Kaunas University of Technology

Faculty of Mechanical Engineering and Design

Estimation of Defects Depths and Lateral Size Using Different Ultrasonic Techniques

Master's Final Degree Project

Ugnė Baskutytė

Project author

Prof. Elena Jasiūnienė

Supervisor

Kaunas, 2020

Kaunas University of Technology

Faculty of Mechanical Engineering and Design

Estimation of Defects Depths and Lateral Size Using Different Ultrasonic Techniques

Master's Final Degree Project

Aeronautical Engineering (6211EX024)

Ugnė Baskutytė

Project author

2020 05 15

Prof. Elena Jasiūnienė

Supervisor

Assoc. Prof. Daiva Zeleniakienė

Reviewer

Kaunas, 2020

Kaunas University of Technology

Faculty of Mechanical Engineering and Design

Ugnė Baskutytė

Estimation of Defects Depths and Lateral Size Using Different Ultrasonic Techniques

Declaration of Academic Integrity

I confirm that the final project of mine, Ugnė Baskutytė, on the topic „Estimation of Defects Depths and Lateral Size Using Different Ultrasonic Techniques" is written completely by myself; all the provided data and research results are correct and have been obtained honestly. None of the parts of this thesis have been plagiarised from any printed, Internet-based or otherwise recorded sources. All direct and indirect quotations from external resources are indicated in the list of references. No monetary funds (unless required by Law) have been paid to anyone for any contribution to this project.

I fully and completely understand that any discovery of any manifestations/case/facts of dishonesty inevitably results in me incurring a penalty according to the procedure(s) effective at Kaunas University of Technology.

Ugnė Baskutytė — (name and surname filled in by hand)

(signature)

Kaunas University of Technology

Faculty of Mechanical Engineering and Design

Study programme: Aeronautical Engineering (6211EX024)

Task of the Master's Final Degree Project

Given to the student: *Ugne Baskutyte*

1. Title of the Project:

Estimation of Defects Depths and Lateral Size Using Different Ultrasonic Techniques

Atstumo iki defektų ir defektų dydžio įvertinimas naudojant skirtingus ultragarsinių matavimų metodus

2. Aim of the Project:

to compare accuracy of different ultrasonic techniques for the sizing of defects / determination of depth of defects in composite materials.

3. Tasks of the Project:

- *to analyze the type of defects and their causes in composite materials;*
- *to analyze the scope of application of ultrasonic method and suitability for estimation of defects size/depth*
- *to determine the most appropriate parameters (transducers' parameters, positioning) so that defects can be detected in the carbon fiber composite materials;*
- *to create a computer model for the investigation of influence of the defect size/ depth on detectability and correct sizing*
- *to verify the results experimentally*

4. Structure of the Text Part:

1. Introduction

2. Carbon Fiber Composite Materials: Structure, Properties, Defects, Inspection Methods

3. Computer Simulation

4. Experimental Analysis

5. Conclusions

5. Structure of the Graphical Part:

Author of the Final Degree Project	Ugnė Baskutytė	2020 05 15
	(abbreviation of the position, name, surname, signature, date)	
Supervisor of the Final Degree Project	Prof. Elena Jasiūnienė	
	(abbreviation of the position, name, surname, signature, date)	
Head of Study Programmes	Prof. Artūras Keršys	
	(abbreviation of the position, name, surname, signature, date)	

Ugnė Baskutytė. Estimation of Defects Depths and Lateral Size Using Different Ultrasonic Techniques. Master's Final Degree Project, supervisor Prof. Elena Jasiūnienė; Faculty of Mechanical Engineering and Design, Kaunas University of Technology.

Study field and area (study field group): Aeronautical Engineering (E14), Engineering Sciences (E).

Keywords: ultrasound, phased arrays, NDT, carbon fiber, Omniscan

Kaunas, 2020. Number of pages 78.

Summary

Polymer composites are increasingly used in aerospace structures, mainly due to the relatively high specific strength and stiffness, and relatively low density and mass. Aviation safety requires reliable testing techniques that allow for the timely detection of defects in individual components or assembly units. In this master's final project, possible defects in composite materials and non-destructive testing methods used to identify defects are examined. The aim of this work is to compare accuracy of different ultrasonic techniques for the sizing of defects / determination of depth of defects in composite materials. Using CIVA software, the test sample was designed and inspected virtually with two techniques of ultrasonic method, i.e., with single-element transducer and phased array probe. "OLYMPUS OMNISCAN$_{MX}$" flaw detector was used for the verification of the results experimentally. It provided an opportunity to examine the propagation of ultrasonic waves in the sample and the interaction with the defects. Studies have shown that using the ultrasonic measurement method, more accurate results are obtained in the presence of a defect inside the carbon fiber reinforced polymer, compared to the results when the defects are relatively close to the surface of the object under study. However, after estimating the absolute errors, deviations from the actual defect sizes are minimal and justify the use of the chosen method. The more accurate determination of the depth of the defect and its lateral size in the composite using a phased array compared to the single-element transducer, obtained in the experimental studies, allowed to conclude that the phased array probe is one of the best of non-destructive test methods for evaluation quality of aerospace structures of polymer composites for in-service application.

Ugnė Baskutytė. Atstumo iki defektų ir defektų dydžio įvertinimas naudojant skirtingus ultragarsinių matavimų metodus. Magistro baigiamasis projektas, Prof. Elena Jasiūnienė; Kauno technologijos universitetas, Mechanikos inžinerijos ir dizaino fakultetas.

Studijų kryptis ir sritis (studijų krypčių grupė): Aeronautikos inžinerija (E14), Inžinerijos mokslai (E).

Reikšminiai žodžiai: ultragarsas, fazuotos gardelės, NDT, anglies pluoštas, Omniscan

Kaunas, 2020. Puslapių sk.78 p.

Santrauka

Polimerinės kompozitinės medžiagos vis plačiau naudojamos aviacijoje, daugiausia dėl santykinai didelio savitojo stiprio ir standumo bei santykinai mažo tankio ir masės. Saugumui aviacijoje užtikrinti reikalingos patikimos kontrolės sistemos, leidžiančios laiku nustatyti defektus atskirose detalėse ar surinkimo vienetuose. Magistro baigiamajame projekte išnagrinėti galimi pasitaikantys defektai kompozitinėse medžiagose ir defektų nustatymui naudojami neardantys kontrolės metodai. Šio darbo tikslas - palyginti skirtingų ultragarsinių metodų, taikomų defektų dydžiui / defektų gyliui nustatyti kompozitinėse medžiagose, tikslumą. Naudojant CIVA programinę įrangą, suprojektuotas tiriamasis bandinys buvo patikrintas dviem būdais taikant ultragarsinį matavimą, t.y., naudojant vieno elemento pjezokeitiklį ir fazuotą keitiklių gardelę. Eksperimentinių tyrimų rezultatams patikrinti buvo panaudota „OLYMPUS OMNISCAN$_{MX}$" defektoskopas. Tai padėjo išanalizuoti ultragarsinių bangų sklidimą realiame bandinyje ir sąveiką su defektais. Tyrimai parodė, kad naudojant ultragarsinį matavimo metodą tikslesni rezultatai gaunami esant defektui anglies pluoštu sustiprinto polimero viduje, lyginant su rezultatais, kai defektai yra sąlyginai arti tiriamojo objekto paviršiaus. Tačiau įvertinus absoliutines paklaidas, nukrypimai nuo realių defektų dydžių yra minimalūs ir pateisina pasirinkto metodo panaudojimą. Eksperimentinių tyrimų metu gautas tikslesnis defekto gylio ir jo matmens kompozite nustatymas panaudojant fazuotą gardelę, lyginant su vienu ultragarsiniu keitikliu, leido padaryti galutinę išvadą, kad fazuotos keitiklių gardelės naudojimas yra vienas iš tinkamiausių neardomųjų kontrolės metodų, skirtų polimerinių kompozitinių medžiagų eksploatuojamų aviacijoje, kokybės įvertinimui.

Table of contents

List of figures

List of tables

List of abbreviations and terms

Abbreviations:

NDT – non-destructive testing;

AE - acoustic emission;

UT - ultrasonic testing;

IR – infrared;

FBH - flat bottom hole;

CFRP – carbon fiber reinforced polymer;

PAN – polyacrylonitrile;

CAD – computer-aided design;

ROI - region of interest.

Terms:

OLYMPUS OMNISCAN$_{MX}$ - ultrasonic measurement system.

CIVA – non-destructive testing simulation software.

Lamb waves - a specific case of surface-guided waves that travel within a thin single elastic and homogeneous plate of large areal extent.

A/D converter – analog-to-digital converter.

Poisson's ratio - is the ratio of transverse contraction strain to longitudinal extension strain in the direction of stretching force.

Young's modulus - mechanical property that measures the stiffness of a solid material.

A-scan - ultrasound biometry, commonly referred to as an amplitude scanning.

B-scan – refers to the image produced when the data collected from an ultrasonic inspection is plotted on a cross-sectional view of the component.

1. Introduction

Carbon fiber composite materials have gained popularity in recent years in high-quality products which need to be light but strong enough to withstand high loads, such as aerospace structures (ailerons, fuselages, tails, wings, panels), car parts, bicycle frames, boat bodies, storage vessels, the sporting goods industry (oars, poles, outdoor tennis rackets, fishing rods, ice hockey sticks, etc.). This can be explained by the fact that these materials are characterized by low density, high energy absorption on impact, high strength and fracture toughness, good thermal conductivity, relatively low thermal expansion, high creep and corrosion resistance and acceptable cost.

Composites are different from traditional materials because they consist of two distinctly different components - fiber and matrix material (usually polymer resin), which, in combination, remain discreet, but interactively create a new material whose properties cannot be predicted by simply adding its components properties.

Carbon fiber is made of thin (about 5-6 μm in diameter), strong crystalline filaments of carbon. Carbon fibers are combined with a polymer matrix to form a new material - composite. Currently, in the world approximately 90% of the carbon fibers produced are manufactured from polyacrylonitrile or PAN. The rest 10% are made from petroleum pitch or rayon. The matrix can be thermosetting (i.e. polyester, epoxy, phenolic, and polyimide resin) or thermoplastic (polypropylene, Nylon 6.6, poly (methyl methacrylate) and polyether ether ketone) [1].

Hypothesis: by applying a non-destructive ultrasonic testing method, defects, which may occur during fabrication and operation, can be detected in carbon fiber composite materials.

Aim of the Project: to compare accuracy of different ultrasonic techniques for the sizing of defects/determination of depth of defects in composite materials.

Tasks of the Project:

- to analyze the type of defects and their causes in composite materials;
- to analyze the scope of application of ultrasonic method and suitability for estimation of defects size/depth
- to determine the most appropriate parameters (transducers' parameters, positioning) so that defects can be detected in the carbon fiber composite materials;
- to create a computer model for the investigation of the influence of the defect size/ depth on detectability and correct sizing
- to verify the results experimentally

2. Carbon Fiber Composite Materials: Structure, Properties, Defects, Inspection Methods

The structure and fabrication of carbon fiber composite materials requires understanding and knowledge of the strength and stiffness of the basic component parts – fibers and matrix. Due to the high composite stiffness and strength resulting from the prepreg technology, combined with the low component density, the fabricated components are suitable for the aforementioned products. Composite materials are increasingly used in aeronautical parts production, so it is important to detect potential defects in a timely manner, as they can have severe consequences. Therefore, composite materials testing methods, which must be reliable, non-destructive to the composite material, quick, convenient, and relatively inexpensive, are becoming a very important factor.

2.1. Properties of Carbon Fiber Composite Materials

Let's briefly look at the key features of carbon fiber composites that make it possible to say that these polymers are a specific substance with exceptional properties.

- Carbon fiber has a relatively high strength to weight ratio, called a specific strength.

- Low density compared to other materials (Table 2.1). This is one of the key factors for easy weight of structures and parts.

- Carbon fiber has relatively rigidity (stiffness). This property is evaluated by Young's modulus and measures deflection under stress. Compared to other materials, carbon fiber reinforced composite is over 4 times stiffer than glass-reinforced composite, almost 20 times more than pine, and 2.5 times greater compared to aluminum [2].

- Carbon fiber is sufficiently chemically stable and has high corrosion resistance.

- Although carbon fiber itself does not deteriorate, the epoxy matrix is sensitive to sunlight and needs protection. Other matrices, irrespective of carbon fiber mixing, may also be reactive.

- Carbon fiber is known as an electrically conductive material. Depending on the field of use, this property may or may not be desirable.

- Good fatigue resistance. While resistance to fatigue greatly depends on the orientation of the fibers, this is especially true when cyclic stresses match with the orientation of the fiber.

- Carbon fiber has good tensile strength. Tensile strength, also known as ultimate strength, is the stress maximum at which material can safely withstand while being pulled or stretched before failing or necking.

- Low thermal expansion coefficient. This is a parameter of how much a material expands and contracts under heating or cooling respectively. Low coefficient of thermal expansion makes carbon fiber to be adaptable for purposes where slight movements can be very important.

- Chemical stability. This ensures the durability of structures and parts in aggressive environments, particularly in strong acids.

- Good fire resistance. Depending on the manufacturing path and the precursor material, carbon fiber can be quite soft and can be manufactured or more often integrated into protective clothing for fighting a fire [3]. A typical example could be nickel coated fiber.

• Carbon fiber is nonpoisonous and X-ray permeable. Both features make it possible to use in medicine.

In the case of disadvantages of carbon fibers, first of all, anisotropy and low strain to failure is to be mentioned. Furthermore, compressive strength is relatively low compared to tensile strength.

Table 2.1 presents the materials properties of carbon fibers along with their rival materials [4-5].

Table 2.1. Properties of carbon fiber and its rival materials

Property	**Unit**	**Carbon Fibers**	**Steel**	**Aluminum**
Tensile strength	MPa	3530-6370	276-1882	230-570
Density	g/cm^3	1.75-1.8	7.7-7.85	2.6-2.8
Elongation at break	%	0.7-2.1	10-32	10-25
Melting point	C^o	3650	1500	477-660
Thermal conductivity	W/m·K	10-150	24-65	237
Specific heat	$J/C^o \cdot g$	0.71-0.75	0.45-2.1	0.9-0.96
Young's modulus	GPa	80-680	190-214	69-73
Poisson's ratio	T	0.1-0.34	0.27-0.3	0.32-0.35

The review of the literature showed that the properties of carbon fibers vary greatly depending on the fibers structure. For example, for the same precursor material (polyacrylonitrile or mesophase pitch), Young's modulus, tensile strength, and strain to failure vary greatly.

2.2. Faults and Defects in Carbon Fiber Composites

Defects in structures and parts of carbon fiber composite materials may occur in two circumstances: during the manufacturing process and during the exploitation, i.e. in-service life.

Let us observe the composites' damage situations in-service life. During the exploitation, the parts and structures of the composite material are subjected to impact loads, tensile forces, bending, compression, fatigue, etc. Composites can also be affected by high temperatures, humidity, and various chemicals. This results in various defects in carbon fiber composite materials.

Compression damage in carbon fiber composites occurs when the material is subjected to axial compression. Due to this effect, the composite losses elastic stability. Due to axial compression, the part takes an undulatory shape. The compressive stress values that cause such buckling are determined by the stiffness of fiber bending and the stiffness of the matrix compression. If the compression load is increased, the buckling is further exacerbated. As a result, local failure occurs in the form named kink-bands [6] (Fig.2.1).

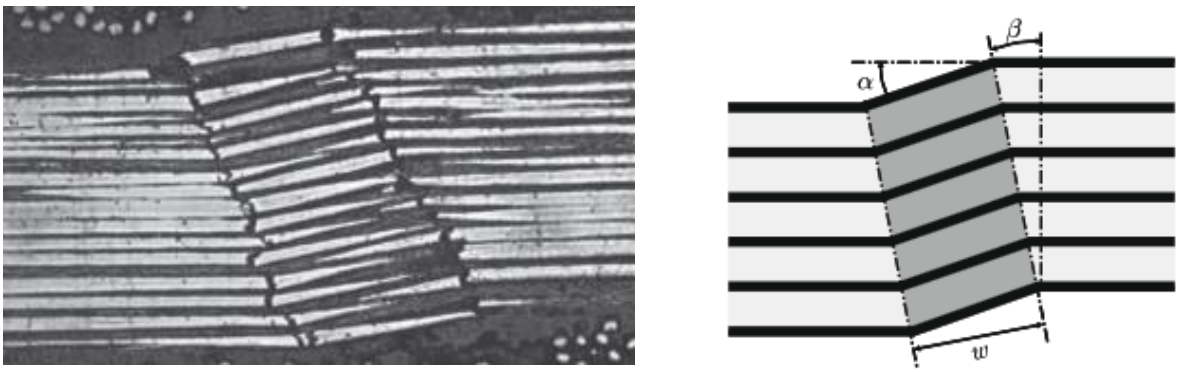

a b

Fig. 2.1. Kink-band due to compression damage of carbon fiber composite: a- micrograph of kink-band formation, b – schematic kink-band local failure (α – fibre angle, β – band angle, w – band width) [7]

Tension damage in composites occurs when the material is under the axial tension. The most common defects are matrix cracking in the transverse lamina, splitting of the longitudinal lamina and the delamination between two L and T plies when the material is under axial tension (Fig.2.2) [1]. It is known that the strength of the fibers is much higher than the strength of the polymeric matrix [8].

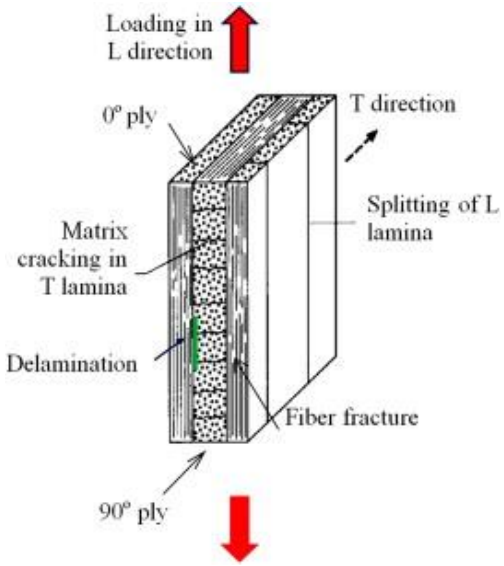

Fig. 2.2. Defects due to axial tension of a composite laminate

As a result, the along strength of the fiber of the lamina (L direction) is much higher than the across strength of the fiber of the lamina (T direction). Consequesntly, at the early stage in the loading cycle, matrix cracking of the 90° ply occurs. When the axial tension load increases, further damage in the form of delamination between the 0° and 90° lamina with extreme different properties occurs. If the load continues to gradually increase, the 0° plies will finally fail because of the fracture of the fiber, as the load can no longer be supported.

Impact damage in composites occurs due to impact onto composite part. The impact can cause these defects, named as delamination, crater, cracks, spalling, fiber breakage, surface buckling (Fig.2.3). Impact defects can be visually observed (surface buckling, craters), however, in some cases, the impact can damage the composite without any significant visible marks on the material surface, e.g. the delamination in the composite layup. The stronger impact can also indicate spalling on the backside of the part, although there may be no visible damage on the front side. Delamination in the composite layups can drastically reduce the composite compression strength.

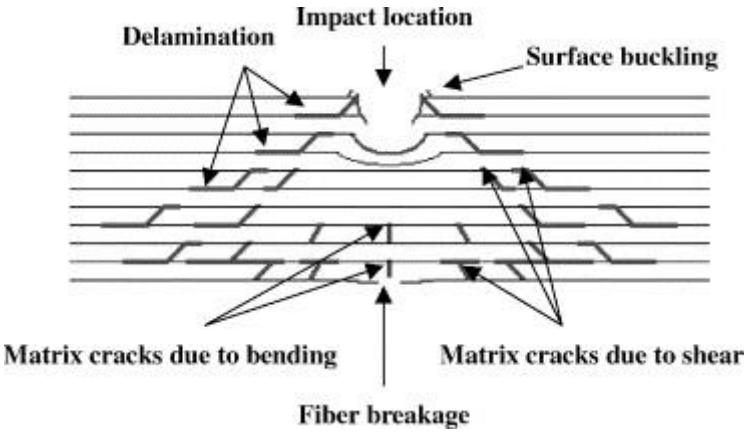

Fig. 2.3. Schematic representation of impact damage effects on carbon fiber composites [9]

Other types of defects appear under the impact load on the structures of sandwich composites. The sandwich composite construction comprises of rigid thin strength faces of the composite which are adhesively jointed on the bottom and top of low density core as shown in figure 2.4a.

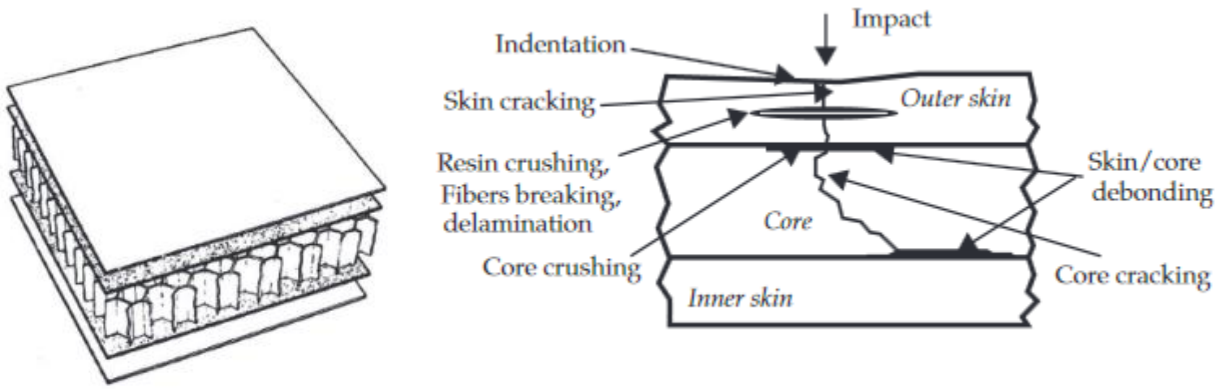

a b

Fig. 2.4. Impact damage in sandwich composites: a- sandwich composite construction, b - possible damage types [10]

Figure 2.4b illustrates possible damage types in sandwich composites. Fiber breaking, skin cracking, resin crushing, or delamination can occur under impact in the top layer skin indentation. The appearance of such damages is highly dependent on the nature of the material of the skin. In parallel with outer skin damage, the core can be damaged by cracking and crushing. There is a risk that both skin-core interfaces may be damaged by debonding.

Fatigue damage of composites causes these effects: delamination, matrix cracking, composite fracture, fiber breaking, crack coupling (Fig. 2.5).

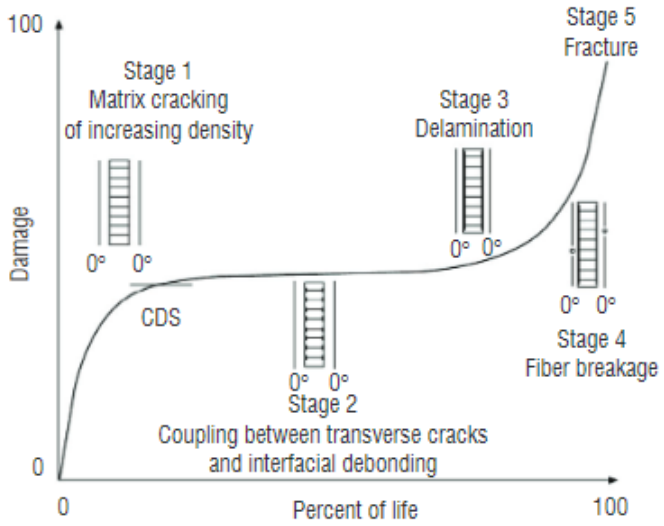

Fig. 2.5. Fatigue crack growth in a cross-ply laminated composite [11]

In the first stage when cycling loading starts, there is a relatively negligible drop in stiffness related to the formation of damage. During the second stage, the stiffness reduces progressively and damage increases relatively slowly and linearly. In the third stage, more noticeable processes are associated with fiber breakage and unstable delamination growth. During the fourth stage an intensive increasing amount of damage is observed, and, finally, as the fifth stage is reached, catastrophic failure takes place. Because of this growing damage under cycling loading, the parts of composites affected by high fatigue loads should be checked regularly for progressive damage.

It is very important to evaluate the state of riveted or other types of joints during the operation of constructions from composite materials. It is, therefore, important to consider the fastener hole damage in composites. A typical example of failure modes in bolted composite plates under tension is shown in figure 2.6. There are four typical modes of failure in composite joints: net-tension, shear-out, bearing, and cleavage [7].

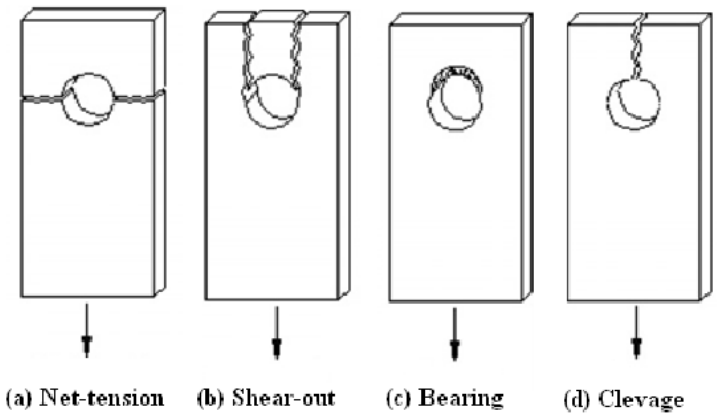

Fig. 2.6. Modes of failure in bolted composite parts under tension [12]

Net-tension mode is observed at the location between the side edge of the part and hole and usually occurring when the parts' cross-sectional area is relatively small and due to exaggerated tensile stress. The shear-out failure takes place when the distance between the edge of the part and hole is particularly small. Bearing mode occurs in the area near the edge of the hole caused by pressure stress acting on the boundary of the hole. Net-tension, shear-out, and cleavage failures may be partially avoided due to improved geometrical parameters of the joint, while the bearing failure cannot be eliminated by any part design.

Under compression the damage composite joints are divided into three types, names as buckling of the part, local buckling of the area weakened by the hole, and micro buckling in the area close to hole names as a zone of highest compression strength (Fig. 2.7).

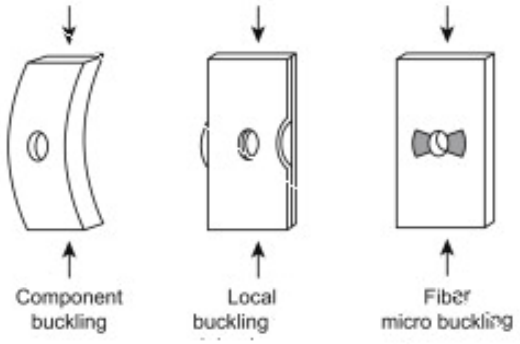

Fig. 2.7. Compression failure types [1]

Overall, practically buckling can be avoided by proper geometrical modification of the joined parts, unfortunately, damage caused by cycling loading would finally weaken the part. It comes up with the thought that composite joints should be done using adhesive joining techniques instead of mechanical fasteners. But the reliability of adhesive joints may not be always guaranteed, especially in tensile loads.

Because of the variety of techniques used for composite materials manufacturing, the variety of defects that occur during manufacturing is also very wide. The main task during the manufacturing of composite material is a combination of the fiber and resin into a well consolidated product. The resin and fiber can be separated before the manufacturing process, or they both can be combined in the form of a pre-preg product. For aerospace parts, where it is essential to reduce the mass, higher quality polymers are usually required, so more modern techniques, such as hot pressing or autoclaving are used.

The manufacturing defects. The manufacturing process of composites can cause a variety of defects. The misalignment of the fiber may occur when the fibers are laid up. Fibers in the same layer may be misaligned for one another or may be misalignment between layers. During manufacturing, the sequence of the layers might be incorrect or a layer could be completely missed. If the layers are omitted or dislocated at the wrong angle, the reduction in composite mechanical characteristics or possible deformation of the structure may occur. Resin rich zones is a result of local divergence in the volume of fiber fraction and the ability of reduced performance. Composites must be properly cured. Improper curing cycles with incorrect temperature, heating rate, or pressure will cause cracking or delamination.

The manufacturing defects of carbon fiber composites usually divided into three categories: matrix, fiber, and interface defects. Matrix defects can be voids/blisters and pores, and incomplete curing. Voids are the most common defects (Fig 2.8). Too little resin causes an inadequate bonding between layers. Thus results the formation of voids and pores. A void is a pore that is not filled in a composite material. Voids' formation is the outcome of imperfection from the manufacturing of the composite.

Fig. 2.8. Voids in a matrix of carbon fiber composite (highlighted by a white arrow) [13]

The voids can be found in different sizes, shape and spatial location. Voids/blisters weaken the material and they also stimulate the formation of other types of defects.

The formation of voids can be controlled to a certain extent by parameters of the manufacturing process. Such parameters could include vacuum pressure, curing temperature, viscosity of the resin, etc. Incompletely cured matrix could be as the result of improper curing cycle or faulty material.

Fibre defects can be broken fibres, waviness (wrinkles) and fibre misalignment. Deviations due to fibres misalignment (Fig. 2.9.) can reduce mechanical properties of the composite, first of all, stiffness and compression strength.

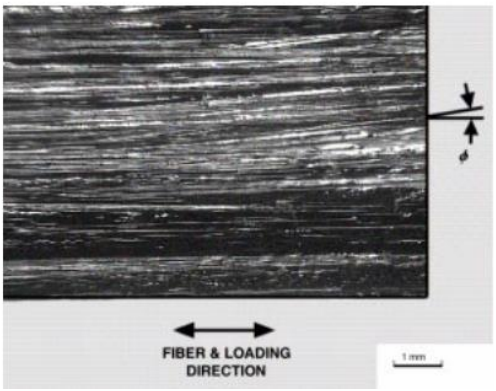

Fig. 2.9. Level of fibre misalignment of a carbon fiber composite [14]

Wrinkles and waviness (Fig. 2.10) are among the most common defects meet in the manufacturing process when adding new layers. This is mostly influenced by pressure from other layers or when different layers of composite are cured in different configurations. Fibre waviness along fiber length causes delamination and subsequent failure of the material.

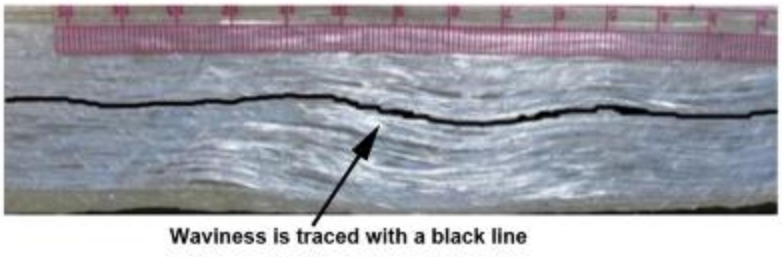

Fig. 2.10. Cross-sectional view of the fiber composite illustrating the waviness [15]

Broken fiber defects more often occur in-service life of material, but some authors [1] attribute them to defects arising in manufacturing route as well, due to inadequate conditions of technological process. Too much resin during manufacturing lowers the volume fraction of carbon fibers and this fact increases the risk of fiber breakage (Fig. 2.11).

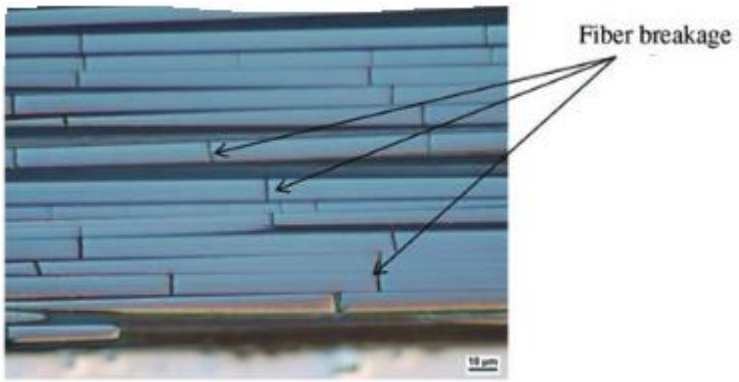

Fig. 2.11. An example of broken carbon fibres [16]

Figure 2.12. presents typical delamination and debonding defects of carbon fiber composite.

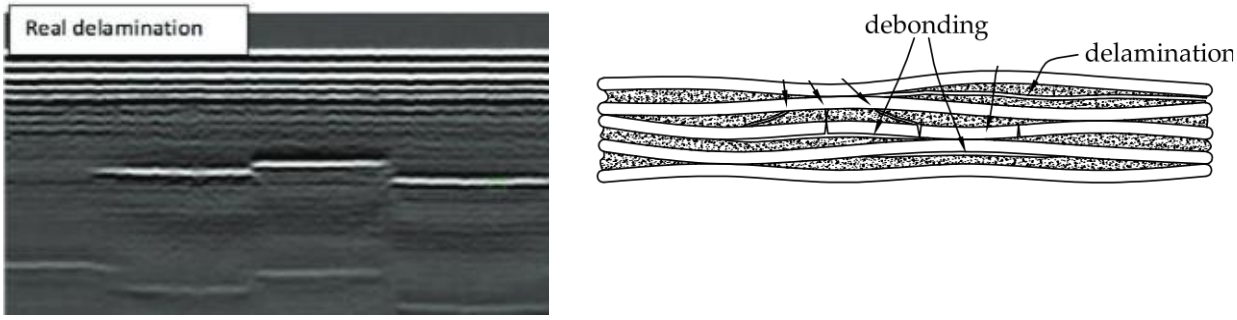

Fig. 2.12. Delamination and debonding defects of carbon fiber composite [17-18]

Foreign objects (Fig. 2.13) also appear in the material during manufacturing process. The most common foreign objects are grease, dust, hair and other impurities. Around foreign inclusions, stresses can develop and cause delamination and other damage.

Common defects (arised during manufacturing process and during exploitation) of carbon fiber composite are nicely shown in figure 2.13.

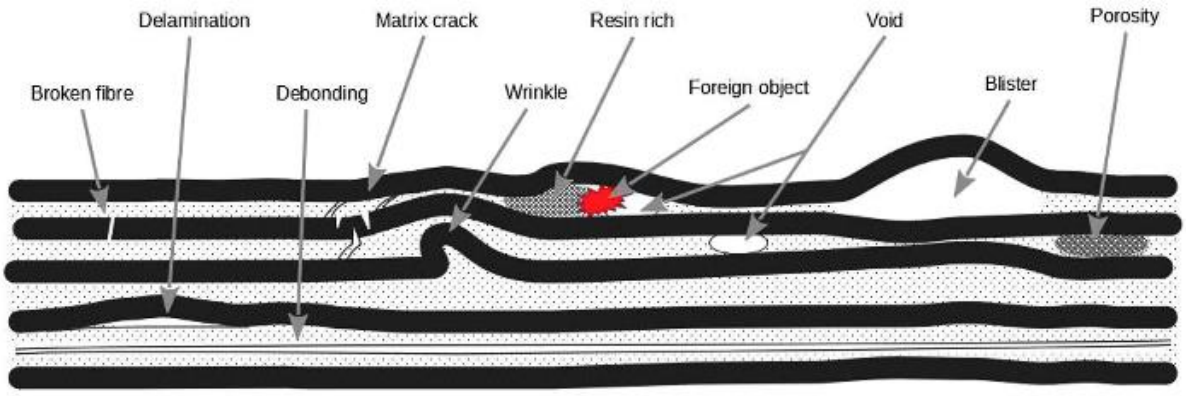

Fig. 2.13. Typical types of defects of carbon fiber composites [19]

It is important to note that in order to avoid the painful consequences due to defects in composite materials, it is necessary to check carbon fiber structures both at the time of service and while in manufacturing.

2.3. Testing Methods of Damage in Carbon Fiber Composites

Like for other materials as well as for carbon fiber composites, all testing methods can be divided into two groups. The first includes techniques that damage the test material itself during the testing, i.e. destructive methods. The second group consists of techniques without causing damage to the material during the testing, i.e. non-destructive testing (NDT) methods. This chapter provides a review of techniques for non-destructive methods.

One of the simplest and cheapest non-destructive testing methods is a **visual inspection**. The accuracy and reliability of this method is highly dependent on the operator's experience. This method can be used to determine surface damage, surface porosity, resin rich zones, delamination, some types of wives [20]. The most important advantages of this method is quick testing procedure and accessibility of the method. In some cases, additional measures such as a microscope may be used during visual inspection.

Another very simple NDT method is **coin tapping** [1, 21]. This method is used for testing laminated structures to detect delamination and voids. The method requires the operator to touch the coin every point of the inspected structure and listen to the sound generated by the structure. The sound of defective points changes and defective regions can therefore be identified.

Thermography testing. Thermography or infrared testing is based on registration of the thermal radiation emitted by a sample surface by means of an infrared (IR) camera (Fig 2.14). The thermal conductivity of the composite material may change due to the presence of defects [20]. Using this method, testing surface is heated in some manner. After that such a surface will emit infrared radiation. Since the heat is partially reduced inside the material, the surface emissions will change in time. If the internal defect exists, it will disorder the heat flow. This fact will result in a change of infrared emission from the surface. This phenomenon can be captured by the IR camera. The thermography method is used for thin carbon fiber composite parts when the defect is in a relatively

non-deep layer from the surface. If the defects are deployed deeper from the surface of the part, they tend to produce fewer heat fluctuations than the defects visible closer to the surface.

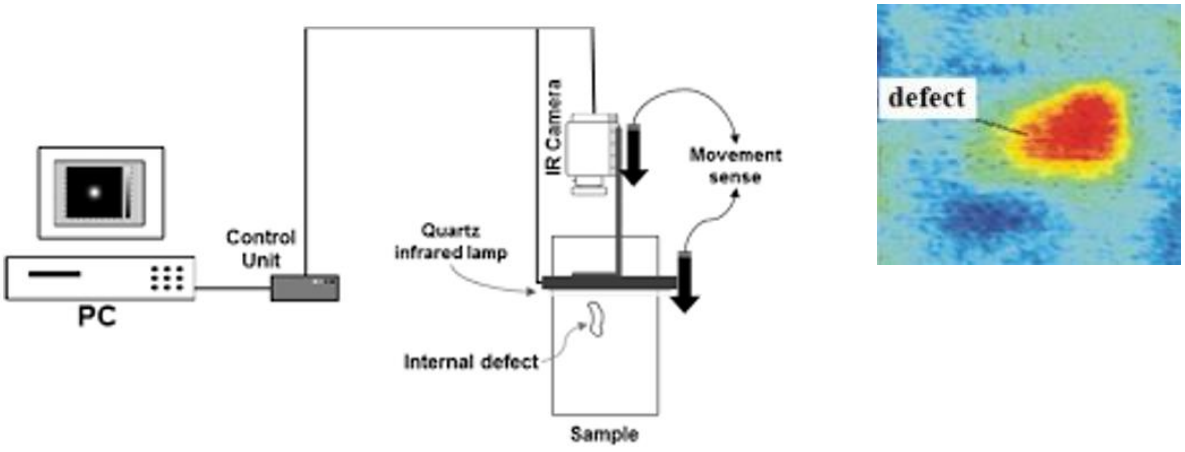

Fig. 2.14. Thermography carbon fiber composites inspection: a – experimental setup of thermographic testing, b – sample from carbon fiber composite material with the defect [22]

Infrared thermography is divided into passive and active approach [23]. The passive method mostly is used for predictive maintenance. Thermography testing is very useful for the detection of composite structures and parts in-service damage. An example could be the situation, when an aircraft coming down from a high altitude warms, thermographic views of the structure can be used to visualize some subsurface state (Fig. 2.15) [23]. This method is relatively rare in the manufacturing level of carbon fiber composites.

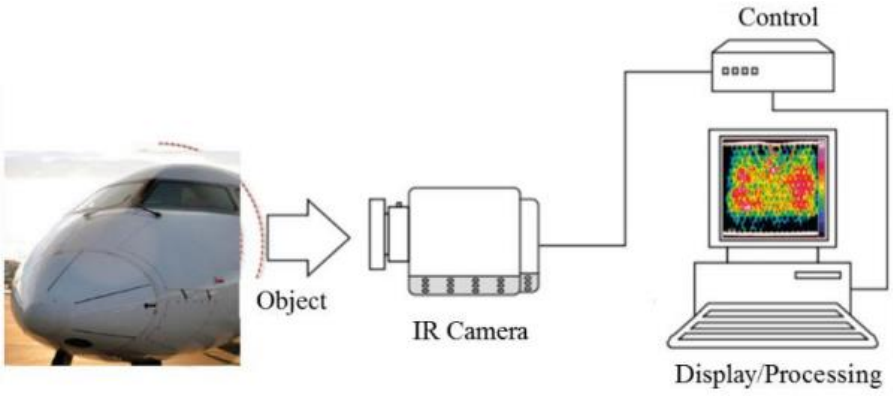

Fig. 2.15. Passive thermography for predictive maintenance in aerospace industry [23]

One of the advantages of thermography testing is that it can test a relatively large area of a part without much time for procedure. Moreover, it is possible to inspect the parts where only one side of the object is accessible to testing.

The drawback to this type of testing includes the requirement for sensitive and relatively expensive equipment, the demand for highly qualified inspectors and the shortage of clearness about defects if they are located too deep from the surface of the part.

Acoustic emission. The acoustic emission (AE) method is different from other NDT methods. Firstly, there is the origin of the signal. When microstructural changes take place in composite materials,

transient stress waves are excited by the influence of energy generation. Secondary, the AE performs with the dynamic processes in the composite. The ability to distinguish between developing and stagnant defects is significant [20]. These stress waves, generated by material defects such as delamination, matrix cracking, debonding, fiber breakage, or fiber pull-out, are called AE (Fig. 2.16). The stress waves are detected by using highly sensitive piezo transducers [24] or fiber optics sensors [25].

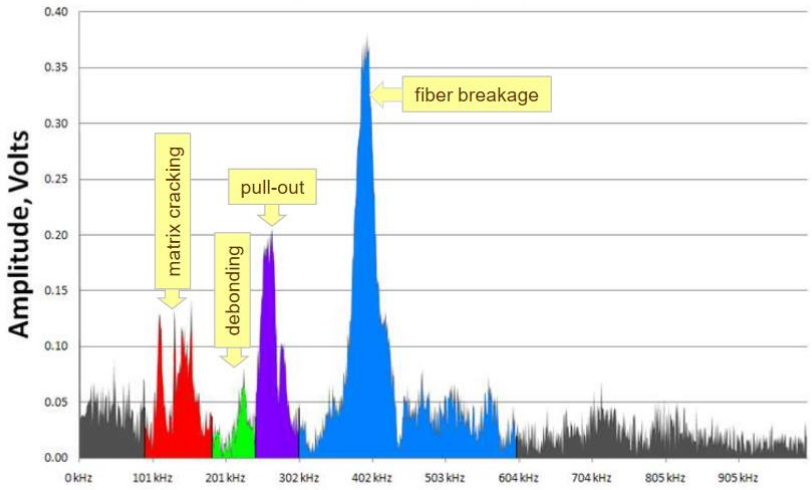

Fig. 2.16. Frequency distribution depending on type of defect in carbon fiber composite using AE method [26]

AE signal is also generated under loading because of the different properties of the fibers and matrix materials. Typical signal of stress wave as the result of the initial impact recorded by piezo transducer is presented in figure 2.17.

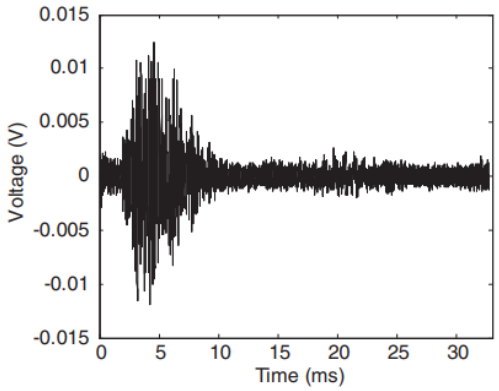

Fig. 2.17. Impact response registered by a piezo transducer on a carbon fiber reinforced plate [24]

The main advantages of AE method are high sensitivity, use of multiple sensors for fast and global testing, and no need to clean and prepare the inspecting part. The disadvantages of AE include the need for highly qualified staff, who would be able to correlate AE inspection results to specific types of failures of carbon fiber composites.

By measuring AE signals, it is possible to obtain and monitor structural changes in the composites. Due to phenomenon that micro damage in composites generates AE, the acoustic emission method is useful for obtaining damages and monitoring them long before they become serious. Also these data

could be used for predicting the service life of the structures and parts of composites and eliminate the risk of unexpected failure thus extending the service life of the part.

Radiographic testing. With radiography it possible to detect cracks, delamination and foreign inclusions as well as to evaluate composites for changes in density and thickness. There many types of radiographic testing: conventional radiography, gamma rays' radiography, low voltage radiography, penetrant enhanced radiography [20]. Each of these testing has specific applications. For example, for thin parts (1-5 mm) low voltage radiography is used, for thick – gamma rays' radiography method, for small matrix cracks and delamination - penetrant enhanced method. One of the most effective radiographic methods is X-ray computed tomography. This method allows to monitor 3D visualized imagines of the structure while the projection radiology allows to see only 2D visualization.

Figure 2.18 presents a typical radiographic set-up.

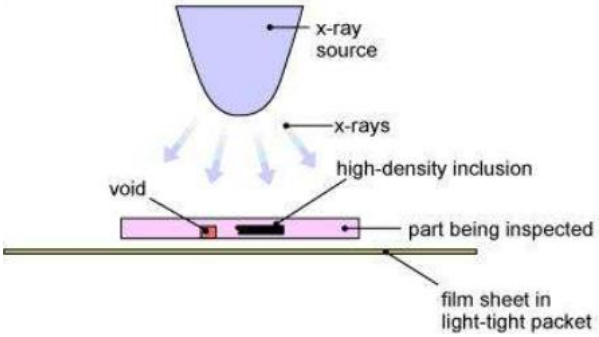

Fig. 2.18. Schematic presentation of set-up for X-ray radiography inspection [21]

Figure 2.19 shows how X-ray passing through the specimen changes its intensity due to an internal void in the material. The X-ray intensity is recorded by radiation sensitive target, usually film or a digital imaging system.

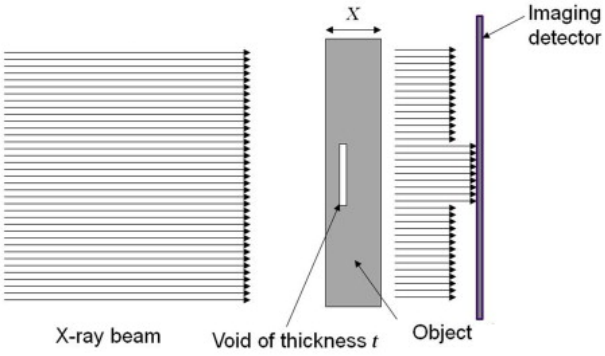

Fig. 2.19. Transmission of X-ray though the part for obtaining voids in composite [1]

The main advantage of radiographic inspection is that it can test thicker parts than other NDT methods and to inspect closed hollow parts. The major disadvantages of radiographic testing are relatively high cost and specific strict health requirements. Also, X-rays are not useful for inspecting in-service damage in composites and cannot detect delamination without penetrant.

Shearography. Shearography is a laser optical technique commonly used for composites. Figure 2.20 shows the principle of shearography inspection.

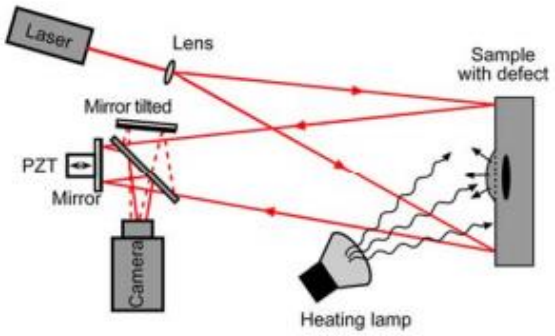

Fig. 2.20. Configuration of shearography inspection system [27]

Composite failure usually occurs at stress concentrations. Defects emergency is easily evaluated from the degree of strain concentrations close to the defect [27]. The essence of the method consists of interferometric comparison of the inspected part in two states - unloaded and loaded one (Fig. 2.21). This interference phenomenon is named as a shearogram.

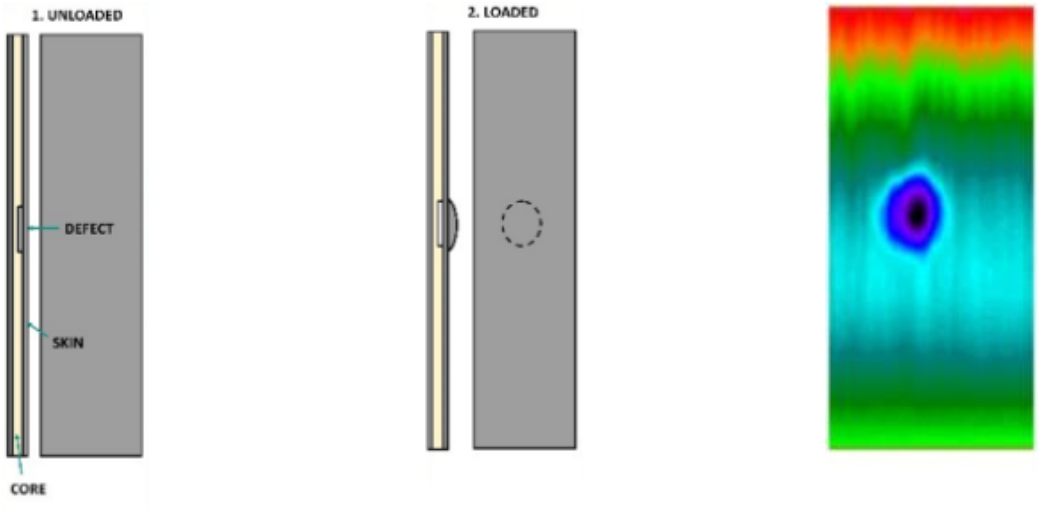

a b c

Fig. 2.21. Shearography operation principle: a – unloaded part, b – loaded part, c – shearogram [28]

This method is well used for showing disbands in the composite. The advantage of shearography method is that this method is less sensitive to noise in comparing with other NDT methods. Another advantage of the method is relatively rapid inspection with a high degree of sensitivity.

The method's wide applicability has limited that the technique can only be used for the parts in which the roughness of the surface is of the order of one wavelength of light or more. Parts with smoother surfaces will give random interference. Moreover, the method requires considerable experience for the interpretation of the results and influence of lighting has significant importance on the resultant image.

Electromagnetic testing. Electromagnetic methods are not typical testing methods for carbon fiber composites, but they can be applied in some cases [29]. Electromagnetic methods include eddy current inspection, magnetic flux leakage, remote field testing, and alternating current field

measurement [20]. Electromagnetic inspection is used to find and evaluate fractures, faults, and some other conditions of materials. Eddy current technique may be used to determine defects for carbon fiber reinforced composites because carbon fibers are electrically conductive [30]. Eddy current based inspection techniques are sensitive to the volume fraction of fibers, broken fibers or waviness (Fig. 2.22) due to impact damage [30,31].

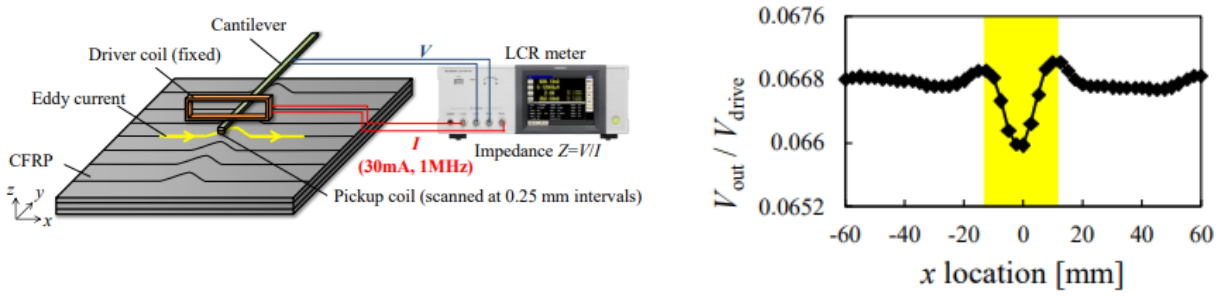

a b

Fig. 2.22. Eddy current method for waviness detection in carbon fiber composites: a- an experimental setup for eddy current imaging, b – results of eddy current testing obtained from scanning part [32]

The greatest limitation of the use of this testing for carbon fiber reinforced composites is that these composites are mildly conductive and they are only useful for sensing very near the surface. Moreover, damages which are located parallel to the scan direction are undetectable.

Ultrasonic testing. Ultrasonic testing (UT) is probably the most commonly used NDT method for the testing of composite materials. There are many ultrasonic testing variants, but several of them have the greatest applicability for the inspection of carbon fiber composites: pulse echo, through transmission ultrasound, acoustic-ultrasonic, back scattering and ultrasonic spectroscopy [33]. UT uses waves which are generated by a mechanical vibration due to transducer that transforms an electrical signal into a mechanical movement and vice versa. Ultrasound for composite testing is most widely generated by piezo electric transducers [1]. UT is useful for defecting wide variety of defects such as porosity, inclusions, voids, delamination, broken fibres, and some other flaws [34].

Pulse echo method uses the single transducer which serves as the transmitter and the receiver (Fig. 2.23).

a b

Fig. 2.23. Configuration of pulse echo method: a - typical pulse echo inspection setup, b- delamination image from an amplitude C scan [35]

When ultrasonic waves smash into impact damage, the reflective energy in the form of pulse-echo amplitude differs from the normal situation when there is the absence of damage. The method can be used in cases when it is possible to get access only from one side of the object.

Advantages of the pulse echo method: large objects can be investigated, can be adapted to the complex form of the research object, relatively simple equipment.

Disadvantages of the pulse echo method: hard to detect defects close to the surface, slow testing, limited detection and characterization of heterogeneity, bad signal-to-noise ratio in strongly inhibiting materials.

The through-transmission ultrasound method is also one of the most often used methods of ultrasonic testing for composite structures. By applying the through-transmission ultrasound method, the transducers are mounted on both sides of the test object (Fig. 2.24). The act of one transducer is sending (transmitter) and the other – receiving (receiver).

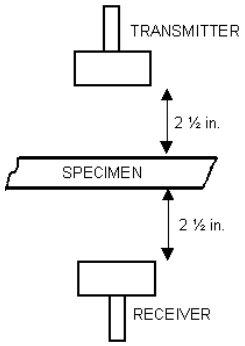

Fig. 2.24. Location of transducers in through-transmission ultrasound technique [36]

Advantages of the through-transmission ultrasound method: easy to use for thickness measurement, for heterogeneity determining, for material composition changes.

Disadvantages of the through-transmission ultrasound method: the transducers must be exactly opposite, the characteristics of the transducers must be the same, they must be calibrated, the surfaces of the test object must be flat and parallel, both sides of the object must be accessed, the depth of heterogeneity cannot be determined, only the transverse coordinates can be determined.

The pitch catches variant uses two different but in one body transducers – transmitter and receiver (Fig. 2.25). In this case, the emitted pulse will not be visible on the monitor screen, only reflection from the defect or bottom with different signal amplitudes will be visible.

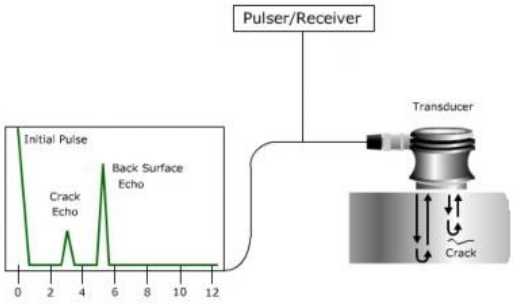

Fig. 2.25. Ultrasonic testing using pitch catch variant [37]

Advantages of the pitch catch method: defects can be found close to the surface, measurements can be made in thin objects, each piezoelectric transducer can be combined separately, different piezoelectric elements can be used.

Disadvantages of the pitch catch method: part of the signal goes directly from the transmitter to the receiver and an interference echo occurs, so it is difficult to detect low heterogeneity near the surface.

Polymer structures have significant anisotropy of layers that makes shear waves more problematic to use effectively. In this situation where composite testing is carried out, it is better to use guided waves which include Lamb waves. In addition, Lamb waves are easy to use for thin parts and for measurements over long distances [33]. Typical Lamb waves use scheme is shown in figure 2.26.

Fig. 2.26. Configuration of Lamb waves variant for inspection [38]

Advantages of the guided waves which include Lamb waves method: it is possible to study thin structures, especially composite materials, convenient measurements at long distances, various configurations of measurements.

Disadvantages of the guided waves method: a high qualification of staff is needed because of the requirement of considerable interpretation.

When the ultrasonic waves are incident with an oblique angle, the ultrasonic testing variant is named as back scattering technique (Fig. 2.27).

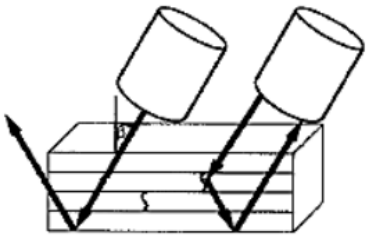

Fig. 2.27. Back scattering measurement configuration [38]

The signal used to find defects is reflected from the bottom. This method can be used to find heterogeneous areas close to the surface of the part and which are not parallel to the surface of the part. For example, a perpendicular transducer may not detect perpendicular to the surface defects, while the use of an angular transducer can easily detect such defects. The back scattering measurement is applicable for detecting matrix cracks.

Advantages of the back scattering method: it is possible to find heterogeneities that are not parallel to the surface of the object, there are no problems with the “dead zone”.

Disadvantages of the back scattering method: it is difficult to determine the size and location of heterogeneity, it is difficult to distinguish between short and deep heterogeneity from long and shallow.

For traditional ultrasound examination, the coupling medium (water or gel) is always required for transmitting the ultrasound. However, contact fluids are not always suitable for the part's geometry or when the properties of the object may change due to immersion in the medium. Recently with advanced signal processing techniques, it is possible using air-coupled ultrasonic measurement (Fig. 2.28) to determine the location of defects in ultrasonic systems for composite testing.

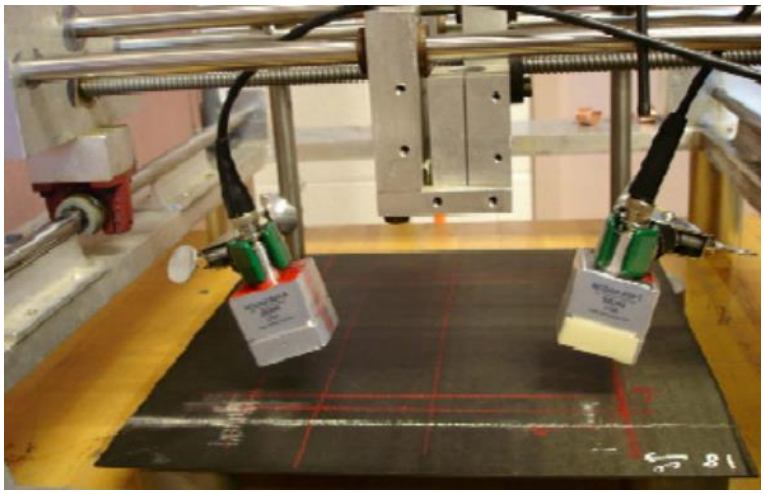

Fig. 2.28. Air coupled transducers for inspection of delamination [38]

Advantages of the air-coupled measurement: it is easy to find heterogeneities that are not parallel to the surface of the object, convenient to use for perpendicular heterogeneities to the surface.

Disadvantages of the air-coupled method: it is necessary to accurately position the transducers in one line.

The experimental setup of ultrasonic spectroscopy technique with laser ultrasound source and time profile of ultrasound pulse are shown in Fig. 2.29.

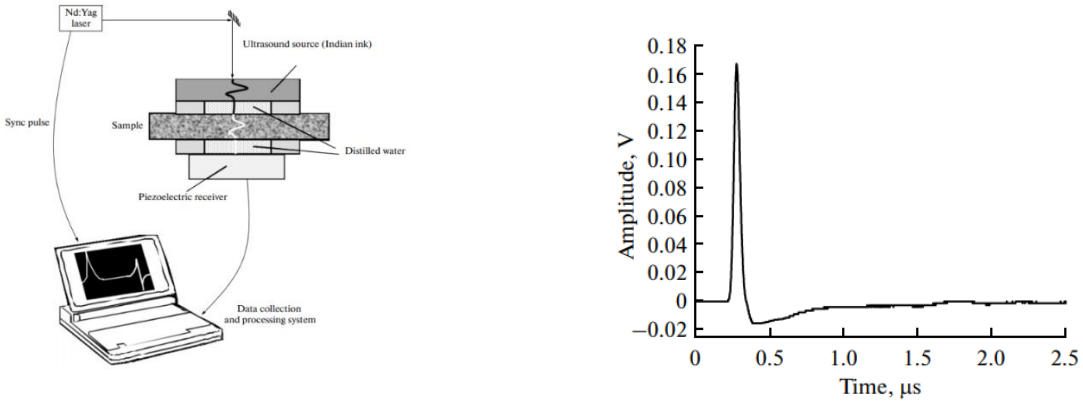

a b

Fig. 2.29. Ultrasonic spectroscopy technique: a - block diagram of ultrasonic spectroscopy with laser ultrasound source, b – time profile of an ultrasound pulse in acoustic spectrometer [39]

This method is widely used to determine porosity and delamination because it is possible to study parts of different forms, higher measuring speed.

Advantages of the ultrasonic spectroscopy method: it is possible to study objects of different forms, higher measurement speed compared to contact method, no loss of contact due to surface roughness of the object under investigation.

Disadvantages of the ultrasonic spectroscopy method: stationary sophisticated apparatus, not suitable for corrosive objects, expensive equipment, problematic positioning of the transducer in relation to the object.

Time of flight diffraction method is used to estimate defect sizes in the composites and other materials. This method uses tandem transducers. As shown in figure 2.30, firstly the surface wave 1 comes from the transmitter to the receiver, then diffuses from the upper defect edge wave 2, after that the wave 3 has been diffractioned from the bottom edge of the defect and finally the reflection from the rear wall of the tested object 4 [33].

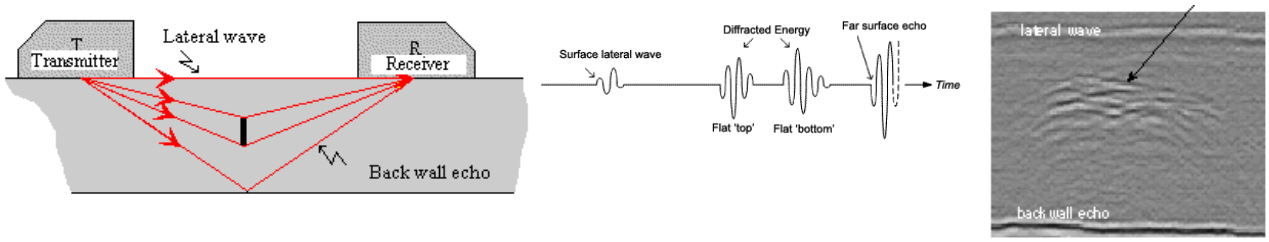

a b c

Fig. 2.30. Time of flight diffraction method: a – typical setup, b – signals of waves, c – imagine projection of defect [40]

The duration of the spread of the signal from the edge of the defect can be measured during the study. Knowing the duration, it is possible to find the depth that contains the defect. Knowing the duration of diffractioned signals from both edges of defects, it is possible to determine the depth of the upper and lower defect edge and determine the height of the defect.

The main advantage of this method is that it is possible to determine not only the place of heterogeneity but also its size.

Disadvantages of the flight diffraction method: need to put the transducers in one line, it is difficult to determine the lower edge of the defect due to the weak reflected signal.

2.4. Determination of Defects in Polymer Composites using Ultrasonic Phased Arrays

Multichannel ultrasonic phased array method is designed for ultrasonic non-destructive testing and measurements by analyzing the internal structure of various metals and their alloys, carbon and glass fiber reinforced composites, plastics and their alloys, in the search for internal defects.

Typically, the ultrasound transducers used for non-destructive inspection consists of either a single piezoelectric element, which can transmit and receive reflected waves or of two paired piezoelectric elements, one of them serves for transmitting and the other for receiving waves. Piezoelectric element is the main component of the phased array probe (Fig. 2.31).

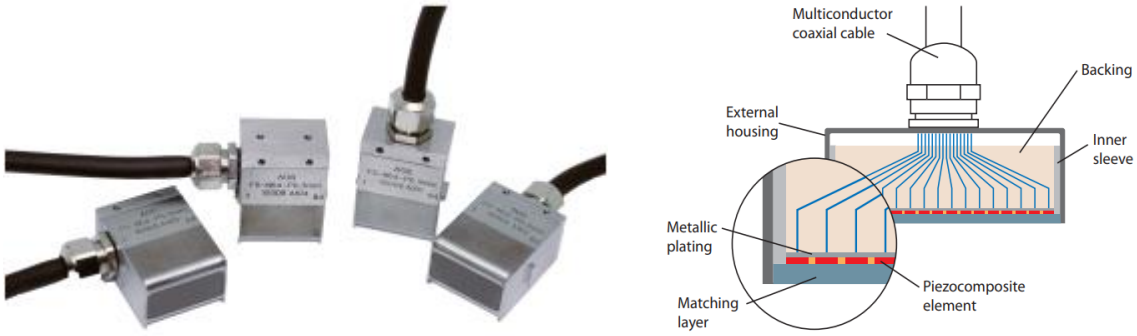

a b

Fig. 2.31. Phased array probes: a – general view of phased array probes; b – cross-section of phased array probe [41]

In the production of phased array probe, the piezoelectric element is cut into many small individual elements (Fig. 2.32), usually between 16 and 256 [41]. More elements increase the capability of focusing and steering by increasing area under inspection but requires higher cost of the equipment.

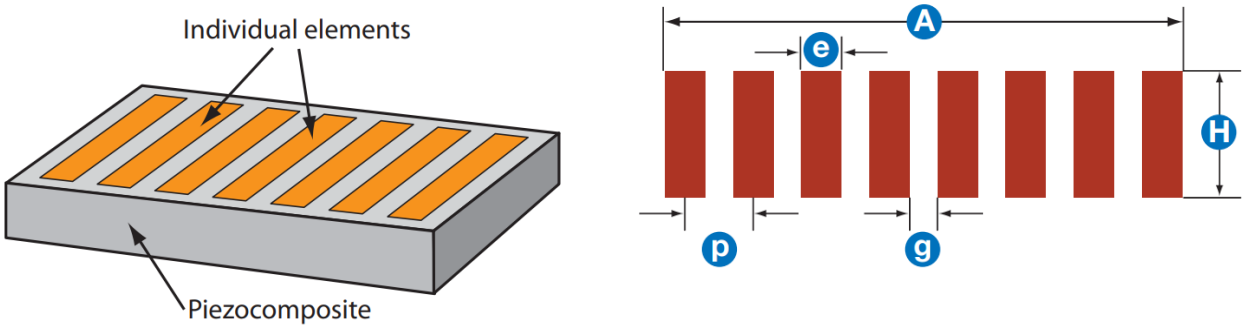

a b

Fig. 2.32. Phased array probe: a - typical multi-element view; b- dimensions of a phased array probe, where A – total aperture, H – height of individual element, p – pitch between elements, e – width of individual element, g – spacing between elements [41]

Each of these elements has its own connector, circuit of time delay and A/D converter. All elements are acoustically insulated from each other. Individual elements are pulsed in groups, have calculated time delays for each element. This phenomenon is called phasing. Pulsers are usually multiplexed. The more elements, the better distinction can be obtained by measuring. The types of arrays can be linear (a), circular, ring (b), and 2D matrix (c), as shown in figure 2.33 [33]. The frequency used for the transducer is between 2 MHz and 10 MHz.

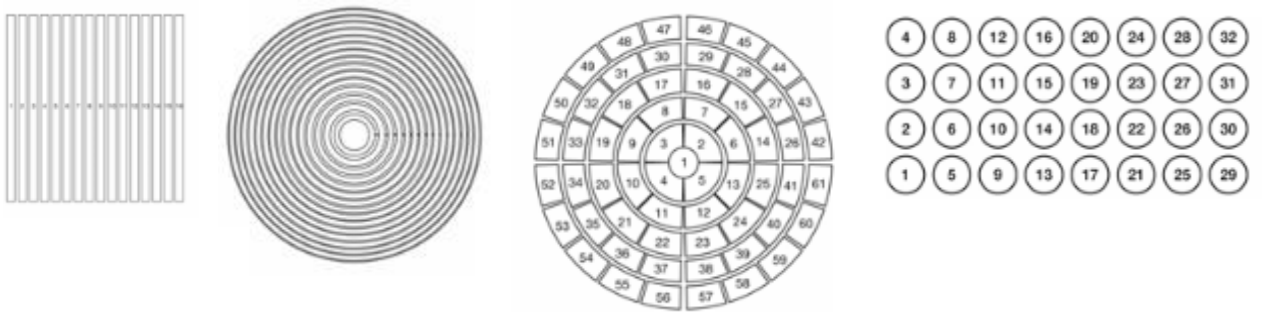

a b c

Fig. 2.33. Types of arrays: a – circular; b – ring; c – 2D matrix [33]

The simplest manner is to locate the phased array parallel to the surface of the material that has been inspected and either couple it directly or through a specific intervening coupling medium (Fig. 2.34) [42]. The aperture is then electronically transferred along the array to create an image. Angular sweeps are more commonly used with the angle wedge (Fig. 2.34, d), but also can be performed with directly coupled arrays (Fig. 2.34, c).

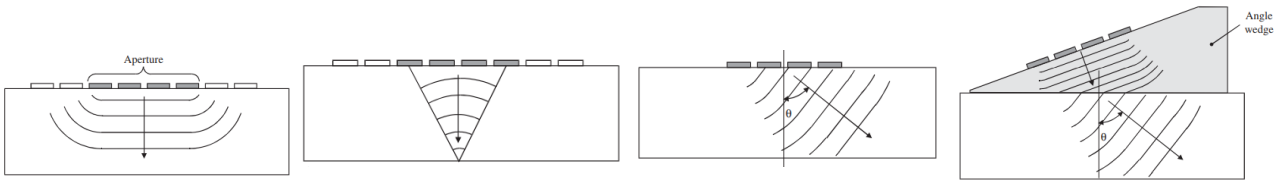

a b c d

Fig. 2.34. Array test modes: a – simple scanning; b – focused scanning; c – angular sweep; d – angular sweep with angle wedge [42]

In most cases, the angular sweep is more informative as defects that are perpendicular to the surface can be detected (Fig. 2.35).

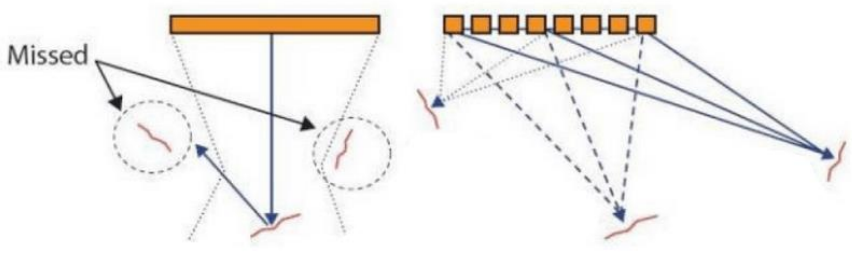

a b

Fig. 2.35. Detection of the defects: a – with limited beam angle; b – with angular sweeping beam [43]

As we can see from figure 2.35, a, using limited beam angle, the defects oriented in the material perpendicular to the surface can't be noticed.

The principle of ultrasonic phased arrays is to excite all or group individual piezo elements of the transducer. The result is beam forming which requires precise pulsing and time delays. Receiving process is the reverse of pulsing (Fig. 2.36) [43]. As shown in figure 2.36, the echo reaches various transducer elements from a desired focal point with a calculated time offset. The echo signals from each transducer element are shifted over time before summation. The amount received is an A-scan, which highlights the response from the flaw and weakens various other echoes from other material points.

In the emitting stage the acquisition unit (Fig. 2.36) sends a trigger signal to the phased array. The phased array tool turns the signal into a high-voltage pulse whose pre-programmed width and time delay is defined in the focal laws. Each piezo element receives only one pulse. This creates a beam of a certain angle, oriented to a certain depth. The beam impacts a defect and returns back. Received signals then are shifted in time taking into account the receiving focal law. Then they unite to form one ultrasonic pulse, which is sent to the acquisition unit.

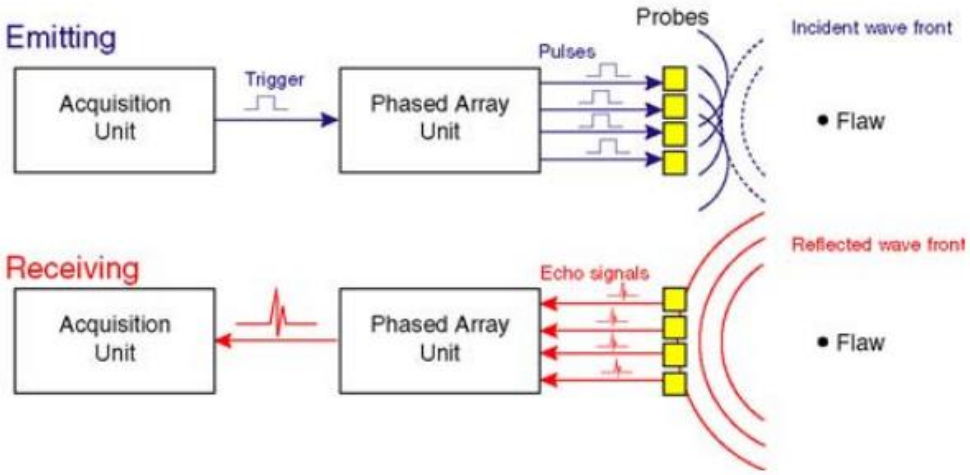

Fig. 2.36. Transmitter and receiver components for ultrasonic phased array beam forming [43]

Using phased array technique, focalization, deflection (also called angular scanning) or electronic linear scanning are possible.

Illustration of beam generation and focusing is shown in figure 2.37 [44]. There the elements are pulsed with different time delays. Applied delay to each element is in green color and elements in the array are marked in yellow.

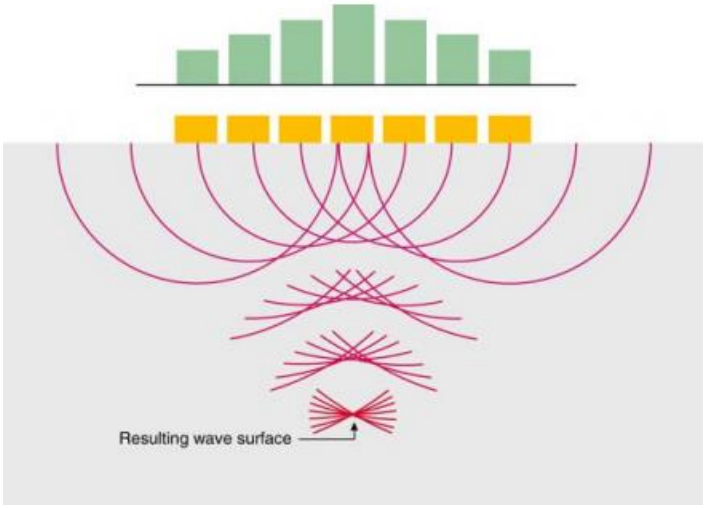

Fig. 2.37. Beam generation and focusing [44]

Beam focalization is a convergation of the acoustic energy into a relatively small focal spot. In practice, focalization technique scanning process is fulfilling with different focal depths. Using focalization only one transmitted pulse is used, and refocusing is performed at all programmable depths.

Using deflection technique, the beam is shifted through a sweep range in a specific direction for a certain focal depth. This allows the single transducer to perform testing at various angles (Fig. 2.38).

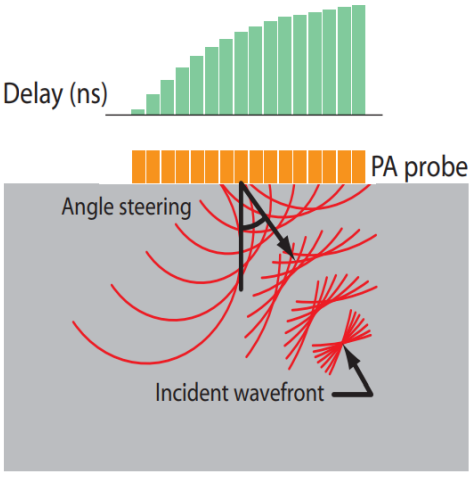

Fig. 2.38. Angled beam generation [44]

Steering diapason can be changed using an angle wedge which is usually made of plastic. Using this method, it is possible to inspect multiple angle with a single probe.

Electronic linear scanning. This method allows to move the acoustic beam along the axis of the array without mechanical movement (Fig. 2.39). The beam movement is performed by active

elements multiplexing in time. Scanning is limited by number of array elements and number of channels in the system.

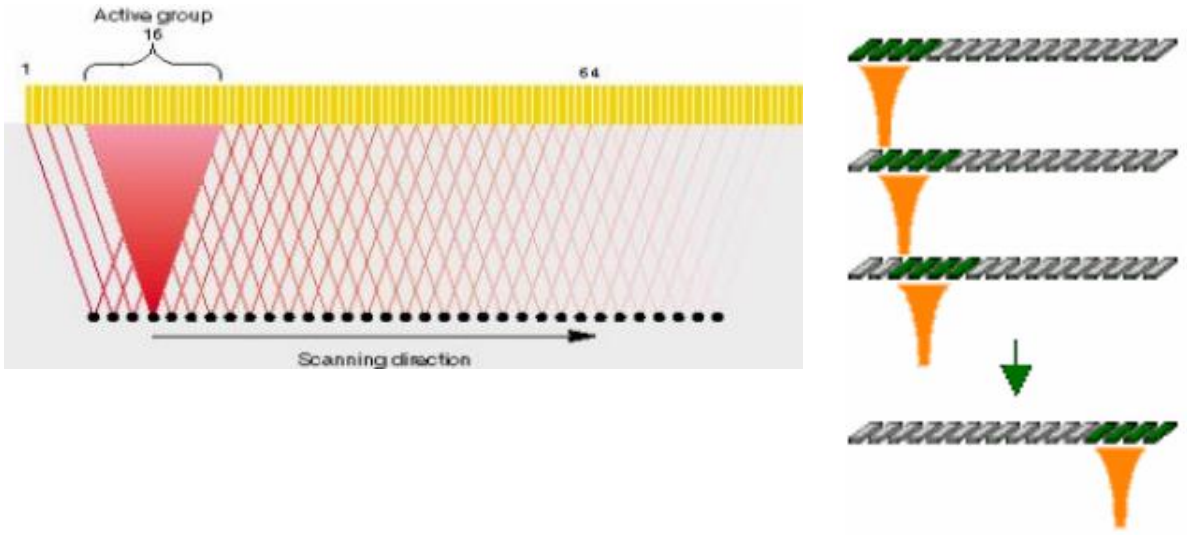

Fig. 2.39. Electronic linear scanning [44]

Figure 2.40 presents examples of linear scanning to detect defects in the material.

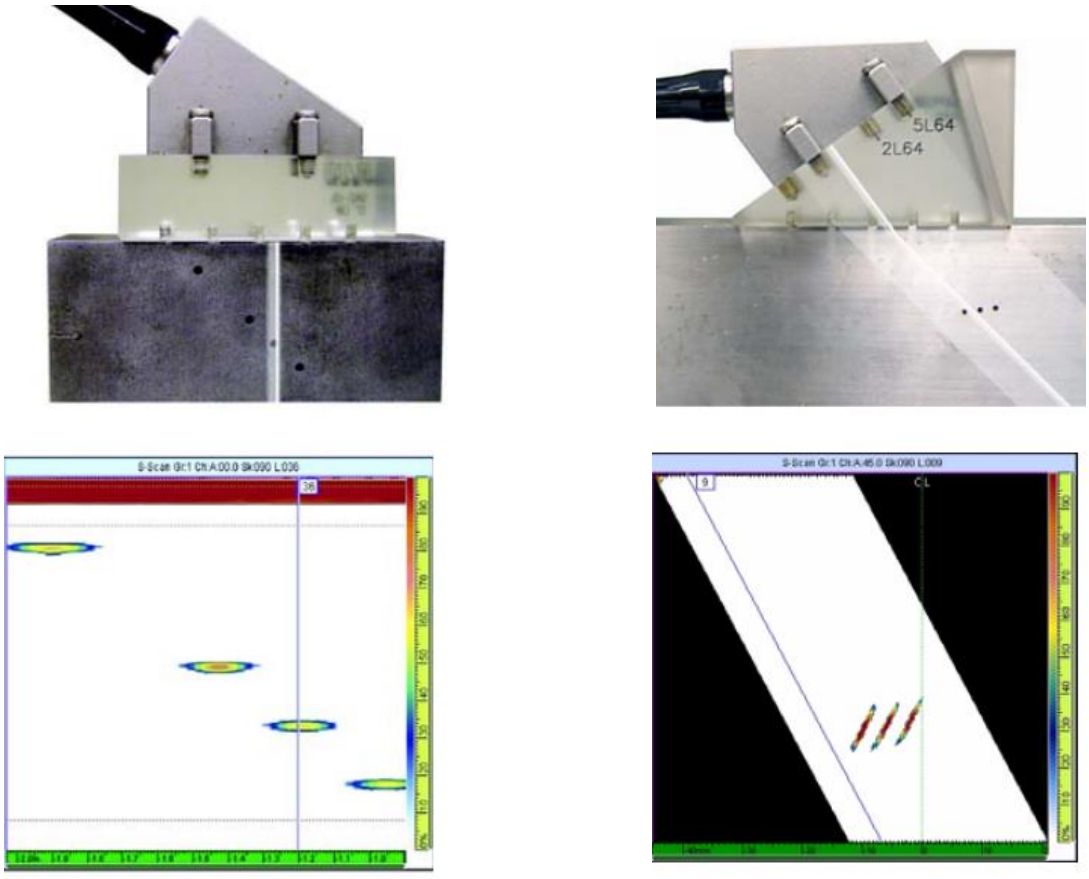

a b

Fig. 2.40. Imagines of electronic linear scanning: a – normal beam linear scanning; b - angle beam scanning [41]

There is also a possible combined beam processing because the phased array method can be used in almost any combination of testing, for example, focalization and steering or linear scanning and steering.

2.5. Summing-up

After reviewing the NDT methods and after examining the possibilities of the inspection methods for carbon fiber composites, the appropriateness of the methods to determine the defects is summarised in table 2.2.

Table 2.2. Applicability of NDT methods depending on defect

Defect	**Inspection Method**							
	Visual	**Coin tapping**	**Ultrasonic**	**Thermo-graphy**	**Acoustic emission**	**Radio-graphy**	**Shearo-graphy**	**Electro-magnetic**
Porosity	□		○					
Fibre breakage			○		○	□		○
Delamination	○	○	○	○	○	□	○	
Matrix cracks			□	□	○	□		
Fibre-matrix bond	□				□			□
Foreign inclusions			○	○		○	□	
Voids		○	○					
Wrinkles							○	□
Resin rich	○		□					
Blisters		○	○					
Impact damage	○			○			○	

Note: NDT research is a continuous process and can change the status of different inspection methods

○ the method has proven the ability to detect specified defect

□ limited application

As shown by the results of the analysis, the most appropriate NDT method for carbon fiber composite materials is ultrasonic testing.

The main advantages of the ultrasonic testing methods compared to other NDT methods would be the following:

- high sensitivity of the method to both surface and subsurface discontinuities
- equipment for the inspection can be very portable or at a high level of automatization
- depth of penetration for defects inspection or measurement is superior to other NDT methods
- only a minimal sample preparation for inspection is required
- only one-sided access is required to use pulse echo method for inspection

- method is highly accurate in determining the position of the defect and evaluating the shape and size
- method provides instantaneous results
- comprehensive imagines can be obtained using automated systems
- equipment is not a health hazard to operators or staff nearby and does not affect the substance being inspected
- in addition to defect inspection, the method has other uses, such as thickness measurement.

However, like all inspection methods, ultrasound testing also has some drawbacks:

- staff skill and training is more extensive than with some other NDT methods
- material should be accessible to transmit ultrasound waves
- a coupling medium is usually required to promote the transfer of sound energy to an inspected sample
- it is problematic to test objects that are rough, relatively very small, irregular in shape, exceptionally thin or not homogeneous
- it may be difficult to make measurements due to the undesirable internal structure of the materials, impurities and so on
- standards need to be followed for both equipment calibration and defect specification.

The main advantage of the phased arrays is the inspection speed. An analysis of the literature review suggests that it is several times faster than conventional ultrasound tests. So, that is a useful and effective way to detect defects in polymer composites.

3. Computer Simulation

The aim of this part of the project is to develop a model that can determine the most appropriate parameters (transducers' parameters, positioning) so that defects can be detected in the real specimen. The results obtained will also allow to evaluate whether the chosen research method will be suitable for real measurements. In order to select the most suitable defect detection method in carbon fiber composite material, and to select the most suitable parameters for this study, a computer model was developed in CIVA environment. With the CIVA program it is possible to perform a full simulation of the study, i.e. create a sample CAD model, select the sample material, the ultrasonic transducer, its frequency, and compare the results for determining the most appropriate parameters.

3.1. Description of the Sample Model

The real specimen is composed of carbon fiber layers. The image of a real specimen is shown in Fig. 3.1. This is a specimen of COTESA with flat bottom holes (FBH).

Fig.3.1. Image of a real specimen

The length, width and height of the test piece are 110 mm, 90 mm and 5.4 mm respectively (Fig. 3.1). The most important elements in this sample are artificial defects – boreholes. The sample has flat bottom boreholes with a diameter of 3 mm; 4 mm; 5 mm and 6 mm. The depths for each diameter hole are 0.4 mm, 2.7 mm and 5.0 mm. All artificial defects could be easily measured in their position with a caliper gauge.

The sample has a porosity volume content of less 0.5 vol. -%, according to standard EN2564 [45]. The porosity (void fraction), is a measure of voids, i.e., "empty" spaces in the material and is a fraction of the voids volume over the total volume, from 0 to 1, or as a percentage from 0 to 100%.

The real specimen shown in Fig. 3.1 is made of 10 carbon fiber reinforced polymer (CFRP) layers.

The CAD model of the sample is designed in CIVA environment as shown in Fig. 3.2. Technical parameters of the materials used for model description in the program are presented in table 3.1.

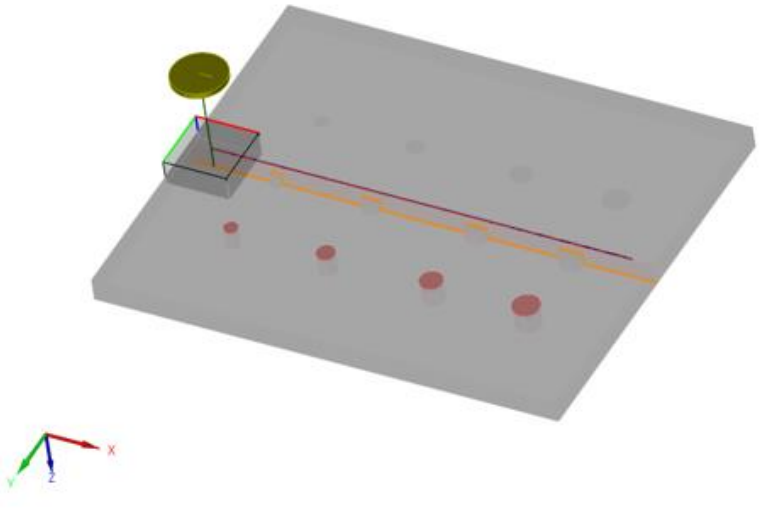

Fig.3.2. Model of the sample

Table 3.1. Basic materials' parameters

Parameter material	**Water**	**CFRP**	**Air**
Density	1000 kg/m^3	1494 kg/m^3	0,0012 kg/m^3
Velocity of longitudinal waves	1483 m/s	2400 m/s [46]	333 m/s

The object under investigation is described below. The geometry of the object and the characteristics of the material are listed. Also, the number of layers of the composite specimen, the total thickness of the composite (5.4 mm), their angle of rotation, and the type of composite part are presented. The material type chosen is multilayer homogeneous composite (figure 3.3). This characteristic is derived from the compliance of the sample with the program specification.

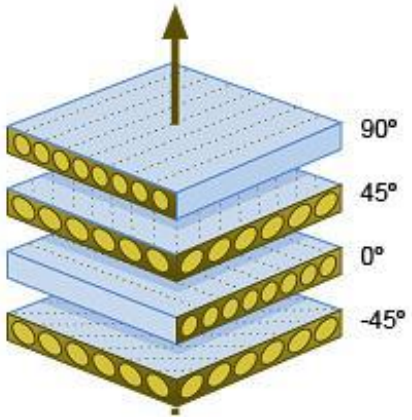

Fig. 3.3. Example of a multilayer homogeneous composite

Because tests will be performed perpendicular to the generation of ultrasonic waves, the most important parameter will be the velocity of acoustic longitudinal waves which in the case of water is 1483 m/s and in the composite is 2400 m/s.

Figure 3.4 shows a model with artificial defects and their numbers. Each defect has an assigned number that will not change throughout the study.

Fig. 3.4. Defects numbering and positioning in the sample

Defects of different sizes will give an idea of what defects can be detected during the actual experiment and which transducers and equipment will be best used. Table 3.2 gives a complete list of defects, their diameter and depth.

Table 3.2. Geometrical parameters of defects

Number of the defect	**Geometrical parameters of defects in mm**	
	Diameter	**Depth**
1	3.0	0.4
2	3.0	2.7
3	3.0	5.0
4	4.0	0.4
5	4.0	2.7
6	4.0	5.0
7	5.0	0.4
8	5.0	2.7
9	5.0	5.0
10	6.0	0.4
11	6.0	2.7

12	6.0	5.0

In modelling, all defects are circular.

3.2. Selection of Transducer and Method

The literature analysis, the evaluation of the sample and the parameters of transducers used in practice revealed that high frequency transducers are used for similar objects. This is due to the relatively small specimen thickness and the higher resolution required to detect defects, which is why 5 MHz single-element perpendicular flat transducer, which has diameter of active element of 12,7 mm is used. Transducers of this frequency are commonly used to study aviation components. After evaluating the structure of the sample it was decided to use immersion method (also known as the immersion pulse–echo method). It is probably the most popular and widely used method, which is perfect to determine depth and diameter of the defect in various forms of objects. Defects are detected by the occurring reflection of a transmitted ultrasonic pulse [47]. Water makes it possible to improve the transmission of the ultrasonic wave from the ultrasonic transducer to the test object. Details of the transducer used provided in Table 3.3 and an experimental set-up is shown in figure 3.5

Table 3.3. Parameters of transducers used in computer simulation

Parameter	**Transducer: Olympus V109 (serial No 919732)**
Frequency	5 MHz
Diameter of active element	12.7 mm
Shape of element	Round

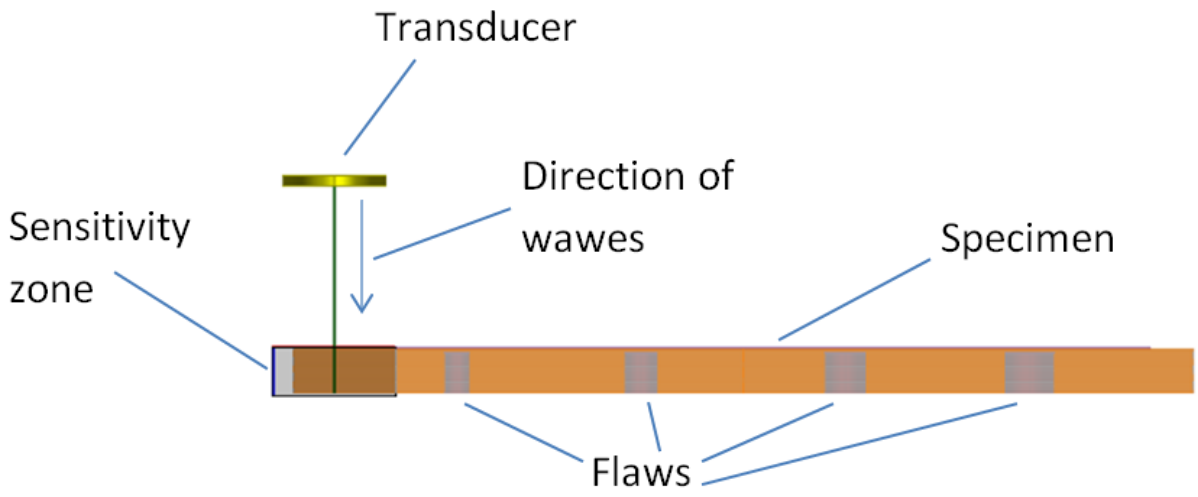

Fig.3.5. Experimental set-up

3.3. Investigation using Single-Element Transducer

Single-element ultrasonic transducer consists of an active element (piezoelectric or single crystal material) housed in a casing. A single active element transmits and receives sound energy. Single-element ultrasonic transducers are used for flaw detection, material research, detecting and sizing delaminations, inspecting plates, bars, billets, and other metallic and nonmetallic components.

3.3.1. Investigation of Fields of Ultrasonic Transducer

A very important parameter of an ultrasonic transducer is its emitted acoustic field. The positioning of the transducer is selected taking into account its nature, the circumstances of the study and the research materials. In this case, a flat ultrasonic transducer is used. It generates longitudinal waves emitted perpendicularly to the test material. During the test, it will be positioned at a certain distance from the test object. The transducer generates an ultrasonic wave not from one point but from a number of adjacent points on the transducer surface. Generated waves in space interact with each other. Two main fields can be distinguished in the acoustic field of the ultrasonic transducer: near field and far field [48]. At a given point in space, called a far field, the amplitude of the acoustic pressure will reach its maximum and will be equal to the sum of all the individual wave amplitudes. The near field is the space near the transducer surface. In the near field, ultrasound wave irregularities and oscillations are quite strong. This field is located between the transducer surface and the field amplitude and the location of the last and maximum peaks.

The length *N* of the near field depends on diameter *D* of the transducer and on ultrasonic wavelength λ in the test environment. Formula 3.1 is used to calculate the near field [48,49]

$$N = \frac{D^2}{4\lambda} = \frac{D^2 f}{4V} \qquad 3.1$$

where: *D* is the diameter of the transducer; λ - ultrasonic wavelength in the test environment; *f* - wave frequency; *V* – velocity of sound in the material.

Knowing the transducer and ultrasonic parameters (*D* = 12.7 mm, *f* = 5 MHz, *V* = 1483 m/s) in the material theoretically calculates the near field.

$$N = \frac{D^2}{4\lambda} = \frac{D^2 f}{4V} = 0.1359\ m = 135.9\ mm$$

Finding defects in the near field and accurately estimating their size is extremely difficult due to ultrasonic pressure fluctuations. Therefore, defect detection should be carried out in the far field. The field is called the far field if it is at a distance *N* from the transducer. In the far field, the field pressure generated by the transducer decreases with increasing distance and the strongest signal is received in the acoustic axis (Fig. 3.7).

In the far field, the ultrasound wave is reflected at an angle β.

$$\beta = \arcsin\left(k\frac{\lambda}{D}\right) \qquad 3.2$$

where: k - constant depending on the edge of the beam indicating the limit of the beam beyond which the acoustic pressure does not exceed a certain level (dotted line in figure 3.6), the shape of the transducer, and method used to determine the angle of expansion of the beam.

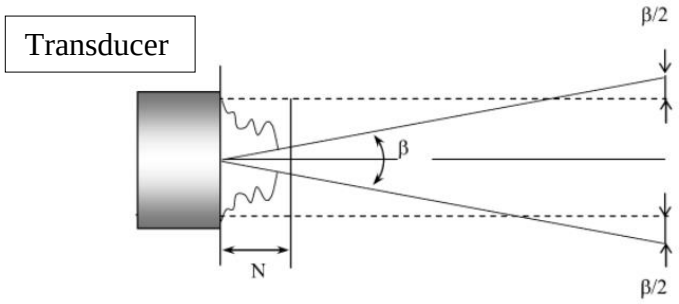

Fig. 3.6. Eradiation of the wave

As can be seen from the formula 3.1, increasing the diameter of the transducer increases the length of the near field without changing the frequency of the transducer. Thus, a small diameter transducer has a shorter near field than a large diameter transducer. In the far field, the beam of the small-diameter transducer extends more than that of the large-diameter transducer. In addition, the near field increases with increasing frequency of the transducer when the transducer has the same diameter.

In computer simulation and changing the transducer distance parameters, a close field is obtained in the CIVA environment. slightly different from theoretical calculations. The simulation uses the near field size obtained by the CIVA program. From the figure 3.7a it can be seen that the amplitude curve to a distance of 138.67 mm is practically without any significant fluctuation. As mentioned above, defects in the near field can be inaccurately sized or located. Therefore, far-field study is necessary. Curve 2 (in CFRP) gradually decreases with increasing distance and behaves predictably.

The curve decreases as the amplitude of the ultrasound signal decreases as the propagation distance of the waves increases.

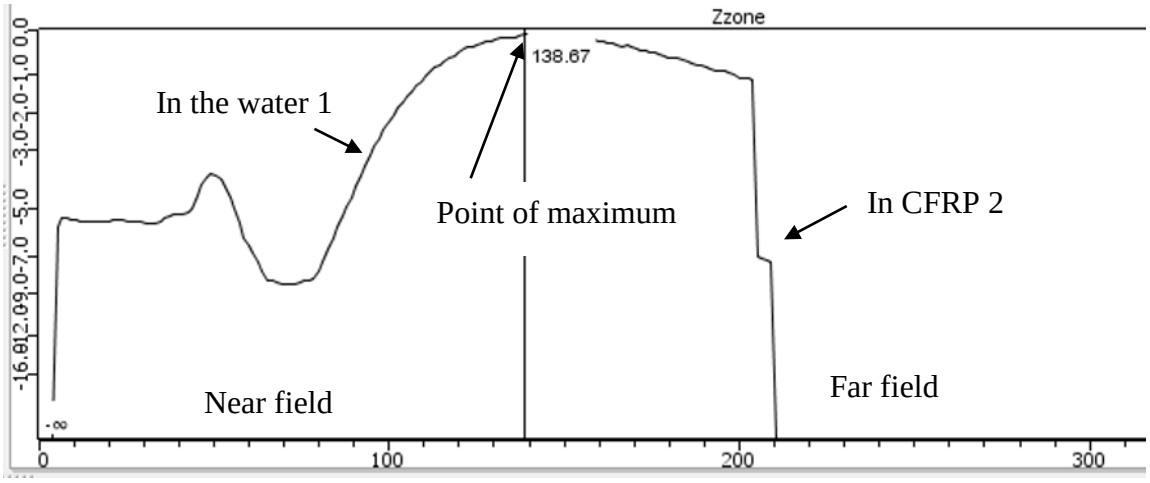

a

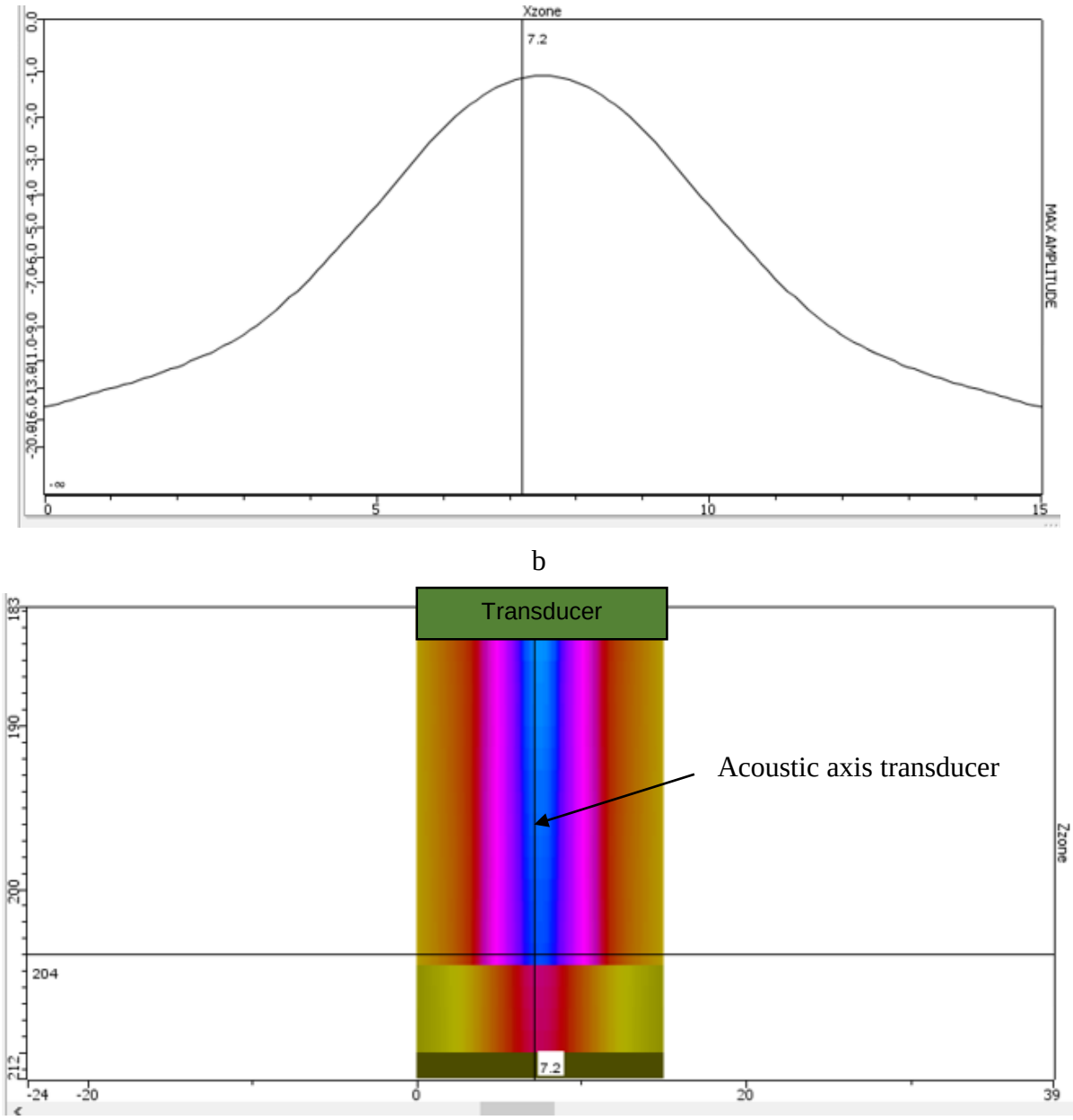

Fig. 3.7. Received near field in CIVA environment: a - near and far fields, b - maximum of acoustic pressure amplitude, c - transducer and its emitted fields, near field – red colour, far field – yellow colour

In this case, a simulation of the reflection immersion method with a non-focused transducer is performed. Therefore, the sample is allegedly immersed in water and the waves emitted by the transducer propagate through the water and then enter the test object. The calculated near field distance *N* from formula 3.1 means that the transducer must be 135.9 ~ 138.0 mm away from the specimen in order to correctly detect the defects and their size.

3.3.2. Simulation Results

Having a sample model and knowing the distance to place the transducer, calculations and simulation results are obtained in a CIVA environment. As mentioned in section 3.3.1, the distance between the transducer and the specimen is 138 mm. Scans are performed through artificial defects (boreholes of different diameter and depth). For this reason, the "Sensitivity zone" parameter is used, which allows to set only a specific zone where the calculation will take place. Using the sensitivity zone (15x15x6

mm) reduces the computation time. In this case, the sensitivity zone parameters are given below (Fig. 3.8).

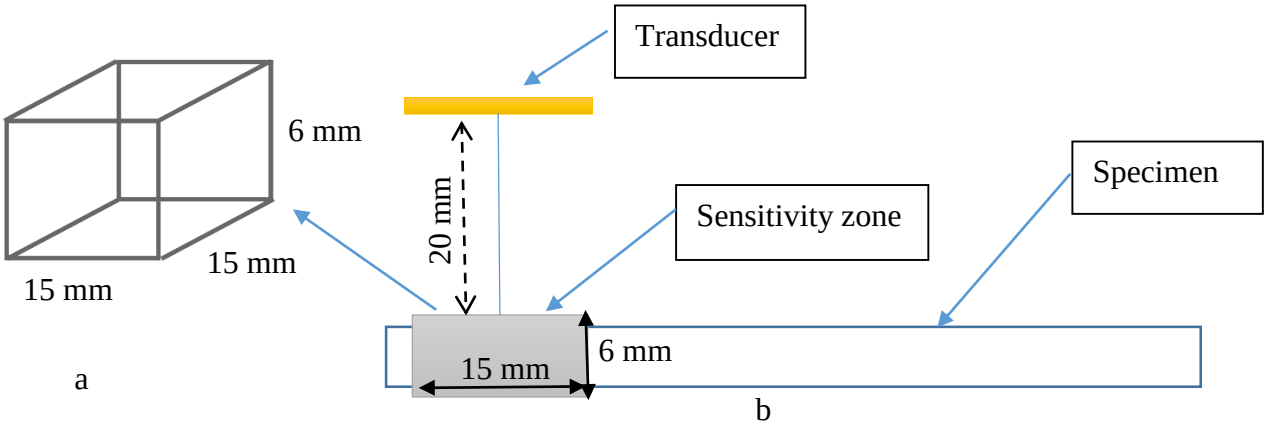

Fig. 3.8. Sensitivity zone: a – size of sensitivity area, b – schematic of scan with 5 MHz transducer

Scanning step was 0.5 mm. 150 steps in y- axis direction and 200 steps in x-axis direction were performed during scanning. Scanning steps scheme along x and y axies is presented in figure 3.9.

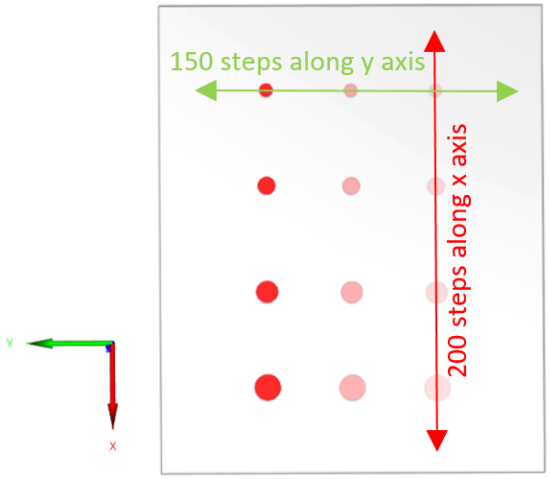

Fig.3.9. Scanning scheme

Scanning prodecure along the test sample for inspecting defects along y axis is shown in figure 3.10. As we can observe, the single-element transducer is moved towards the defects to obtain indications of the defects.

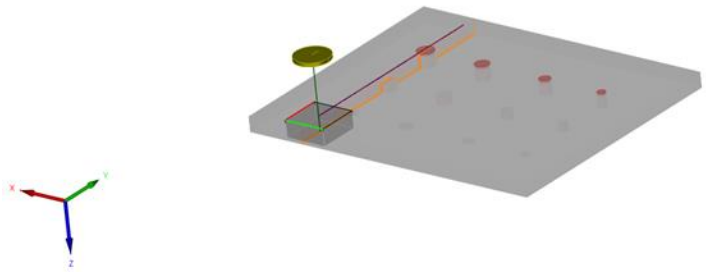

Fig. 3.10. 3D image view of the test sample and single-element transducer using in the scanning procedure along y axis

Simulation results in type A and B scan views of ultrasound scans are presented in table 3.4.

Table 3.4. Images of field views and amplitude vs. time graphs

Image of field view (B scan view)	**Amplitude vs. time graph (A scan view)**
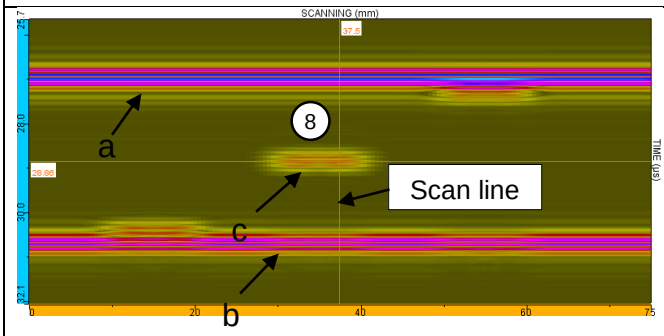 a	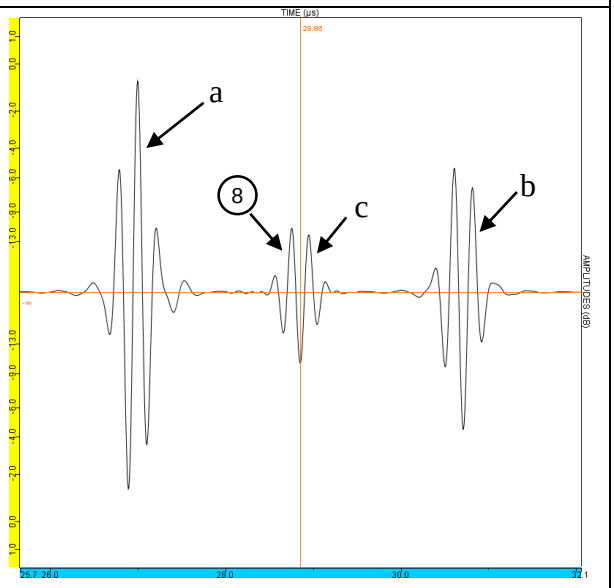 b

Fig.3.11. Scanning of defect no 8 (a – B-scan of Ø5 mm FBH (flat bottom holes), b- A-scan of Ø5 mm FBH) at depth of 2.7 mm

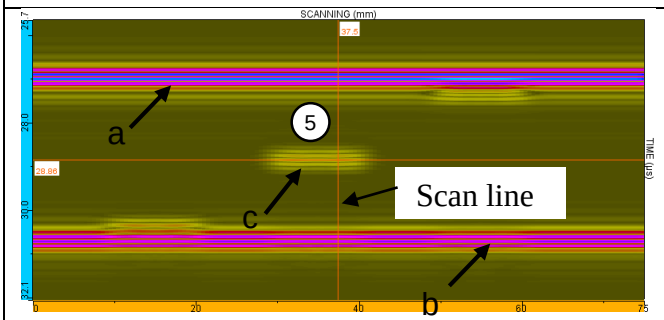

a

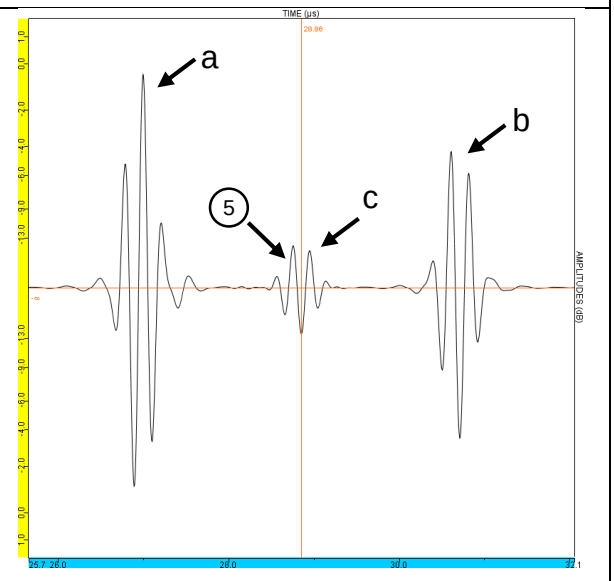

b

Fig. 3.12. Scanning of defect no 5 (a – B-scan of Ø4 mm FBH, b- A-scan of Ø4 mm FBH) at depth of 2.7 mm

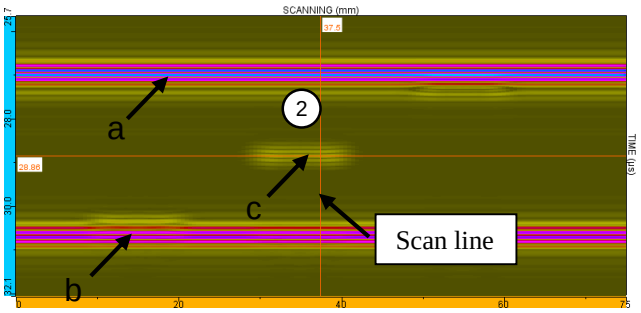

a

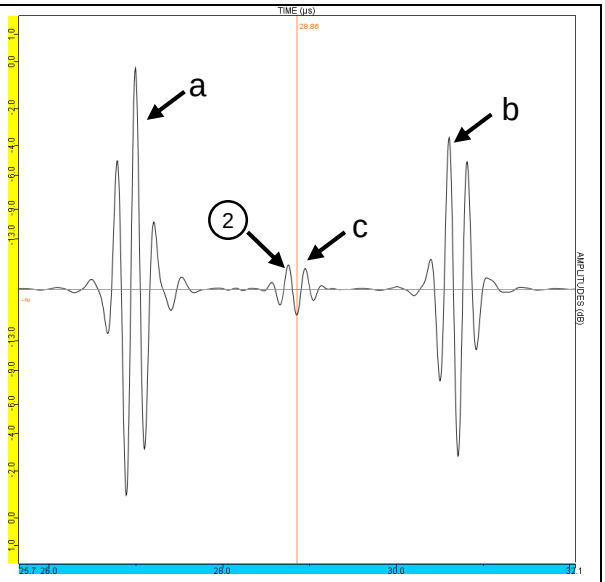

b

Fig. 3.13. Scanning of defect no 5 (a – B-scan of Ø3 mm FBH, b- A-scan of Ø3 mm FBH) at depth of 2.7 mm

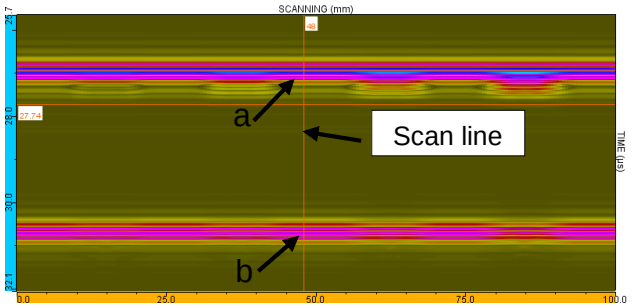

a

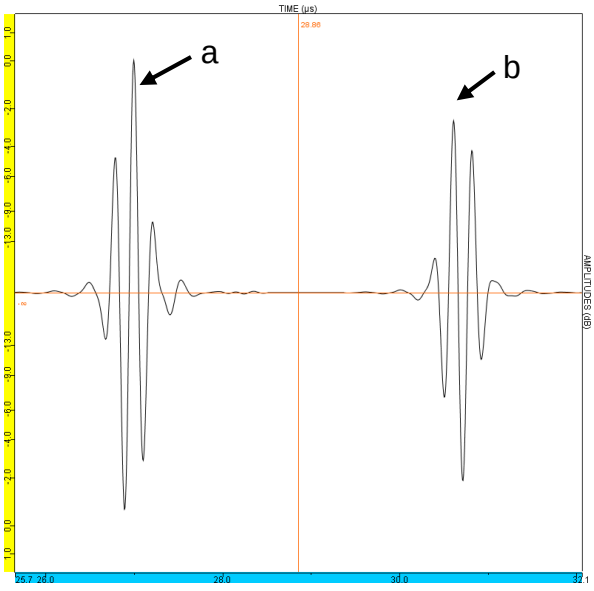

b

Fig. 3.14. Scan line and amplitudes in the absence of defects (scan line does not cross the defect)

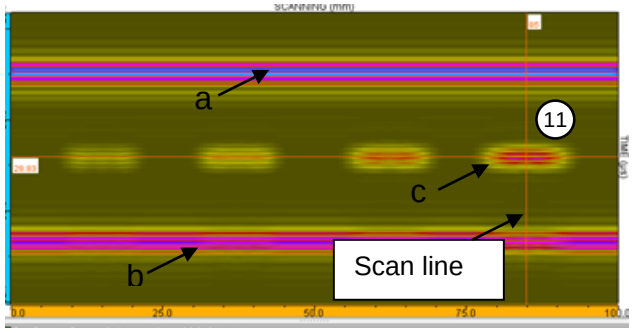

a

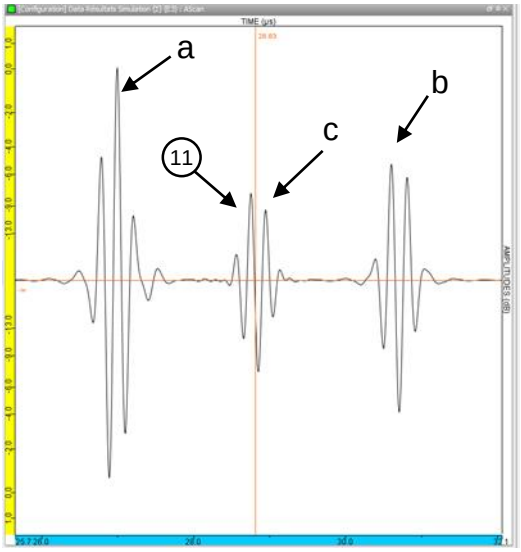

b

Fig. 3.15. Scanning of defect no 11 (a – B-scan of Ø6 mm FBH, b- A-scan of Ø6 mm FBH) at depth of 2.7 mm

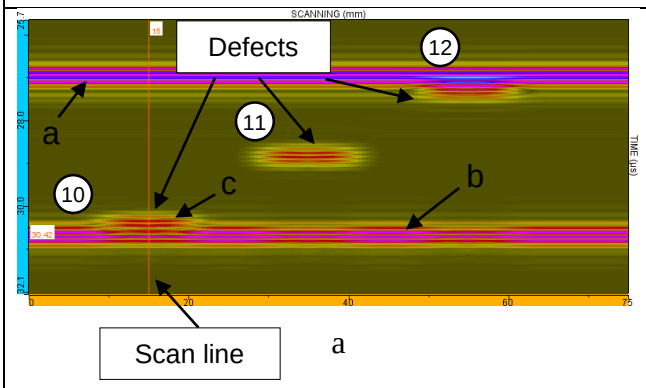

a

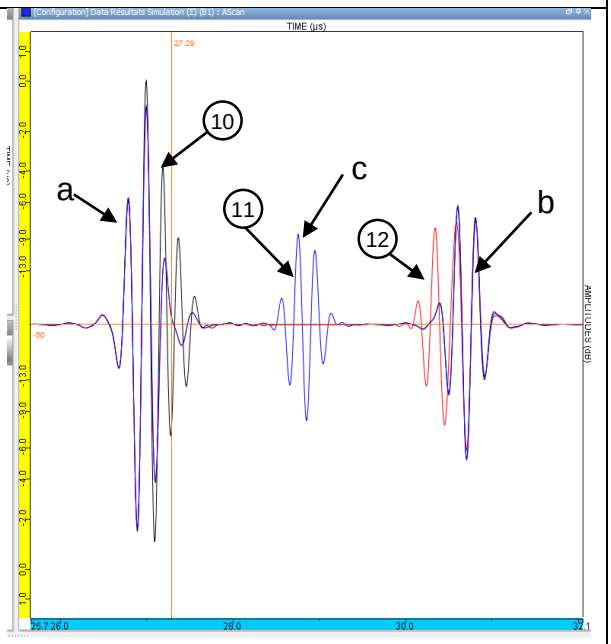

b

Fig.3.16. Scanning of defect no 10,11,12 (a – B-scan of Ø6 mm FBH, b- A-scan of Ø6 mm FBH) at 0.4; 2.7 and 5.0 mm depths

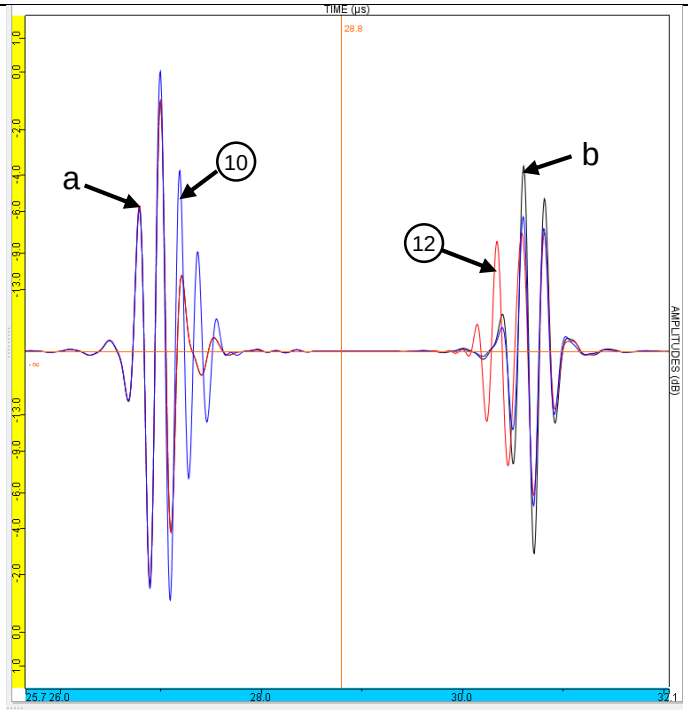

Fig. 3.17. Comparison of amplitudes: black curve – without defects, red – with the defect of 0.4 mm depth, and blue – with the defect of 5.0 mm depth (diameter of the boreholes – 6 mm)

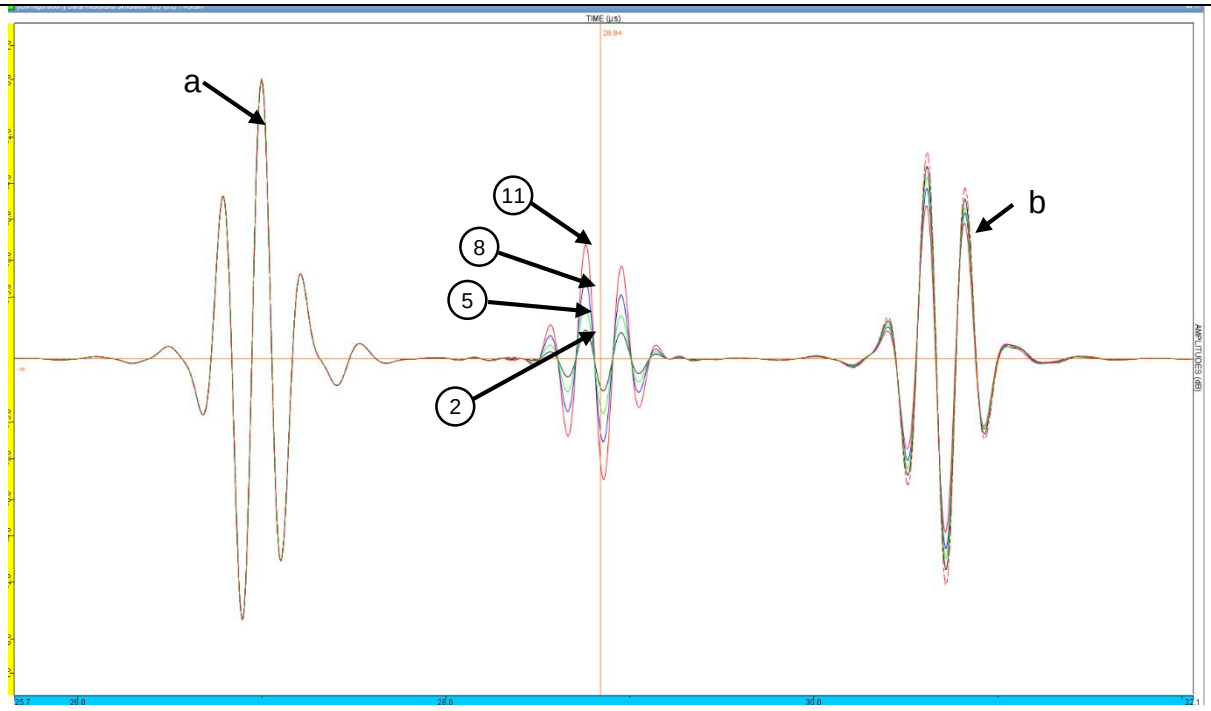

Fig. 3.18. Comparison of amplitudes obtained from the defects with different diameters and the same depth: red curve – 6 mm diameter, blue – 5 mm, green – 4 mm, black – 3 mm

The dependence of the amplitude, measured in logarithmic units called decibels, on the diameter of the defect is given in Fig. 3.19. This graph shows the measurement results of defects no. 2, 5, 8 and 11 with different diameters but the same depth (2.7 mm).

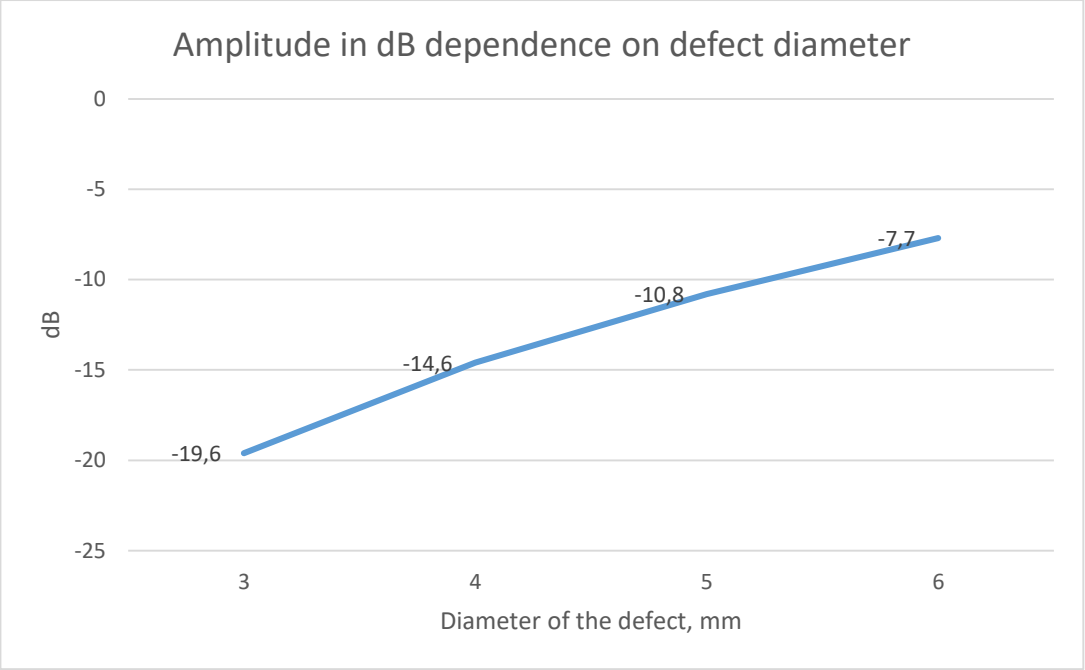

Fig. 3.19. Comparison of amplitudes in dB obtained from the defects with different diameters

The Fig. 3.19 shows that the smaller the defect size, the smaller the signal amplitude, measured in decibels.

From the information in table 3.4 it could be seen that the detected defects are only in the scanning plane. The simulator uses a perpendicular transducer so the waves propagate perpendicular to the transducer along the specimen. The left column of the table represents image of field views (B scan views). The right column of the table represents amplitude vs. time graphs (A scan views). In all figures in the table 3.4 the scan lines are shown (in red) and the numbering means: a – reflection from the surface; b – reflection from the bottom; c – reflection from defect. In addition, the defect numbering in the sample is from 1 to 12 (number of defect is shown in a circle).

Fig. 3.15 presents the scanning results of the defect no 11, but scanning image also allows us to see the defects no 8, 5 and 2, which are with the same depth (2.7 mm), but with different diameters (Ø6, Ø5, Ø4 and Ø3 mm respectively). To determine the amplitude dependence of the defect depth, three defects (no. 10, 11, and 12) with different depths but the same diameter are compared after scanning (Fig. 3.16). The defect no 10 has 0.4 mm of depth, while the defect no 11 has 2.7 mm of depth, and defect no 12 has 5 mm of depth. In the right column (Fig. 3.16, b), red colour curve shows the defect no 12, blue – the defect no 11, and black – the defect no 10. The graph clearly shows the differences in these amplitudes.

The amplitudes of scanned boreholes with different diameters and the same depth (2.7 mm) are shown in figures 3.11, b – 3.13, b. The apparent difference in amplitudes shows the differences in the diameter of the boreholes at the same depth of the defects.

Figure 3.14 a shows the scan line and figure 3.14, b amplitudes in the absence of defects in the material (scan line does not cross the defect). In this case only reflections from the surface and from the bottom are visible.

Figure 3.17 shows the comparison of amplitudes without defects - black curve, with the defect of 0.4 mm depth – red, and with the defect of 5.0 mm depth – blue (diameter of the boreholes – 6 mm).

Figure 3.18 represents comparison of amplitudes obtained from the defects with different diameters and the same depth: red curve – 6 mm diameter, blue – 5 mm, green – 4 mm, black – 3 mm. It is obvious that the height of the amplitude depends on the diameter of the borehole at the same depth of the boreholes.

Obviously, using a single transducer is not easy to detect all defects. Occasionally, defects of a similar size located in the same plane are "invisible." Also, a mechanical scan is required to examine the entire specimen, i.e. moving the transducer along and across the specimen, which is not convenient.

3.3.3. Estimation of Defects Depth using Single Element Transducer

As was mentioned before, pulse-echo method is widely used to determine the depth and transverse dimensions of the defects. The thickness of the sample or the depth of the defect is calculated by measuring the propagation time of the wave according to the formula [49]:

$$H = \frac{V \cdot t}{2} \qquad 3.3$$

where: *H* is the depth of the defect; *V* – velocity of ultrasound in the material*; t* – time of propagation of the signal to the defect of the sample.

As example are given depth calculation of the defects no.8 and no.12.

Defect no.8. V = 1483 m/s; $t = 1.85 \cdot 2 = 3.7$ μs (28.86 – 27.01 = 1.85 μs) data from figure 3.20. When measuring by the pulse-echo method, the wawe propagation is a distance equal twice the thickness of the test object [49].

$$H = \frac{V \cdot t}{2} = \frac{1483 \cdot 0.0000037}{2} = 0.00274\ m = 2.74\ mm$$

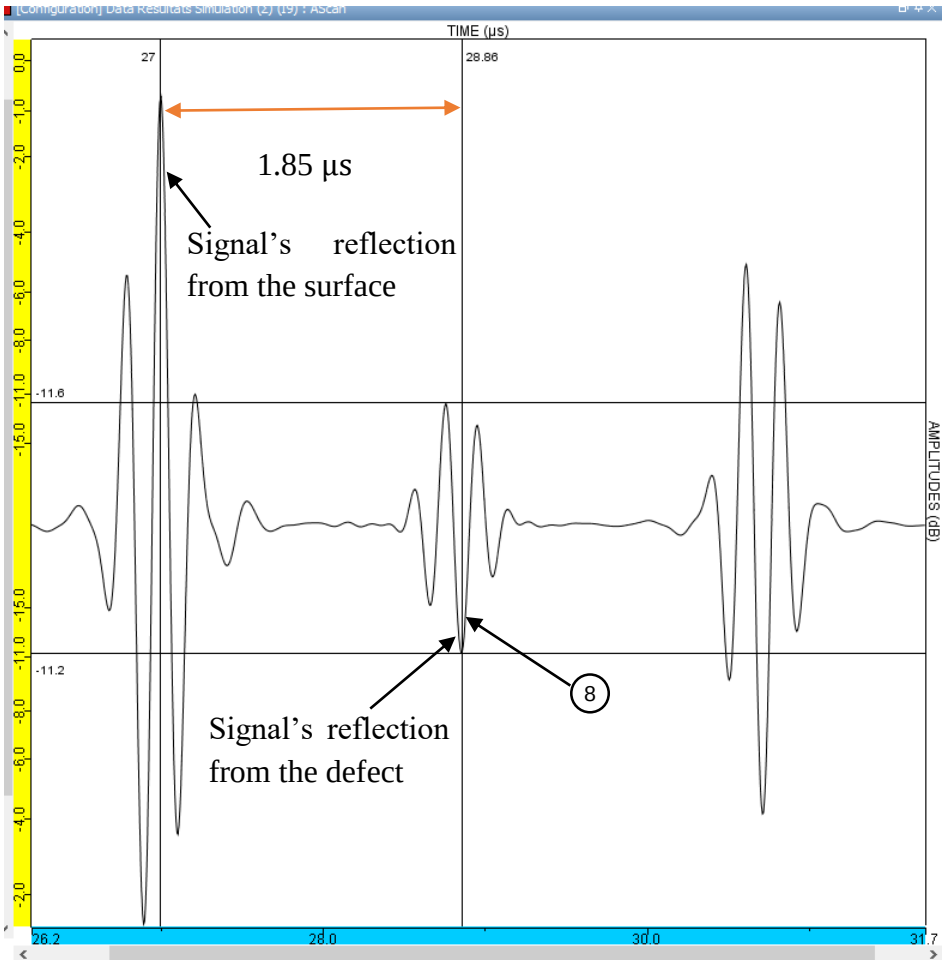

Fig. 3.20. Signals in the time domain: signal's reflection from the surface, signal's reflection from the defect no.8 and signal's reflection from the bottom

The measured depth of the defect no. 8 is 2.7 mm.

Defect no.12. V = 1483 m/s; t = 0.19 · 2 = 0.38 µs (27.19 – 27.00 = 0.19 µs), data from figure 3.21.

$$H = \frac{V \cdot t}{2} = \frac{1483 \cdot 0.00000038}{2} = 0.00028\, m = 0.28\, mm$$

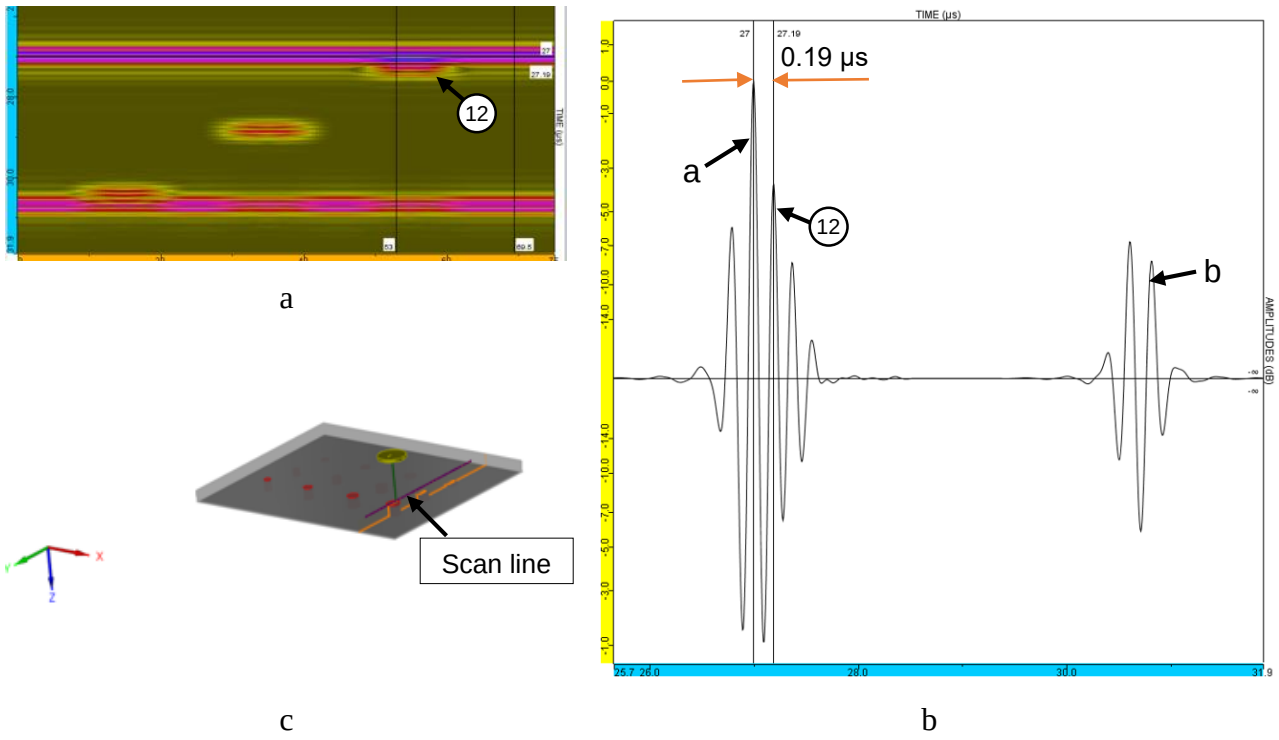

a

c

b

Fig. 3.21. Scanning of the defect no. 12: a - B scan view, b - amplitude vs. time graph (A scan view), c - image of scan line along y axis

The real depth of the defect no. 12 is 5.0 mm. The distance measured from the sample surface to the defect with ultrasound is 0.28 mm. Knowing that the specimen thickness is 5.4 mm, the result of ultrasound measurements to determine the defect depth is 5.12 mm (5.4 – 0.28 = 5.12 mm).

Depths of other defects are calculated analogously. The results are presented in table 3.5.

Table 3.5. Estimated and real depths of the defects in the specimen

Number of defect	Theoretical velocity of ultrasound, m/s	Time interval between adjacent reflections, µs	Estimated depth of the defect, mm	Real depth of the defect, mm	Absolute error, mm
1	1483	0.60	0.45	0.40	0.05
2	1483	3.72	2.76	2.70	0.06
3	1483	0.40	5.10	5.00	0.1
4	1483	0.59	0.44	0.40	0.04
5	1483	3.72	2.76	2.70	0.06
6	1483	0.40	5.10	5.00	0.1
7	1483	0.64	0.48	0.40	0.08
8	1483	3.70	2.74	2.70	0.04
9	1483	0.38	5.12	5.00	0.12
10	1483	0.63	0.47	0.40	0.07
11	1483	3.72	2.75	2.70	0.05
12	1483	0.38	5.12	5.00	0.12

The curves in Figure 3.22. show the dependence of the absolute error variation on the defect depth at various defect diameter. The yellow curve shows the change in absolute error at a defect depth of 0.4 mm at different defect diameters, green at a defect depth of 5.0 mm and blue at a defect depth of 2.7 mm. This data is obtained using single transducer for testing.

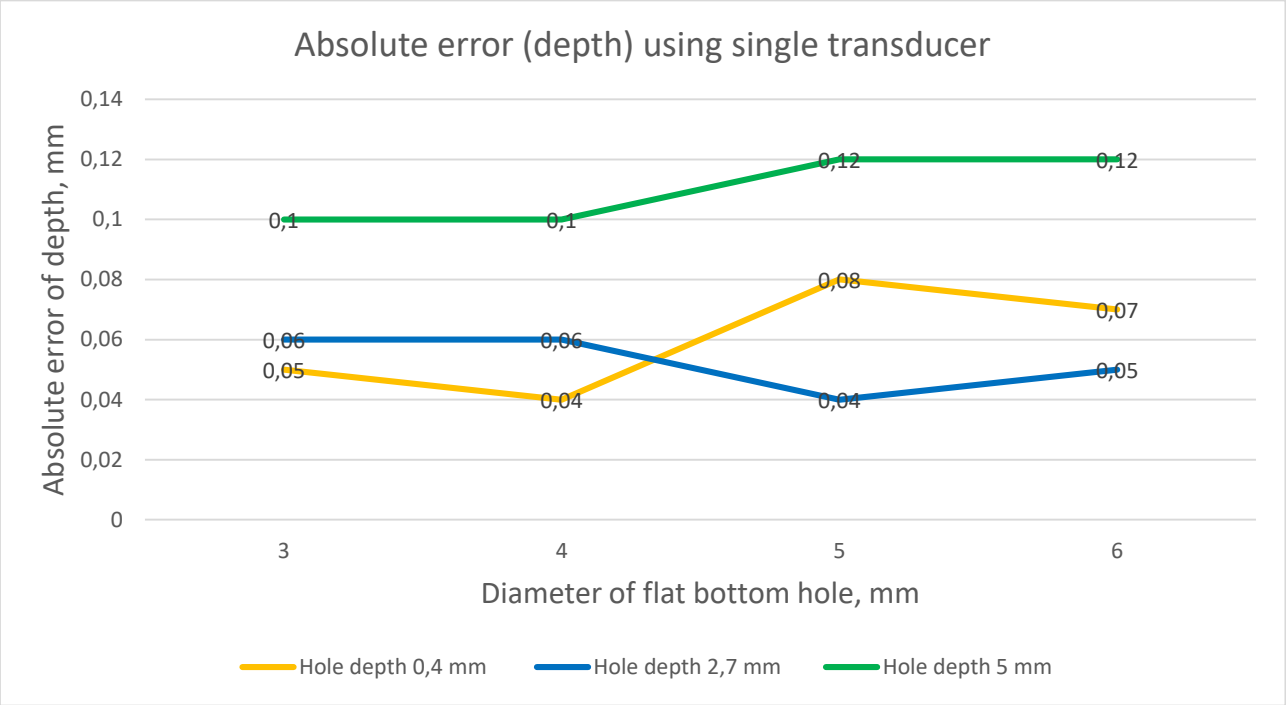

Fig. 3.22. Curves of the absolute error of depth using single-element transducer

As we can see from the graphs, the differences of absolute error are very negligible. However, it can be stated that when measuring the defects close to the surface of the sample, i.e. at a depth of 5.0 mm, when the diameters of the defects are larger (Ø5 mm and Ø6 mm), a slight difference in the magnitude of the absolute error is observed. For other defect diameters, no change in absolute error magnitude was observed at 5.0 mm depth. The same can be said for defects with the depths of 0.4 and 2.7 mm.

3.3.4. Estimation of Defects Diameter using Single Element Transducer

The CIVA modeling software is convenient to use not only for modeling defect depth determination, but for modeling defect size estimation as well. Simulation can be performed with both single-element transducer and phased array. As an automatic tool of CIVA platform the segmentation algorithm was used for modeling. The purpose of the segmentation algorithm is to group signals received from the same defect or part thereof. This grouping is based on an algorithm that provides more efficient coupling than geometric, which is based only on geometrical closeness. The grouping is based on a physical behavior of the ultrasonic wave and reduces the grouping of false signals, for example, noise. Segmentation is the process of using simulated or experimental data to calculate segments that reflect different echoes [50]. Segmentation algorithm assumes that the locally wavefront is planar. The parameters used to identify segments can also be determined using a physical method that increases the reliability level of the grouping based on the band-width, frequency and other technical parameters of the transducer. The band-width defines the frequency spectrum of pulses or receivers that can

absorb them. The band-width is usually expressed at the level of 6 db from the maximum amplitude [49]. The selection of a particular band-width is important to achieve the desired research results. The band-width is determined by many factors, such as the test material, the contact fluid, the pulse emitted by the transmitter, the receiving transducer, and so on. 6db drop technique is a reliable method for determining the width of defects and is widely used for this purpose [51].

After selecting the region of interest (ROI) in the B-scan image, as presented in figure 3.23, the results of ΔX show the size of the defect in mm in the indication table in the CIVA environment.

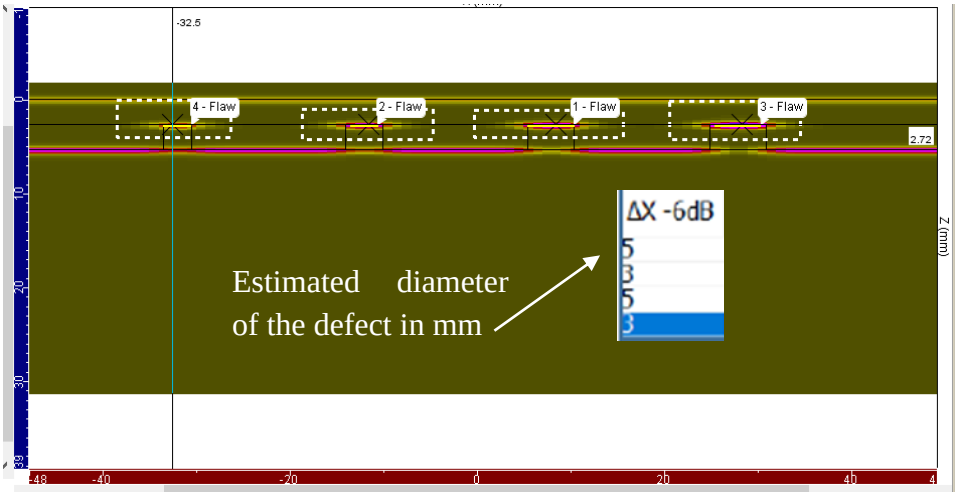

Fig. 3.23. Display of the groups after segmentation using CIVA software for the modeling

Results of the estimated defect diameter using single-element transducer are presented in the table 3.6.

Table 3.6. Estimated and real diameters of the defects in the specimen using single-element transducer

Number of defect	**Depth of the defect, mm**	**Estimated diameter (ΔX) of the defect, mm**	**Real diameter of the defect, mm**	**Absolute error, mm**
1	0.4	6	3	3
2	2.7	9.5	3	6.5
3	5.0	6.5	3	3.5
4	0.4	8.5	4	4.5
5	2.7	11	4	7
6	5.0	8.5	4	4.5
7	0.4	9.5	5	4.5
8	2.7	11	5	6
9	5.0	10.5	5	5.5
10	0.4	9	6	3
11	2.7	10	6	4
12	5.0	11	6	5

The calculated absolute error results for determining the size of the defect using single-element transducer are shown in Fig. 3.24.

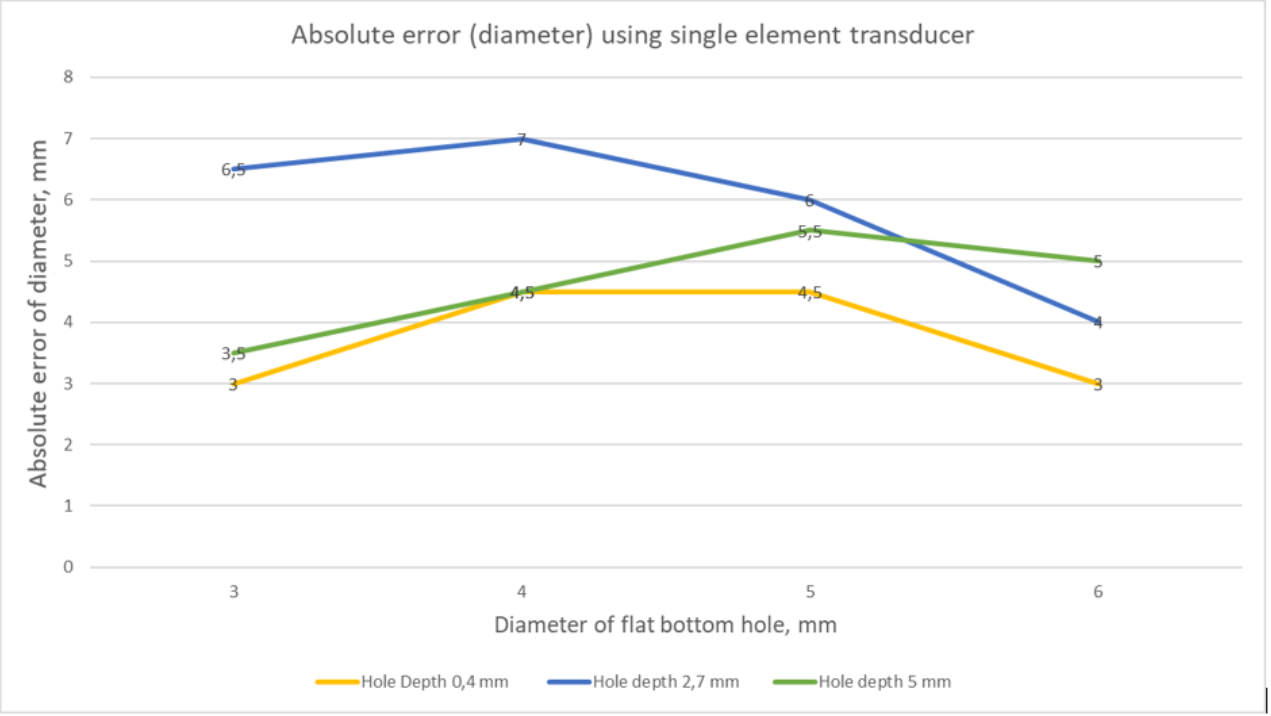

Fig. 3.24. Curves of the absolute error of diameter using single- element transducer

Analysis of the obtained graphs showed that defects with a larger lateral size are detected with a slightly higher accuracy (abosolute error did not exceed 5 mm). In addition, when measuring a large diameter, less dispersion of the measurement results is observed (did not exceed 1 mm). It can also be said that the lateral size of the defects was measured slightly more accurately when the defects are closer to the upper surface of the sample.

3.4. Investigation using Ultrasonic Phased Arrays

After making measurements with a single transducer, it was decided to use ultrasonic phased arrays. Focused ultrasonic phased arrays provide a very convenient and fast ultrasound inspection. Arrays consist of many small transducers. An array can consist of a different number of elements. The measurement principle can be used to flat parts using a linear phased array probe or to rods or tubes using a circular phased array probe. Linear arrays are the most commonly used probes in industry. One of the most important features defining phased array probes is the active probe aperture. Piezoelectric elements can be excited either together or in a sequence [48]. In this case, an Olympus linear array probe 5L 128-128x7-NW3-P-2.5-OM will be used.

If the array covers the entire required surface of the specimen, then we can see all defects in the array area on the scanning equipment screen.

In this study, ultrasonic phased arrays probe type contact with wedge, with the frequency of 5 MHz. Technical characteristics of the 5 MHz arrays are presented in table 3.7.

Table 3.7. Technical characteristics of the 5 MHz ultrasonic phased arrays

Parameter	**Transducer**

Type	Linear
Frequency, MHz	5
Number of elements	128
Pitch, mm	1.0
Active aperture, mm	128
Passive aperture, mm	21
Elevation, mm	7
External dimensions, mm	L= 130, W=21, H=35
Gap between elements, mm	0.1
Element width, mm	0.9

The main parameters of linear array presented in table 3.7 are shown in figure 3.25.

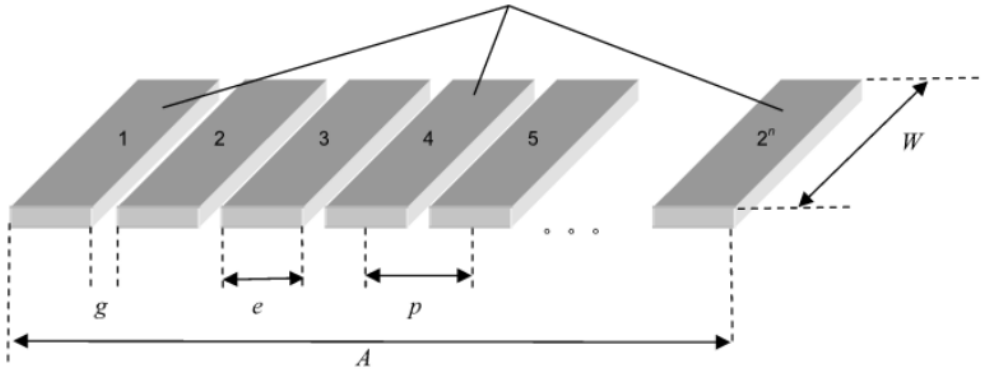

Fig. 3.25. Parameters of linear array: A – active aperture, W – passive aperture, e – width of element, g- interval between elements, p - distance between centres of two adjacent elements [49]

3.4.1. Simulation Results

Scanning prodecure of the sample using linear array for inspecting defects is shown in figure 3.26. As we can see, the phased array completely covers all defects in one axis, so when scanning it is shifted by only one selected coordinate axis to obtain indications of the defects.

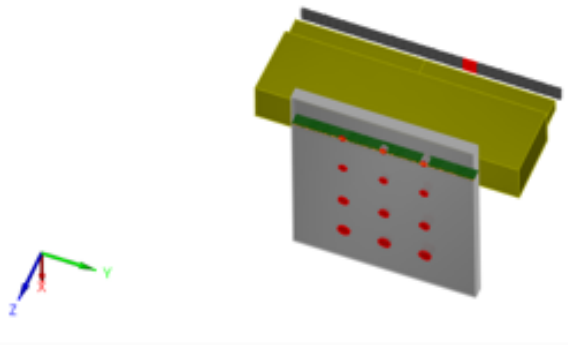

Fig. 3.26. 3D image view of the test sample and linear array using in the scanning procedure along y axis

As in the section 3.3.2, simulation results in type A and B scan views of ultrasound scans using phased linear array are presented in table 3.8.

Table 3.8. Images of field views and amplitude vs. time graphs

Image of field view (B scan view)	**Amplitude vs. time graph (A scan view)**
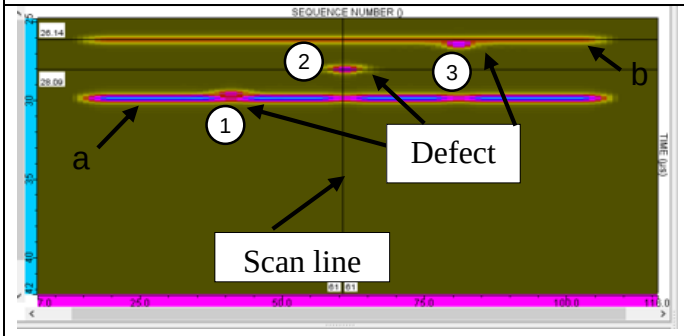 a	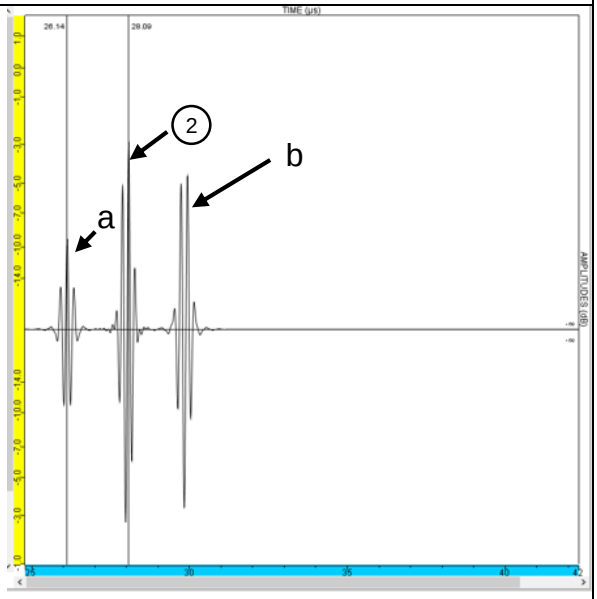 b

Fig. 3.27. Scanning of defect no. 2 (a – B-scan of Ø3 mm FBH, b- A-scan of Ø3 mm FBH) at depth of 2.7 mm

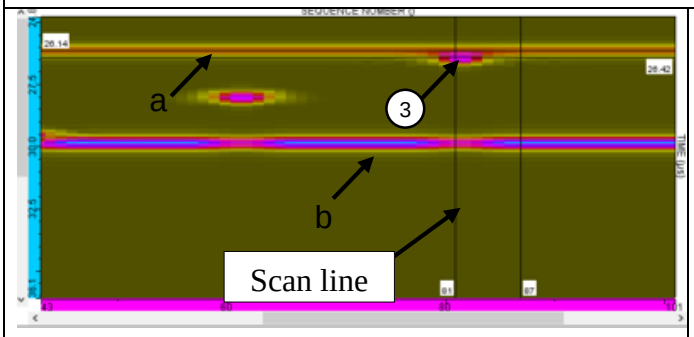 a	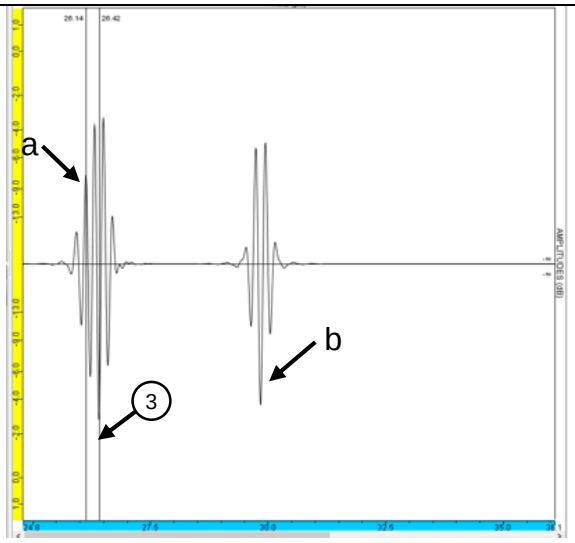 b

Fig. 3.28. Scanning of defect no. 3 (a – B-scan of Ø3 mm FBH, b- A-scan of Ø3 mm FBH) at depth of 5.0 mm

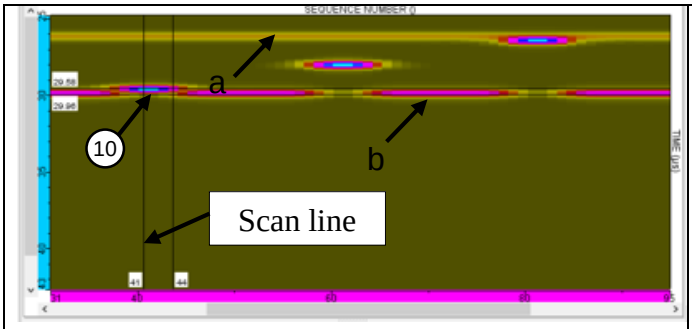

a

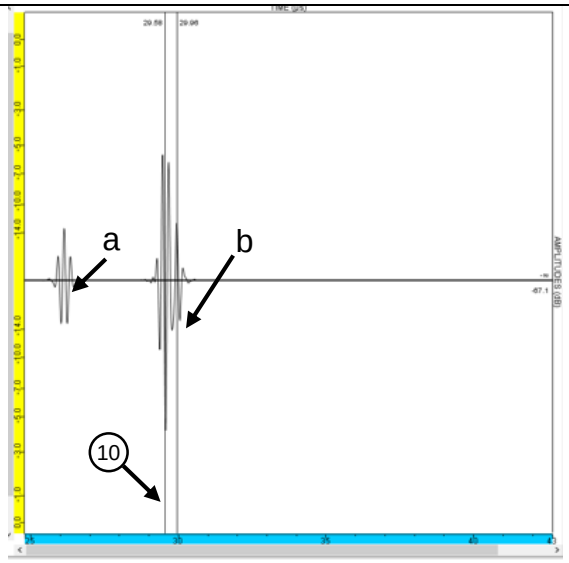

b

Fig. 3.29. Scanning of defect no. 10 (a – B-scan of Ø6 mm FBH, b- A-scan of Ø6 mm FBH) at depth of 0.4 mm

The left column of the table 3.8 represents image of field views (B scan views). The right column - amplitude vs. time graphs (A scan views). In all figures in the table 3.8 the scan lines are shown (in black) and the numbering means: a – reflection from the surface; b – reflection from the bottom. The numbers of defects are shown in the circles. The table 3.8 shows the scan results for three defects of different depths: 0.4 mm, 2.7 mm and 5.0 mm.

3.4.2. Estimation of Defects Depth using Phased Array

As in section 3.3.3, the signal dependence on the depth of the defect is analysed. Defects no 10, 11 and 12, which are at the same diameter but differ in depth, are investigated. The depth of the defects is calculated according to formula 3.3. Time of signals reflection from the surface of the specimen and from the defect are taken from A scan views (figures 3.30 - 3.32).

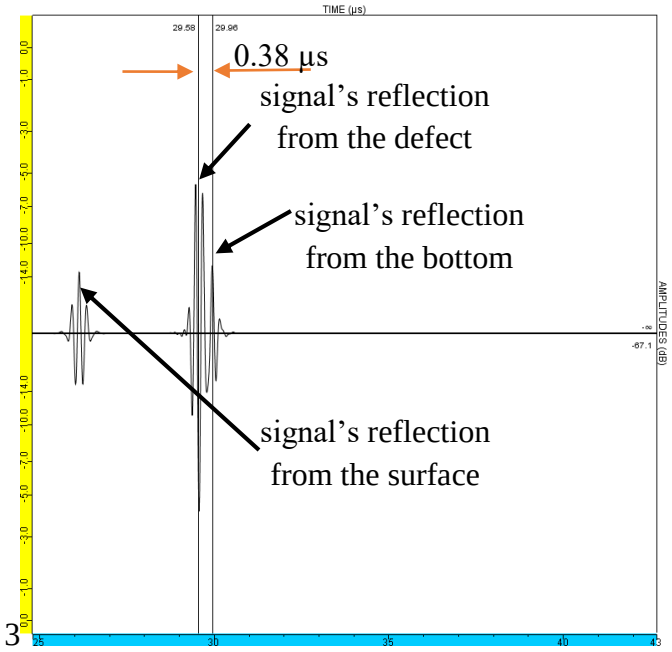

Fig. 3.30. Amplitude vs time graph (defect no 10, depth of the defect 0.4 mm)

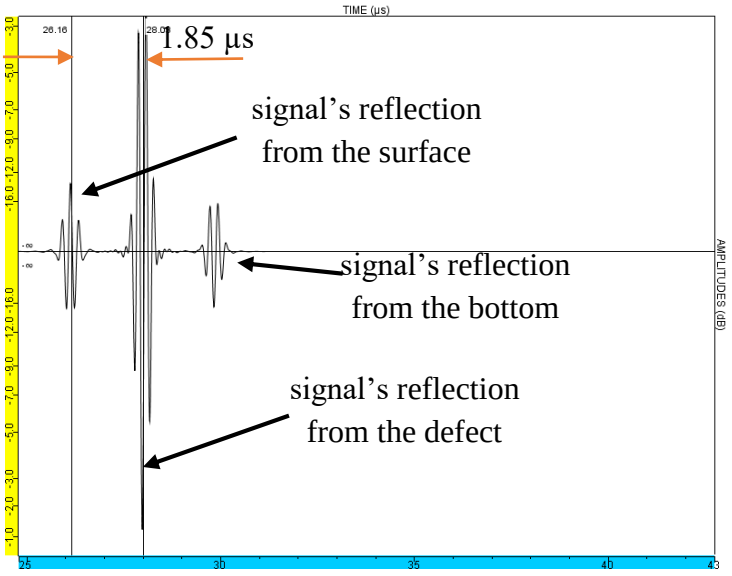

Fig. 3.31. Amplitude vs time graph (defect no 11, depth of the defect 2.7 mm)

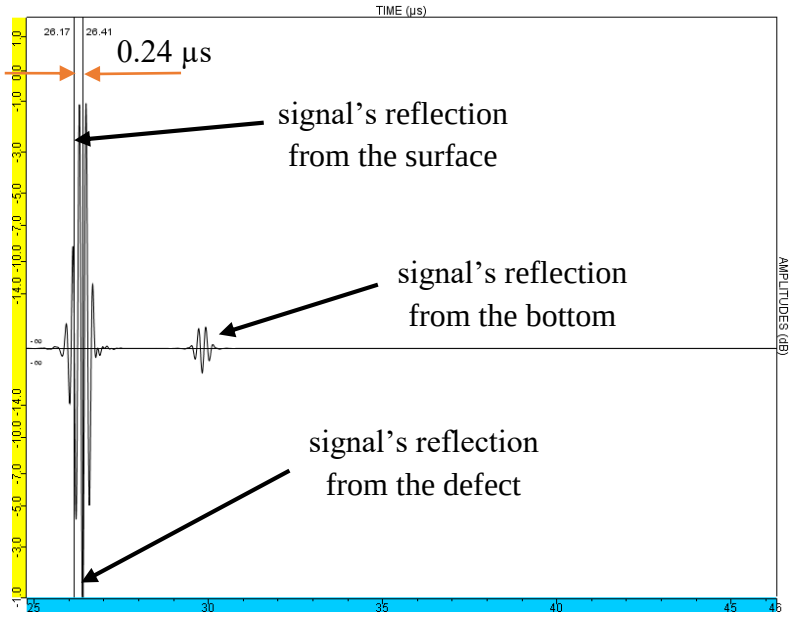

Fig. 3.32. Amplitude vs time graph (defect no 12, depth of the defect 5.0 mm)

The results of estimated depths using ultrasonic phased array probe and real depths of the defects are listed in table 3.9.

Table 3.9. Estimated and real depths of the defects in the specimen

Number of defect	**Theoretical velocity of ultrasound, m/s**	**Time interval between adjacent reflections, µs**	**Estimated depth of the defect, mm**	**Real depth of the defect, mm**	**Absolute error, mm**
1	1483	0.72	0.53	0.40	0.13
2	1483	3.71	2.75	2.70	0.05
3	1483	0.60	4.96	5.00	0.04
4	1483	0.72	0.53	0.40	0.13
5	1483	3.68	2.73	2.70	0.03
6	1483	0.58	4.97	5.00	0.03
7	1483	0.74	0.55	0.40	0.15
8	1483	3.68	2.73	2.70	0.03
9	1483	0.46	5.06	5.00	0.06
10	1483	0.76	0.56	0.40	0.16
11	1483	3.70	2.74	2.70	0.04
12	1483	0.48	5.04	5.00	0.04

The curves in figure 3.33. show the dependence of the absolute error variation on the defect depth at various defect diameters. The yellow curve shows the change in absolute error at a defect depth of

0.4 mm at different defect diameters, green at a defect depth of 5.0 mm and blue at a defect depth of 2.7 mm. This data is obtained using linear phased array for testing.

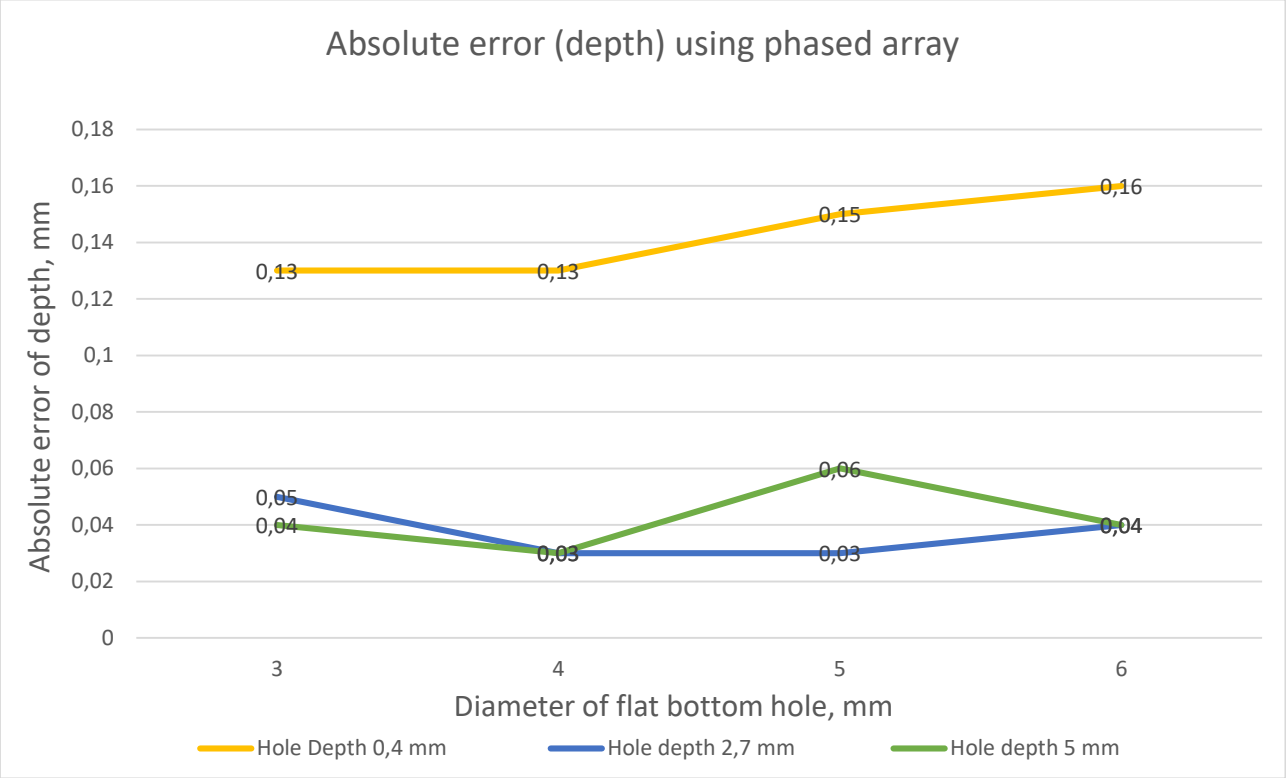

Fig. 3.33. Curves of the absolute error of depth using phased array

As we can see from the graphs, the differences of absolute error are also very negligible. Using phased array probe for testing, the values of absolute errors are even lower than with the single-element transducer. This is especially true for detecting defects in the middle of a specimen. The absolute value of the error is slightly higher when the defect is further from the measuring surface, but the magnitude of the error itself is practically unchanged.

3.4.3. Estimation of Defects Diameter using Phased Array

As in section 3.3.4. CIVA software segmentation tool was used to estimate defects diameter.

Results of the estimated defect diameter using phased arrays are presented in the table 3.10.

Table 3.10. Estimated and real diameters of the defects in the specimen using phased arrays

Number of defect	Depth of the defect, mm	Estimated diameter (ΔX) of the defect, mm	Real diameter of the defect, mm	Absolute error, mm
1	0.4	3	3	0
2	2.7	3	3	0
3	5.0	3	3	0
4	0.4	3	4	1
5	2.7	3	4	1

6	5.0	3	4	1
7	0.4	5	5	0
8	2.7	5	5	0
9	5.0	5	5	0
10	0.4	5	6	1
11	2.7	5	6	1
12	5.0	5	6	1

As can be seen from the curves presented in figures 3.24 and 3.34 and the data presented in tables 3.6 and 3.10, the defect sizes are determined much more accurately using phased array. When using phased array, the value of the absolute error does not exceed 1 mm, while using a single-element transducer for measurements, the value of the absolute error can be up to 7 mm in individual cases.

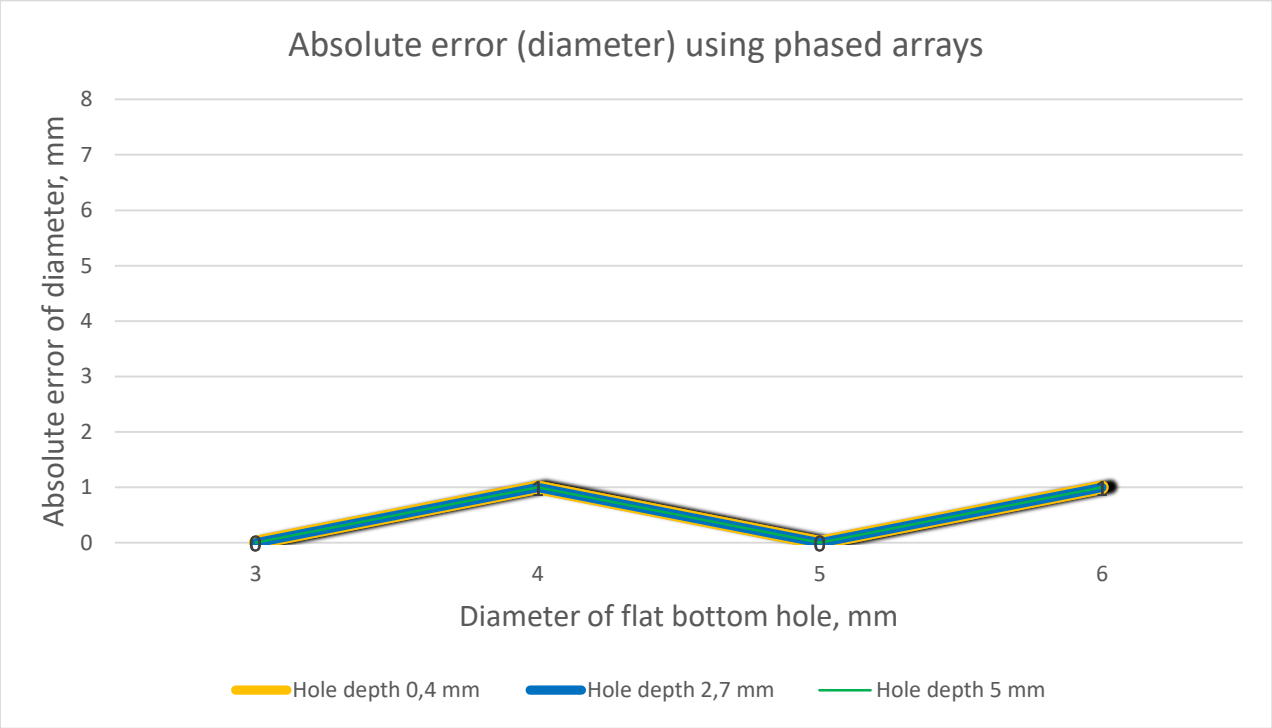

Fig. 3.34. Curves of the absolute error of diameter using phased array

3.5. Comparison of Single-Element Transducer and Phased Arrays Results

Comparing the calculations results of defect depth in tables 3.5 and 3.9 , it can be stated that a little more accurate results are obtained using ultrasonic phased array probe. This statement can be confirmed by comparing graphs (Fig. 3.35, 3.36) showing the results of defects depth measurements using single-element transducer and phased array. Fig. 3.35 shows comparison of absolute error of same diameter but different depth FBH using single-element transducer and Fig. 3.36 shows comparison of absolute error of same diameter but different depth FBH using phased array. It is interesting to note that with the single-element transducer, higher errors were obtained for defects

closer to the upper surface, and with the phased array, higher defect errors were obtained for defects closer to the lower surface of the sample.

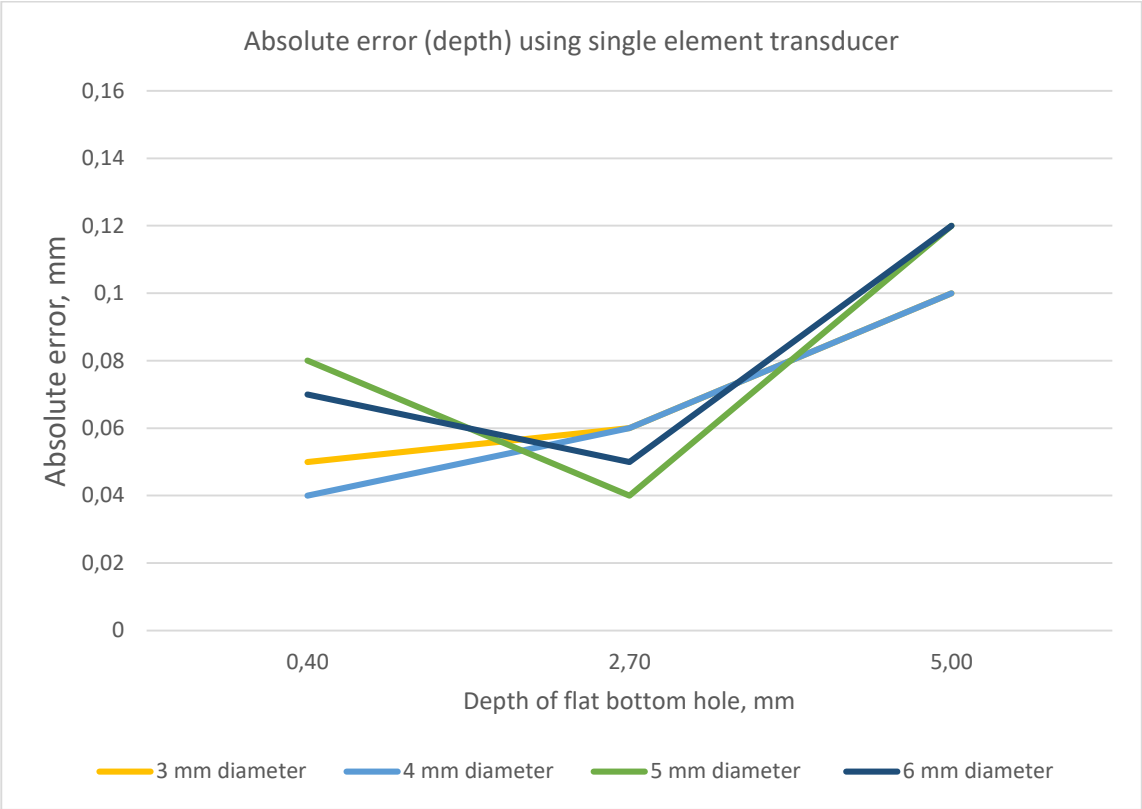

Fig. 3.35. Comparison of absolute error of same diameter but different depth FBH using single-element transducer

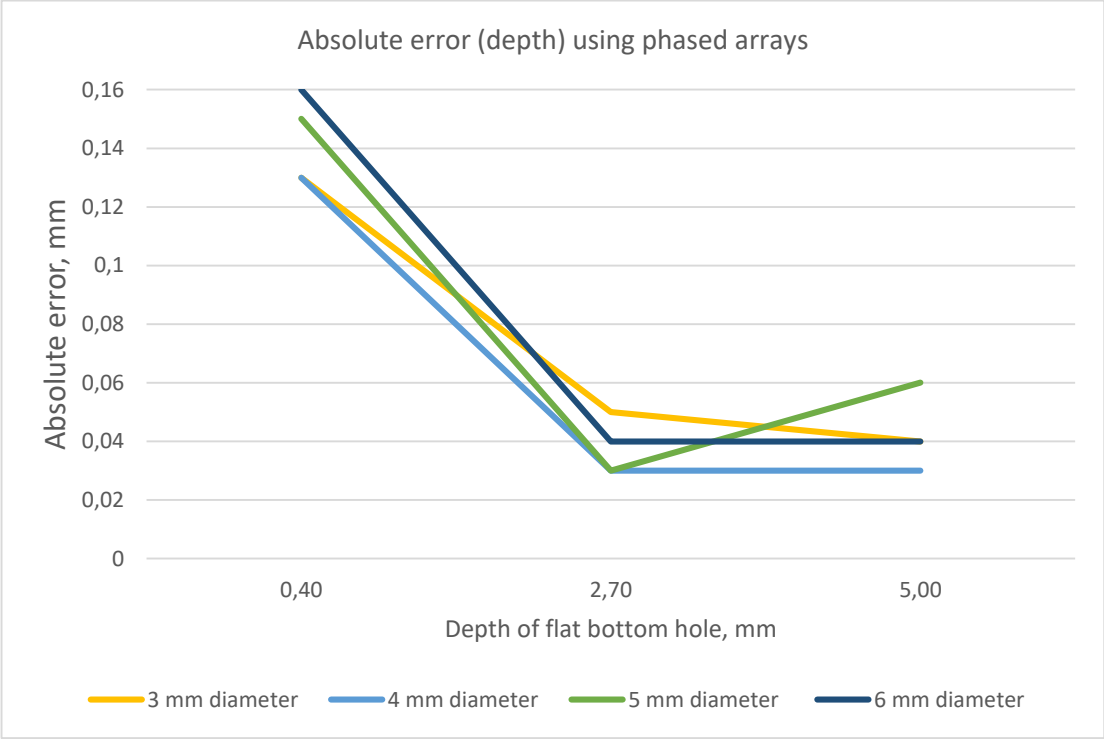

Fig. 3.36. Comparison of absolute error of same diameter but different depth FBH using phased array

In any case the defect depth results obtained with both the single-element transducer and the ultrasonic phased array probe are very close to the real defects depth results. However, it can be seen from the obtained experimental results, which are presented in tables 3.5 and 3.9 and figures 3.22, 3.33, 3.35, and 3.36, that using the ultrasonic measurement method, defects in the material are more accurately detected in the deeper part of the material that closer to the surface. Examining our specific sample, we see that for defects with depths of 2.7 mm, i.e. in the deeper layer both from the upper surface and from the lower surface of the sample, the absolute measurement errors are slightly smaller than for the measured defects close to the upper surface of the sample or lower surface of the sample (i.e. with depths of 0.4 mm and 5 mm).

After examining the influence of the size of the defect on the accuracy of determining the depth of the defect, it can be concluded from the obtained results using phased array probe, that the size of the defect practically does no affect the accuracy of defect depth determination (e.g., for defects Ø3 mm and Ø4 mm at a depth of 2.7 mm, the absolute error for determining the depth is 0.05 mm, and 0.03 mm respectively, and for larger defects Ø5 mm and Ø6 mm, the absolute errors for determining the defect of the same depth are 0.03 mm and 0.04 mm. respectively).

However, it can be concluded that in all cases the defects in the material are determined with relatively very small errors and the obtained values of absolute errors have no influence on the practical inspection of defects that may occur in the material, parts or products from carbon fiber composite materials during its fabrication or exploitation.

Comparing the results of absolute error of defects diameter using single element transducer and phased array bigger variance can be seen. This is especially evident in the comparison of the curves of the obtained results with the phased array and single-element transducer in one graph (Fig. 3.37). Here, solid lines show the results of measurements with a single-element transducer, and dotted lines with a phased array.

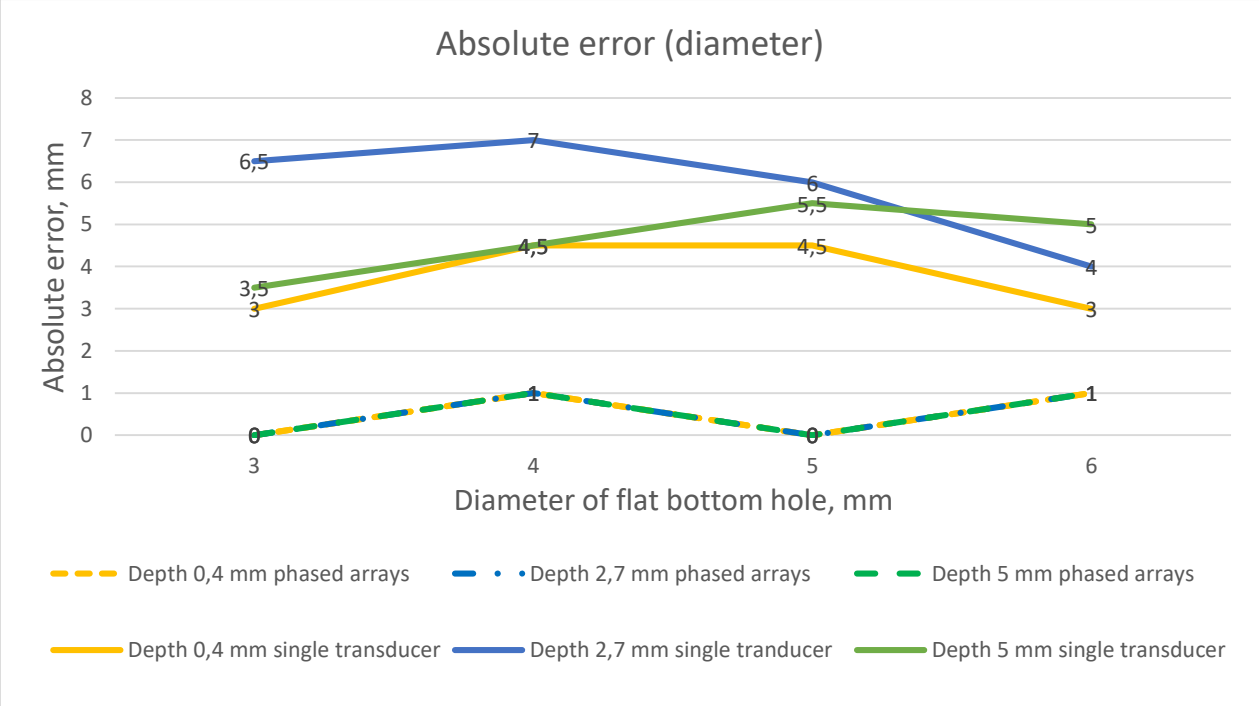

Fig. 3.37. Curves of the absolute error variation versus defect diameter at various defect depths using phased arrays and single transducer

With a single-element transducer, in some cases, an absolute error of up to 7 mm may be unacceptable when it is necessary to identify the size of the defect in parts and components that perform important functions in the product. The relatively low accuracy of defect sizing can have severe consequences for the operation of responsible units. Therefore, the obtained results and their comparison allow us to state that it is recommended to use phased array for determining the lateral size of defects.

4. Experimental Analysis

The purpose of the experimental analysis is to verify whether or not the phased arrays method is suitable for quality control of carbon fiber composite.

The computer simulation model made in chapter 3, theoretically allows us to detect the defects. Further task is to apply the developed model to detect defects in the sample by making real experimental analysis. The main problem of this part is that the measurement model is based on ideal laws, while in the experimental measurements, the quality of the analysis depends on many ambient influences, which complicates the process of measurement and affects the final result. After evaluating the results of computer simulations, a 5 MHz phased array probe was selected for experimental studies, which were connected to the OmniScan system shown in figure 4.1.

Fig. 4.1. Olympus OmniScan measurement system

OLYMPUS OMNISCAN$_{MX}$ ultrasonic measurement system was used in this experimental analysis. OLYMPUS OMNISCAN$_{MX}$ ultrasonic measurement system can be easily combined with other components to form a complete inspection system. The system be expanded by including phased arrays, probes, scanners, software for analysis and other accessories that can be easily integrated into application for specific solutions.

The experimental equipment used for testing is shown in Fig. 4.2.

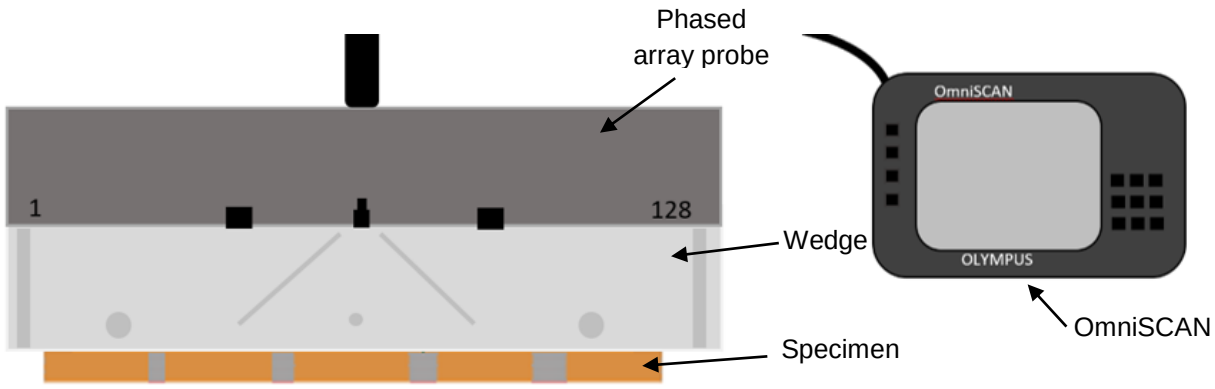

Fig. 4.2 Experimental setup

Phased array probe Olympus 5L 128-NW3 was used for the testing (Fig. 4.3). The measurement scheme is relatively simple so it is easy to carry out such an experiment under industrial conditions and get quick evaluations of the quality of the parts or construction.

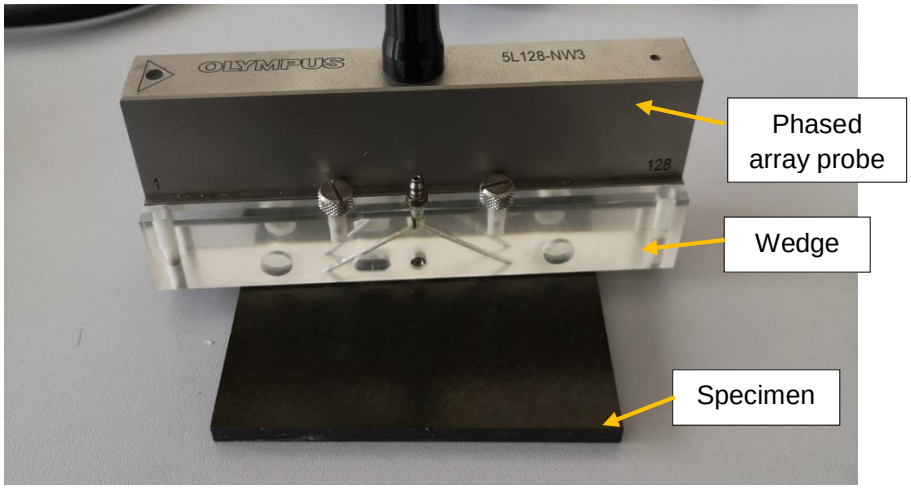

Fig.4.3. Common view of phased array probe Olympus 5L 128–NW3 with the specimen

Phased array probes typically have between 16 and 128 elements, some with as many 256, and frequency ranging from 1 MHz to 17 MHz. More elements increase focusing and steering capabilities and area coverage as well. Each of these 128 elements is pulsed individually to create a wavefront of interest.

Description of the phased array probe Olympus 5L 128-NW3 presented in table 4.1:

Table 4.1. Technical parameters of phased array probe Olympus 5L 128-NW3

Parameter	**Mark/Value**
Identification mark	5L 128-NW3
Frequency, MHz	5
Type	Linear (L)
Number of elements	128

Probe type	NW – near wall probe
Casing type	3
Active aperture, mm	128
Pitch, mm	1
Elevation, mm	7
External dimensions LxWxH, mm	130x21x35

Probe type NW is designed for near-wall and close accessed applications. The advantages of using the near-wall probes could be shortened dead zone at both ends (1.5 mm between the center of first or last element and housing edge), well suited for composite channel inspections and possibility to use for C-scan inspections of composites.

After measurements, the images of the results with signal reflections are shown in figures 4.4 – 4.7. With the 5 MHz phased array probe, images from the surface, bottom, and defects can be seen in the resulting images. Due to the higher phased array probe frequency of 5 MHz and the complex multilayer structure of the specimen, not only defects are reflected, but also very high noise due to the structure of the specimen. However, the resolution of defects in the sample is quite clear. Fig. 4.4 depicts scan images of the defects no 3, 6, 9 and 12 with the same depth (5 mm) but different diameters (3, 4, 5 and 6 mm), respectively.

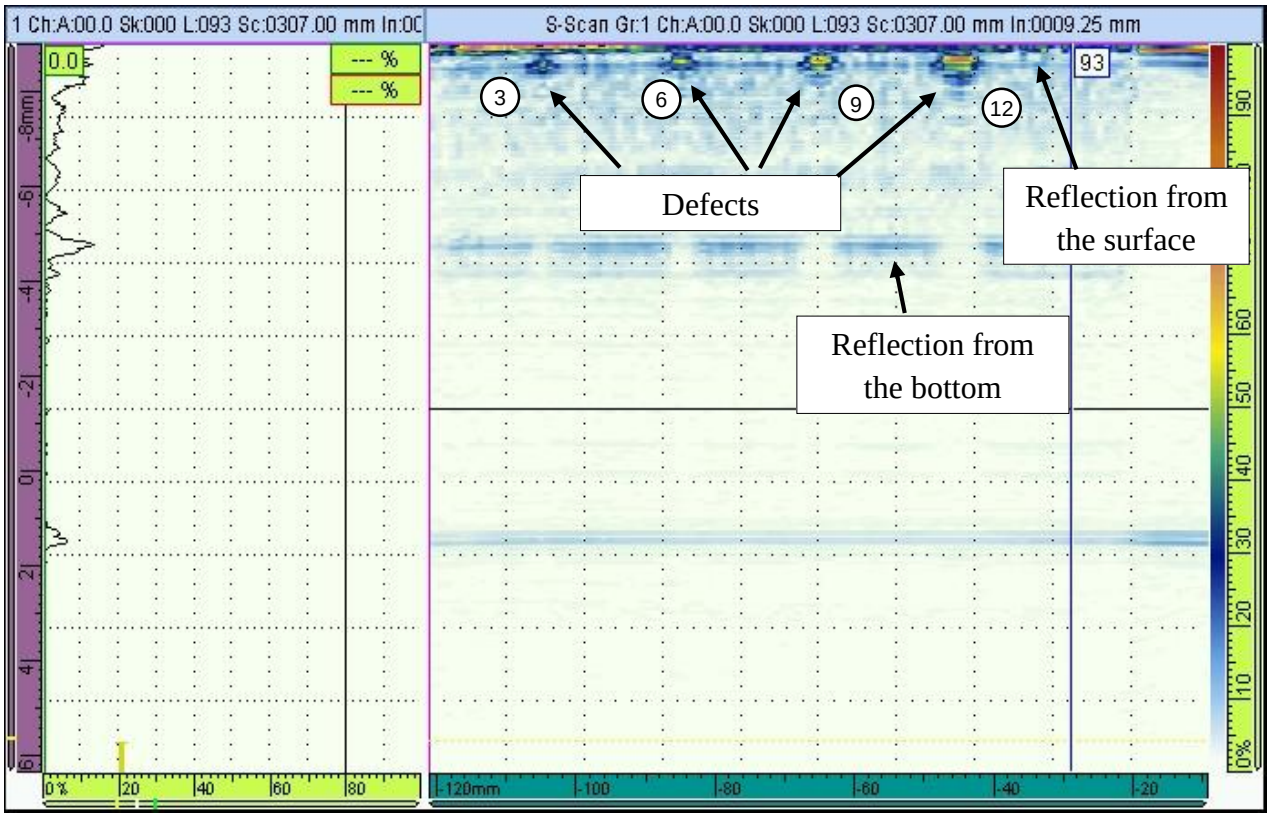

Fig.4.4. Scan images of defects no 3,6,9 and 12 with the same depth of 5 mm but different diameter

Fig. 4.5 shows scan images of the defects no 1, 4, 7 and 10 with the same depht (0.4 mm) but different diameter (3, 4, 5 and 6 mm), respectively.

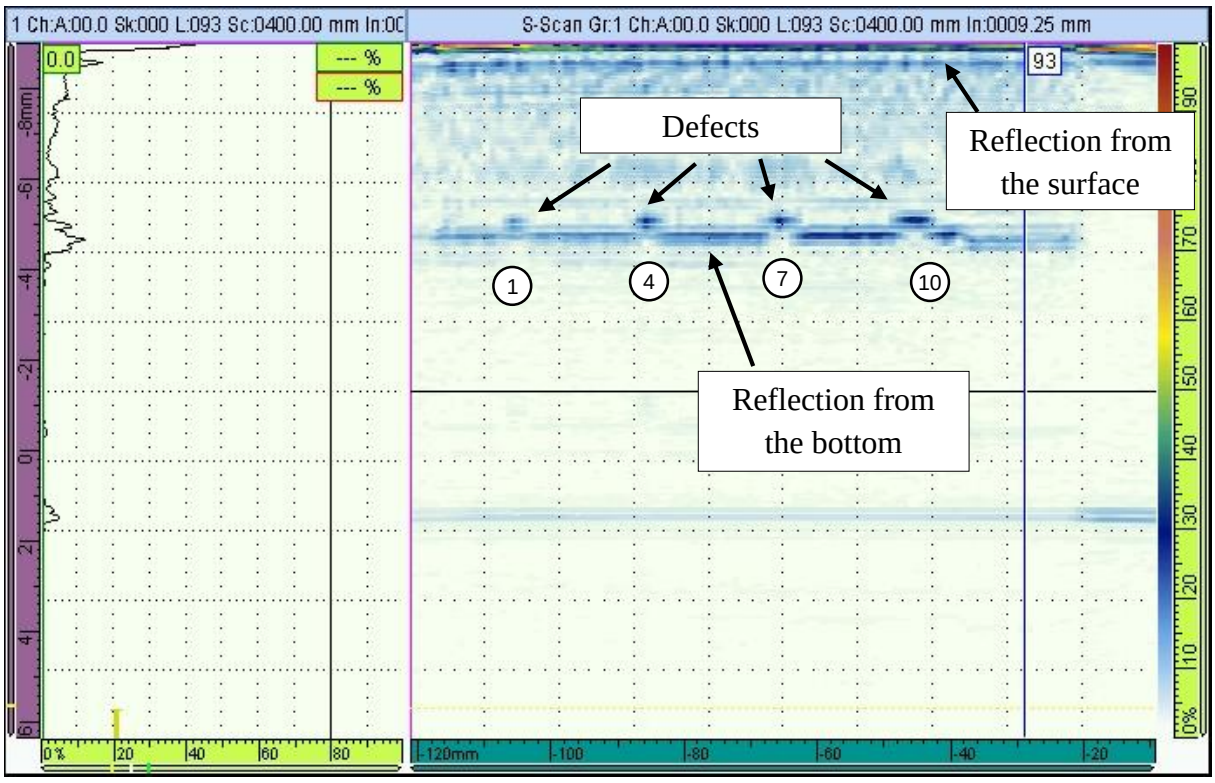

Fig.4.5. Scan images of defects no 1,4,7 and 10 with the same depth of 0.4 mm but different diameter

Fig. 4.6 presents scan images of the defects no 10, 11, and 12 with the same diameter (6 mm) but different depth (0.4, 2.7 and 5 mm), respectively.

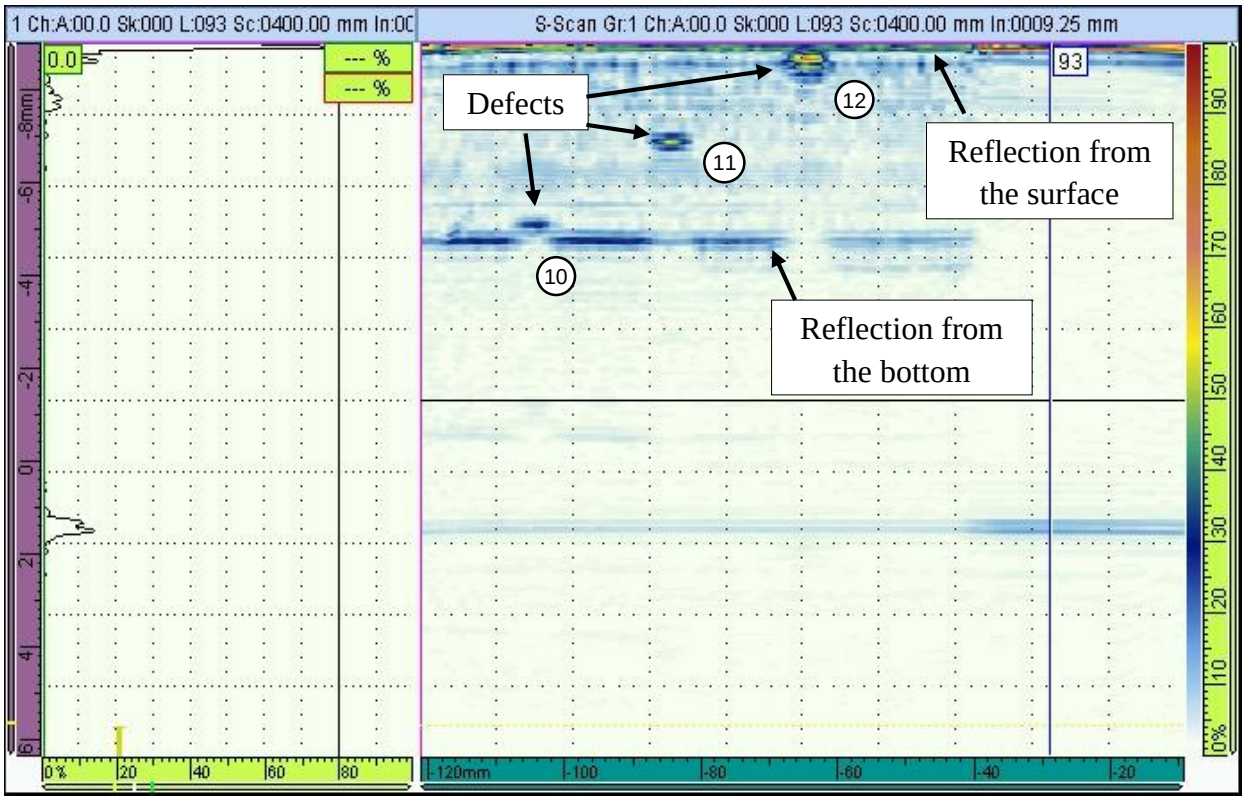

Fig.4.6. Scan images of defects no 10,11 and 12 with the same diameter of 6.0 mm but different depth

Fig. 4.7 shows scan images of the defects no 1, 2, and 3 with the same diameter (3 mm) but different depth (0.4, 2.7 and 5 mm), respectively. Obviously, a brighter image is obtained when there is a defect inside the material (defect no 11) than when it is very close to the surface (defects no 12 and 10).

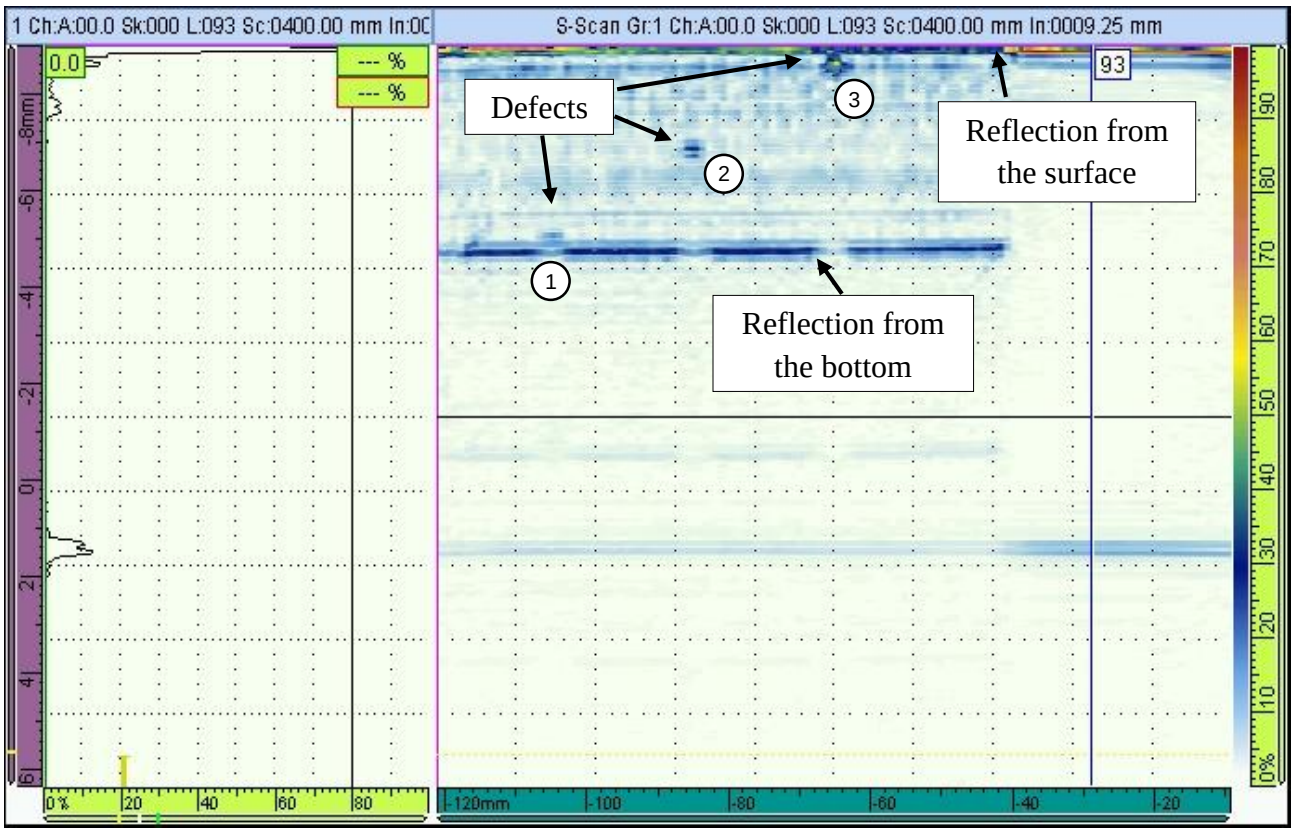

Fig.4.7. Scan images of defects no 1,2 and 3 with the same diameter of 3.0 mm but different depth

Experimental studies can only confirm the fact established during CIVA modeling that the accuracy of determining the location of a defect in a material depends on its distance from the surface. The location of the defect is more accurately determined when it is inside the material than when it is close to the surface.

Analyzing experimental results of a specimen with defects of different diameter and depth, the 5 MHz phased array probe was found to be suitable for detecting defects in constructions and parts made of carbon fiber composites. Using the aforementioned phased array probe, it is relatively easy to find defects in the composite material.

5. Conclusions

1. The analysis of non-destructive control methods has shown that the most suitable method for investigating the quality of carbon fiber composite parts and constructions is ultrasonic. The ultrasonic method is more appropriate when specimens are to be tested under field conditions because the equipment of the method is much simpler and results are obtained faster.
2. In the CIVA environment, a computer-based experimental model was developed and a computer-based measurement simulation was performed. Based on CIVA results, it is concluded that 5 MHz phased array probes are more suitable for real experiment than 5 MHz single-element transducers used in aviation because the absolute errors with phased array probe did not exceed 1 mm in all measurements.
3. Based on CIVA results, the parameters of the phased array probe were determined for the real experiment: the frequency of the phased array probe is 5 MHz, and the necessity of the delay line (wedge). The delay line is used to facilitate the analysis of received signals in relatively thin parts tests when a phased array probe is also used for transmitting and receiving signals.
4. The obtained measurement results allow us to maintain that for ultrasonic measurements for carbon fiber composite using both the single-element transducer and the phased array, the distance to the defect can be determined more accurately in the presence of a defect inside the material (at a 2.7 mm depth). In this case, the maximum absolute error obtained is only 0.06 mm while when the defect is close to the surface of the sample, the error can reach 0.16 mm.
5. Studies performed in determining the lateral size of the defect in the carbon fiber specimen allow to state the fact that significantly more accurate results were obtained using a phased array than that using a single-element transducer, because the use of a phased array allows to determine the defect size with 1 mm absolute error, while measuring with a single-element transducer, in individual cases, the absolute error can increase up to 7 mm.
6. Experimental studies with OLYMPUS OMNISCAN$_{MX}$ flaw detector confirm the results of the CIVA simulation and allow to conclude that ultrasonic measurements are reliable in detecting defects of various sizes and dislocations in composite materials.

List of references

1. IRVING, P.E., SOUTIS, C. Polymer composites in the aerospace industry. Cambridge: Woodhead Publishing (2015), 520 p.
2. CHANDA, M. Plastics technology handbook. Fifth edition. CRC Press (2017) 1012 p.
3. HECHT, K., TEXTOR, T., GIERLING, E., CLASSEN, E. Innovative finishing approach for improved repellency towards metal splashes. 7th European Conference on Protective Clothing. 23-25 May (2016) Izmir, Turkey, 147-149
4. Metal handbook. Properties and selection: irons, steels and high performance alloys. Vol.1, ASM International (1990) 2521 p.
5. DONNET, J.B., BANSAL, R.C. International Fiber Science and Technology 10 (Carbon fibers), 2nd edition. Marcel Dekker, New York (1990) 267-366
6. JENSEN, A.B., THESBJERG, J., WIND, J.L., JENSEN, H.M. Kink band predictions in fiber composites using periodic boundary conditions. Composite Structures, 207 (2019), 331-339
   https://doi.org/10.1016/j.compstruct.2018.09.055
7. PIMENTA, S., GUTKIN, R., PINHO, S.T., ROBINSON, P. A micromechanical model for kink-band formation: Part 1 – Experimental study and numerical modelling. Composites Science and Technology, 69 (2009), 948-955
   doi:10.1016/j.compscitech.2009.02.010
8. KASHTALYAN, M., SOUTIS, C. Analysis of composite laminates with intra- and interlaminar damage. Progress in Aerospace Sciences, 41 (2015) 152-173
   doi:10.1016/j.paerosci.2005.03.004
9. SHYR, T.W., PAN, Y.H. Impact resistance and damage characteristics of composite laminates. Composite Structures, 62 (2003), 193-203
   doi:10.1016/S0263-8223(03)00114-4
10. GIURGIUTIU, V. Structural health monitoring of aerospace composites. Academic Press (2015), 470 p.
    https://doi.org/10.1016/C2012-0-07213-4
11. KAMINSKI, M., LAURIN, F., MAIRE, J.F., RAKOTOARISOA, C., HEMON, E. Fatigue damage modeling of composite structures: the onera viewpiont. Journal Aerospace Lab. 9, June (2015), 1-12
    doi:10.12762/2015.AL09-06
12. JADEE, K.J., OTHMAN, A.R. Fiber reinforced composite structure with bolted joint – a review. Trans. Tech. Publications, 471-472 (2011), 939-944
    doi:10.4028/www.scientific.net/KEM.471-472.939
13. LIEBIG, W.V., VIETS, C., SCHULTE, K., FIEDLER, B. Influence of voids on the compressive failure behavior of fibre-reinforced composites. Composites Science and Technology, 117 (2015), 225-233
    http://dx.doi.org/10.1016/j.compscitech.2015.06.020
14. LEE, S.H., WAAS, A.M. Compressive response and failure of fiber reinforced unidirectional composites. International Journal of Fracture, 100 (1999) 275-306
    https://www.researchgate.net/publication/30843525

15. SHAMS, S.S., ELHAJJAR, R.F. Investigation into the effects of fiber waviness in standard notched composite specimens. CEAS Aeronaut Journal, 6 (2015) 541-555
DOI 10.1007/s13272-015-0161-4
16. OSTAPIUK, M., BIENIAŠ, J., SUROWSKA, B. Analysis of the bending and failure of fiber metal laminates based on glass and carbon fibers. Sci. Eng. Compos. Mater., 25 (6) (2018) 1095-1106
https://doi.org/10.1515/secm-2017-0180
17. JUAREZ, P., LECKEY, C.A.C. Aerogel to simulate delamination and porosity defects in carbon-fiber reinforced polymer composites. AIP Conference Proceedings, 1949, 120008 (2018) 120008-1 – 120008-9
https://doi.org/10.1063/1.5031595
18. UNNPORSSON, R., JONSSON, M.T., Runarsson, T.P. NDT methods for evaluating carbon fiber composites. Research Gate, (2014) 1-17
https://www.researchgate.net/publication/237699285
19. BOWKETT, M., THANAPALAN, K. Comparative analysis of failure detection methods of composite materials' systems. Systems Science & Control Engineering, 5 (1) (2017) 168-177
https://doi.org/10.1080/21642583.2017.1311240
20. GHOLIZADEH, S. A review of non-destructive testing methods of composite materials. XV Portuguese Conf. On Fracture, PCF 2016, 10-12 February 2016, Paco de Arcos, Portugal. Procedia Structural Integrity 1 (2016) 050-057
10.1016/j.prostr.2016.02.008
21. KAPADIA, A. Non destructive testing of composite materials. Best practice guide. National Composites Network, UK (2006) 52 p.
http://www.twi.co.uk/j32k/index.xtp
22. FERNANDES, H., ZHANG, H., FIGUEIREDO, A., IBARRA-CASTANEDO, C., GUIMARARES, G., MALDAGUE, X. Carbon fiber composites inspection and defect characterization using active infrared thermography: numerical simulation and experimental results. Applied Optics, 55 (34) (2016) D46-D53
DOI:10.1364/AO.55.000D46
23. ZHANG, H., YANG, R., HE, Y., FOUDAZI, A., CHENG, L., TIAN, G. A review of microwave thermography nondestructive testing and evaluation. Sensors, 17 (2017) 1123-1167
doi:10.3390/s17051123
24. RAJU, R., AZMI, A.I., PRUSTY, B.G. Acoustic emission techniques for failure characterization in composite top-hat stiffeners. J. of Reinforced Plastics & Composites, 31 (7) (2012) 495-516
DOI: 10.1177/0731684412437986
25. YU, F., OKABE, Y., WU, Q., SHIGETA, N. Damage type identification based on acoustic emission detection using a fiber-optic sensor in carbon fiber reinforced plastic laminates. Journal of Acoustic Emission, 33 (2016). Selected papers from the proceedings of 32nd European Conf. on Acoustic Emission Testing, Prague, Czech Republic, September 07-09, 2016, S271-S278
26. ABRAHAM, A.R., ANDRADE, E., JOHNSON, K.L., NICHOLS, C.T., SAULSBERRY, R.L., TYLKA, J.M., WALLER, J.M., WENTZEL, D.J. Developing novel acoustic emission procedures for failure prediction of carbon-epoxy COPVs and related composite materials. NASA, Composite Conference 2012, Las Cruces, NM, Wednesday, August 15, 2012, 1-49

27. GEORGES, M., SRAJBR, C., MENNER, P., KOCH, J., DILLENZ, A. Thermography and shearography inspection of composite hybrid sandwich structure made of CFRP and GFRP core and titanium skins. Proc. of 18th Int. Conf. on Experimental Mechanics (ICEM18), Brussels, Belgium, 1-5 July (2018) 1-6
doi:10.3390/ICEM18-05384
28. https://www.dantecdynamics.com/products-and-services/what-is-laser-shearography [viewed at 19.04.2019]
29. SALSKI, B., GWAREK, W., KORPAS, P. Electromagnetic inspection of carbon-fiber-reinforced polymer composites with coupled spiral inductors. IEEE Transactions on Microwave Theory and Techniques, 62 (7) (2014) 1535-1544
DOI:10.1109/TMTT.2014.2325537
30. MIZUKAMI, K., MIZUTANI, Y., KIMURA, K., SATO, A., TODOROKI, A., SUZUKI, Y., NAKAMURA, Y. Visualization and size estimation of fiber waviness in multidirectional CFRP laminates using eddy current imaging. Composites: part A, chapter 4, 90 (2016) 261-270
31. MIZUKAMI, K., MIZUTANI, Y., TODOROKI, A., SUZUKI, Y. Analytical solutions to eddy current in carbon fiber-reinforced composites induced by line current. Advances Composite Materials, 25 (4) (2016) 385-401
http://dx.doi.org/10.1080/09243046.2015.1052132
32. MIZUKAMI, K. Eddy current technique for detection and size estimation of fiber waviness in carbon fiber reinforced composites. Thesis for doctor of engineering. Tokyo Institute of Technology (2016) 158 p.
33. JASIŪNIENĖ, E. Ultrasonic material research. Coursebook. Kaunas, Vitae Litera (2007) 139 p (in Lithuanian)
34. OSTWAL, R.S., SAWANT, A.V. Ultrasonic testing of fiber reinforced polymer composites – an overview. International Journal of Engineering Research & Technology, 3 (6) (2014) 544-547
35. MARGETAN, F.J., LECKEY, C.A., BARNARD, D. Modeling the effects of beam size and flaw morphology on ultrasonic pulse/echo sizing of delaminations in carbon composites. AIP Conference Proceedings, 1511, 955 (2013) 955-962
http://dx.doi.org/10.1063/1.4789147
36. STRYCEK, J.O., LOERTSCHER, H.P. Ultrasonic air-coupled inspection of advanced material. NDT net, 4 (12) (1999) https://www.ndt.net/article/v04n12/qmi/qmi.htm
37. http://www.sdindt.com/Ultrasonic-Testing.html [viewed on 20.04.2019]
38. SHEN, Q., OMAR, M., DONGRI, S. Ultrasonic NDE techniques for impact damage inspection on CFRP laminates. Journal of Materials Science Research, 1 (1) (2012) 2-16
doi:10.5539/jmsr.v1n1p2
39. KARABUTOV, A.A., PODYMOVA, N.B., BELYAEV, I.O. The influence of porosity on ultrasound attenuation in carbon fiber reinforced plastic composites using the laser-ultrasound spectroscopy. Acoustical Physics, 59 (6) (2013) 667-673
DOI: 10.1134/S1063771013060080
40. KENZIE, B., SPECK, J. Developments in integrity management with TOFD inspection. Inspectioneering Journal, July/August (2005)
41. ANDERSON, M. Phased array testing. Basic theory for industrial applications. First edition, Olympus NDT Inc., (2010) 122 p.

42. DRINKWATER, B.W., WILCOX, P.D. Ultrasonic arrays for non-desctructive evaluation: A review. NDT&E International, 39 (2006) 525-541
doi:10.1016/j.ndteint.2006.03.006
43. https://www.tcradvanced.com/phased-array-ultrasonic-testing.html, [viewed 23.05.2019]
44. BISIAUX, B. Ultrasonic inspection technique using multi-element probes (phased array): application to tube inspection. Proceedings of 15th World Conference on Non-destructive Testing, 15-21 October (2000) Rome, Italy
45. BS EN 2564:1998. Carbon fibre laminates – Determination of the fibre, resin and void contents. British standard aerospace series. British Standards Institution [BSi], 25 p.
46. PYLAEV, A.E., et al. Velocity and attenuation of acoustic waves in polymers and polymer composites. Polymer Science, Series D, vol. 11, no 3, 2018, pp. 272-276
47. SCHADOW, F., BRACKROCK, D., GAAL, M., HECKEL, T. Ultrasonic inspection and data analysis of glass- and carbon-fibre-reinforced plastics. Procedia Structural Integrity, 7, 2017, pp. 299-306. Proc. of the 3rd Int. Symposium on Fatigue Design and Materials Defects, FDMD 2017, 19-22 September, Lecco, Italy
10.1016/j.prostr.2017.11.092
48. JASIŪNIENĖ, Elena. Ultragarsinė medžiagotyra. Mokomoji knyga, Kaunas, Vitae Litera, 2007, 140 p.
49. JASIŪNIENĖ, Elena, ŽUKAUSKAS, Egidijus, SAMAITIS, Vykintas. Ultragarsinių matavimų laboratoriniai darbai: mokomoji knyga [interaktyvus]. Kaunas: Technologija, 2013, 92 p. [žiūrėta 2019-11-14]. ISBN 978-609-02-0834-2. Prieiga per:
https://www.ebooks.ktu.lt/einfo/1046/ultragarsiniu-matavimu-laboratoriniai-darbai
50. BANNOUF, S., LONNE, S., GRASSIN, F., LE BERRE, S., ROUE, D. Advanced tools based on simulation for analysis of ultrasonic data. Proc. of 11th Int. Conf. on Non Destructive Evaluation, 2015, 19-21 May, Jeju, Korea, pp. 415-422
51. KUMARAN, S., RANI, S.B. Application of 6db drop technique to estimate the width of sub assembly ring top using pulse echo ultrasonic technique. International Journal of Engineering and Technology, vol.5, no 6, 2014, pp. 4771-4775